The University Of Sheffield.

Biophysical Properties of Zebrafish Hair Cells

By:

Jennifer Olt

A thesis submitted in partial fulfilment of the requirements for the degree of Doctor of Philosophy

The University of Sheffield

Faculty of Science

Department of Biomedical Science

December 2015

Souvienne vous de celui, à qui comme on demandait, à quoi faire il se peinait si fort en un art qui ne pouvoit venir à la cognoissance de guere de gens: J'en ay assez de peu, respondit-il, j'en ay assez d'un, j'en ay assez de pas un.

Michel de Montaigne, Essais, Livre I, Chap. XXXVIII (1595)

(Remember, the person who, when asked why he was working so hard on something that would come to the attention of scarcely anyone: I will be satisfied with a few, he answered, I will be satisfied with one, I will be satisfied with no one.)

Acknowledgements

First of all I want to thank my supervisor Walter Marcotti! Thanks for giving me the opportunity to do this exciting and new project, I couldn't have asked for a better topic. Even more thanks for always providing support and guidance in the lab, for supporting my ideas and shaping them.

Thanks to my grandma, mum and family! Thanks to my biology teacher in school, Herr Kowalski, who inspired me to study biology and thanks to Dr. Barbara Tzschentke who let me do my first steps in electrophysiology at HU Berlin. Thanks to all past and present members of the Marcotti lab, particularly Dr. Laura Corns, who made it an enjoyable place to work and for all their support. Thanks to my amazing and caring friends from Germany, who visited me plenty of times and enjoyed so many happy moments on this beautiful island with me. In no particular order: Julia Benedikt, Lisa Perko, Tom Kulosa, Sandra Reinhardt, Katharina Vogt und Kati Drechsel. I can't wait for many more visits! Thanks to Felix and Simon, for numerous trips to climbing and the pub and feeding me with salad. You made these three years a fun time and your advice was invaluable! Thanks to Dr. Alison Wood for being my gym-buddy! Without you team, I would have never experienced what Zumba feels like. Thanks to Dr. Tina Tong, Dr. Diana Rien and Dr. Nico Vautrelle for being fun and always sharing advice on PhDs and life in general.

Thanks to Dr. Stephen Grebby and Dr. Sophie Bradley for sharing their house with me and so many happy moments. The biggest thanks goes to Sophie, my sister from a different mother. I could not have done any of this without you and your encouragement. You make me laugh like nobody else and we always have the best times together, enjoying the many beautiful things in life. Lastly, but not least, I would like to thank Stella Artois and Schneiders Weisse for everything.

Abstract

Hair cells are specialized mechanosensory receptors in vertebrates that detect and process auditory and vestibular information with remarkable precision, fidelity and efficiency (Schwander et al., 2010). Most of our knowledge about these cells stems from *in vitro* preparations using isolated tissue, which creates the need for a relatively simple *in vivo* vertebrate model to study hair cells.

The zebrafish (*Danio rerio*) is being increasingly used to study the genetic basis of hearing and deafness but also the function and physiology of hair cells (Nicolson, 2005). However, the use of the zebrafish as an *in vivo* model to study hair cell function is currently limited by our poor understanding of their biophysical properties. The aim of this study was to provide a detailed description of the biophysical properties of zebrafish hair cells both in the lateral line as well as inner ear during early and mature stages of fish development. I have used single cell patch-clamp electrophysiology to measure potassium currents and synaptic transmission in hair cells.

I found that hair cells from the lateral line and inner ear show different current types, the expression of which depends upon the position of the cell within the lateral line neuromast or inner ear macula. Moreover, I found that the abundance of hair cell types in the lateral line changes over time, which potentially reflects adaptations to a changing sensory environment for the fish. The synaptic machinery of the lateral line hair cells is comparable in terms of efficiency to its mammalian counterpart, but less sensitive. Lastly, I have also developed an approach to study hair cell properties *in vivo* in the juvenile fish.

Contents

Figures

Tables

Abbreviations

ACh – Acetylcholine

AHP – after hyperpolarisation potential

AMPA - alphaamino-3-hydroxy-5-methyl-4-isoxazolepropionic acid (AMPA) receptor

dpf – days post fertilization

DPBS – Dulbecco's phosphate-buffered-saline

E3 – Embryo medium 3

FM1-43 - (N- (3-Triethylammoniumpropyl) -4- (4- (Dibutylamino) Styryl) Pyridinium Dibromide)

GECI - genetically encoded calcium indicators

hpf – hours post fertilisation

I_A – A- type Na^+/K^+ current

I_{Ca} – calcium current

I_h – hyperpolarisation-activated current

IHC - Inner hair cells

$I_{K,1}$ – inward rectifier K^+ current

$I_{K,D}$ – delayed rectifier K^+ current

I_{Met} - mechanotransducer current

L1 – L 8 –neuromasts originating from primI

LJP – Liquid junction potential

MS-222 - tricaine methanesulfonate

OHC - outer hair cells

PLL – posterior lateral line

pllG – posterior lateral line ganglion

PrimI – first primordium

PrimII – second primordium

PrimD – dorsal primordium

TBE - tri-bromo-ethanol

$V_{\mathbf{m}}$ - resting membrane potential

VOR - vestibulo-ocular-reflex

wpf – weeks post fertilization

α-Btx – α – bungarotoxin

Chapter 1 General Introduction

Both sound and body motion are external physical stimuli that are translated into an internal biological signal by a remarkable cell type, the hair cell. These cells are exceptional in their features since they are able to transduce these stimuli and transmit them to the brain with incredible precision and fidelity.

Hair cells are specialised mechanosensory receptors that are in evolutionary terms very old and found in both lower vertebrates and mammals. Because of the different physiological demand and environment to which these cells are exposed, they have developed specialized biophysical and morphological characteristics. Each hair cell type is built to face and fulfil its unique task.

In this chapter, I will cover how the morphological structure of the sensory organ is shaped and develops (point 1.1), how hair cells are able to transduce stimuli (point 1.2) and how hair cells encode their information at the specialized ribbons synapses (point 1.3). Each of these parts will be described in depth for fish and then briefly compared to hair cells of the auditory and vestibular systems of other lower vertebrates.

1.1 Structure of the lateral line and inner ear in fish

Hair cells are present in organs of different sizes and shapes and a selection will be described below.

1.1.1 Structure of the zebrafish lateral line organ

Fish and amphibians have mechanosensory hair cells on the body surface, along the lateral line organ, which functions to sense 'touch at a distance'. In zebrafish, the lateral line organ is able to detect frequencies up to 200 Hz and consists of two parts: the anterior lateral line (ALL) located at the head and the posterior lateral line (PLL) on the tail of the zebrafish. Because the PLL has been the main focus of research, little is known about the development of the ALL. The cell bodies of the neurons contacting the lateral line are located in two ganglia close to the ear of the fish.

1.1.1.1 Structure of a lateral line neuromast

Neuromasts are the functional unit of the lateral line and are located on the surface of the zebrafish under the skin. Neuromasts contain the hair cells, supporting cells and mantle cells (Figure 1.1 *A*). At larval stages, the neuromast has about 8 – 15 hair cells (Ghysen and Dambly-Chaudiere, 2007) and each of them is surrounded by five to six supporting cells, whose cell bodies are located under the sensory cells (Figure 1.1 *A*, Lopez-Schier et al., 2004). The apical part of the hair cell is sealed by the cuticular plate and all the hair cell cuticular plates are fused together to form a near-impermeable barrier (Ghysen and Dambly-Chaudiere, 2007; Pujol-Marti and Lopez-Schier, 2013).

From the cuticular plates, the hair cells extend their stereociliary bundles and kinocilia into the gelatinous cupula, which forms a protective dome over the hair cells and creates a direct connection with the aqueous environment (Figure 1.1 *A,* Lopez-Schier et al., 2004). The cupula orchestrates simultaneous movement of all hair cells and is thought to be secreted by the mantle cells (for review see Ghysen and Dambly-Chaudiere, 2007).

Hair cells within a single neuromast are subdivided into two groups of different polarity, that are present within the anterior or posterior compartment and can be distinguished by the location of the kinocilium. In the anterior group the kinocilium faces to the posterior and cells are excited by stimuli from the anterior-to-posterior direction. The posterior group faces the opposite way and is excited by stimuli from posterior to anterior as shown in Figure 1.1 *B* (Flock and Wersall, 1962). Because of this opposite polarity, the stimulation of the cupula will simultaneously excite one group of hair cells and inhibit the other, which results in bipolar responses on the fibre. The primary neuromasts show polarity along the anterior-posterior axis, whereas the secondary ones orientate perpendicularly and sense dorsal-ventral direction (Figure 1.1 *B*: Lopez-Schier et al., 2004).

Figure 1.1 Schematic of a neuromasts and its polarity.

A, Lateral view of a neuromast. The hair bundle consists of the kinocilium (K) and the stereocilia (S), that protrude into the cupula. Neuromasts contain two populations of hair cells of opposing hair bundle polarities (*B*). Excitation of the hair cells occurs as follows: Water movement (blue arrow) displaces the cupula along the anterior-posterior axis. This depolarizes (+) one population of hair cells, whilst hyperpolarizing (−) the other. This leads to an increase (+) or a decrease (-) of the firing rate of the afferent neuron associated with each hair cell population. *B***,** Top view of a primary (*left,* parallel) and a secondary (*right*, perpendicular) neuromast. Figure modified from Pujol-Marti and Lopez-Schier, 2013.

1.1.1.2 Development of the lateral line

The lateral line starts developing during embryonic stages and is generated by several waves of outgrowth that start with a primordium. During development this will create ~ 30 neuromasts, which are distributed across each somite and on the fins to maximise sensitivity across the whole fish body.

Posterior lateral line migration

The PLL originates from the cephalic placode close to the head and just posterior to the otic placode (Stone, 1937) as reviewed in Ghysen and Dambly-Chaudiere, (2004). At around 18-20 hpf the PLL placode gives rise to the first primordium (primI). It is formed by two compartments, the anterior compartment that contains approximately 20 cells, which are the future afferent neurons , and a bigger compartment with around 100 cells that will be the future neuromast (Pujol-Marti and Lopez-Schier, 2013). PrimI migrates caudally along the horizontal myoseptum on a pre-existing pathway (Stone, 1922, 1937; Smith et al., 1990). This migration process starts at 20 hpf and is finished by 40-48 hpf.

The primI deposits five pro-neuromasts each containing a group of 20 cells on its journey (termed L1-L5) (Figure 1.2 *A* and *B*), and fragments into another two or three to form the tail neuromasts, so that by 48 hpf there are 8 pro-neuromasts on the larval fish. When this first wave is completed, these pro-neuromasts are assumed to be fully functional since the fish respond to touch (Ghysen and Dambly-Chaudiere, 2004). The primI migration is accompanied by axons extending from the lateral line ganglion (Metcalfe, 1985; Gilmour et al., 2004).

After the first primordium has completed its journey, two more primordia are formed, called primII and primD. PrimII commences its journey at ~ 40 hpf and is much slower than primI. It intersperses four to five secondary neuromasts between L1 and L2 (Figure 1.2 *B*) (Sapede et al., 2002). The secondary neuromasts are on average two somites apart. PrimII takes nearly a week to complete its journey to the anus, which is the halfway point between head and tail. Simultaneously to the primII migration start, a dorsal lateral line is formed by primD.

When the primary and secondary neuromasts are deposited, they start to migrate ventrally (Ledent, 2002; Ghysen and Dambly-Chaudiere, 2004). This means that by 2-3 wpf the PLL consists of two paths of neuromasts, the line with neuromasts deposited by primI and II and a dorsal lateral line (Figure 1.2 *B* and *C*). Over the next weeks, the dorsal lateral line will also migrate ventrally, taking up a position at the midline of the fish. Finally, two new lines of neuromasts form in the very position where the embryonic primI and II and the dorsal ones first appeared (Figure 1.2 *D* green dots). In the final step of the lateral line outgrowth, the neuromasts form ''stitches'', which are dorso-ventrally elongated clusters of neuromasts (Figure 1.2 *E*) (for review see Ghysen and Dambly-Chaudiere, 2007).

Figure 1.2 Development of the posterior lateral line.

A, At 32 hpf the primI is about halfway on its journey to the tip of the tail and has deposited two neuromasts. *B,* At 3 dpf, primI has reached the tip of the tail, primII started migration and primD initiates the dorsal line (D1-D3, blue). *C,* At 3 wpf, intercalary neuromasts are formed (red). PrimD and primII have completed their journey (blue). *D,* At the larval–juvenile transition, the lateral and dorsal lines are complete and are shifted ventrally. Two new lines have formed at the original positions at the embryonic lines: one along the horizontal myoseptum and one along the dorsal midline (light green). *E,* Young adult fish hair cells labelled with caged fluorescein. Neuromasts are organised into stitches. *Inset,* 48-hpf embryo at the same scale as the adult. Scale bars, 1 mm. Modified after Ghysen and Dambly-Chaudiere, 2007.

1.1.2 The zebrafish inner ear

The zebrafish inner ear consists of six sensory patches. The three cristae detect rotational acceleration. The three maculae, which include the utricle, sacculus and lagena, are responsible for sensing linear acceleration. While the utricle carries exclusively vestibular function, the sacculus and lagena are probably involved in both vestibular and auditory sensation (for review see Whitfield et al., 2002).

In the **sacculus**, there are differences in hair cell density, with central regions having on average fewer hair cells than the periphery. Moreover, the goldfish sacculus, has been shown to be tonotopically organised with low frequencies around 100 Hz represented at the most posterior/caudal part and the highest frequencies up to 4000 Hz at the anterior/rostral part (Figure 1.3 *B* and *E*) (Bang et al., 2001; Smith et al., 2011).

The **utriculus** is also divided in regions. The striolar region, which is in the anterior portion of the tissue, contains a low density of hair cells with long bundles, while the cotillus, which is posterior to the striolar region, and the juxtrastriolar region have a greater hair cell density (Figure 1.3 *C* and *F*) (Bang et al., 2001).

In the **lagena,** different hair cell morphologies can be found. The central lagena features hair cells with tall and thick bundles, with a kinocilium matching bundle

height. In the periphery, the hair bundles are much shorter and the kinocilium is at least twice as long (Figure 1.3 *A* and *D*) (Bang et al., 2001).

Figure 1.3 Structure of zebrafish maculae and hair cell density.

Confocal reconstructions of phalloidin-labeled whole-mount preparations of the lagena (*A*), the sacculus (*B*) and the utricle (*C*). Hair cell ciliary bundles are represented by dots in the corresponding lower panels (*D–F*). *C* and *F,* In the utricle, the striola (STR) is a band of relatively few hair cells characterized by large bundles. The cotillus (COT) is a large area located posteriorly. The juxtastriolar regions (JXT) run on both sides of the striola. The lacinia (LAC) is a thumb-shaped extension of the striola pointing towards the ampulla of the lateral semicircular canal. *Inset* in *B* and *E* illustrate the dramatic growth of sensory patches in juvenile fish 29 dpf. Scale bars 100 mm. Modified after Bang et al. 2001.

Similar to the vestibular system of mammals, all of the inner ear maculae show a segregation of hair cell polarity of some kind (Figure 1.4) (Platt, 1993), with hair cells orientating along a line of polarity reversal within the tissue as shown in Figure 1.4 (Platt, 1993).

Figure 1.4 Schematic drawing of polarity of hair cells within the maculae.

Sensory maculae show different polarities of hair cell populations. Arrows indicate the excitatory direction of hair bundles. Dashed lines delineate line of polarity reversal. U – utricle; cot – Cotillus; str - striola L- Lagena; S – Sacculus. Modified after Platt, 1993.

Development of the inner ear

The zebrafish inner ear stems from the otic placode, which comes from the preplacodal region (PPR) at the anterior border of the neural plate and is induced at 10 hpf and becomes visible at 16 hpf. At this stage it begins to form an elongated and hollow epithelial ball, termed the otic vesicle. In amniotes the otic vesicle is formed by invagination and in fish it is formed by cavitation (Abbas and Whitfield 2002).

The first pairs of hair cells are specified at the anterior and posterior portion of the otic vesicle at around 22 hpf. At the same time neuroblasts that will form the statoacoustic (VIIIth) ganglion, are emerging in the anterior ventral region of the otic vesicle. The otic vesicle gives rise to most of the cell types that make up the inner ear, including the afferent neurons of the VIIIth cranial ganglion, which innervates both vestibular and auditory hair cells. There is a population of precursors that makes both hair cells and neuroblasts at the posteromedial part of the zebrafish ear (Sapede et al., 2012). Once the neuroblasts are specified, they leave the otic vesicle and accumulate beneath the inner ear in a so called 'transit amplifying population' (Vemaraju et al., 2012).

The first maculae that arise from the otic placode are the utricle and sacculus at around 2 dpf (Haddon and Lewis, 1996) and the lagena develops much later, with hair cells appearing at 21-25 dpf (Bang et al., 2001). The saccular and lagenar maculae undergo morphological changes from larval and juvenile stages. The sacculus develops from a ball shape at 5 dpf to the characteristic spindle at 29 dpf (Haddon and Lewis, 1996). The lagena starts off as an oval patch at 21 dpf and becomes a pear-shape while the utricle maintains its rounded shape (Haddon and Lewis, 1996; Bang et al., 2001). During the first two weeks the number of hair cells grows dramatically, up to 15 per day (Bang et al., 2001). After one year, there seem to be no more hair cells added, but only replacement of the ones that are damaged (Higgs et al., 2002).

1.2 The hair cell is a mechanosensory transducer

1.2.1 General structure of a hair cell

Hair cells have a remarkably conserved structure both in different end-organs and between species from aquatic fish over to amphibians and mammals (Popper and Fay, 1997).

Hair cell have two distinct parts: The apical pole transduces external physical signals into a biological signal and the basal part, which shapes the electrical

activity and transmits this information into coordinated transmitter release onto the afferent fibre (Figure 1.5). Each part of the hair cell is specialised for its unique task and many of these features are conserved throughout the animal kingdom.

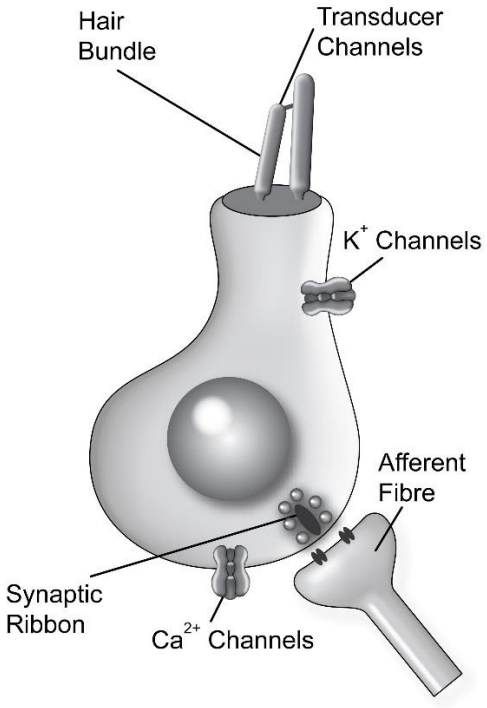

Figure 1.5 Schematic representation of the general structure and ion channels of a hair cell.

Schematic drawing of hair cell. The apical part contains the stereociliary bundle and the basolateral membrane contains ion channels (K^+-channels) and the synaptic machinery with the calcium channels and vesicles tethered to ribbons.

1.2.1.1 The apical pole performs transduction

The apical pole of hair cells contains the structure from which they get their name: the hair bundle. The hair bundle consists of tens to a few hundred stereocilia, which are modified microvilli. They are composed of actin filaments that are cross-linked by fimbrin and espin (Hackney et al., 1993). The stereocilia are rooted into the cell via the cuticular plate, which is an actin dense region. The thickness and length of each stereocilium varies between hair cell types, species

and location. For example, for hair cells sensing higher frequencies, the stereocilia are typically shorter and more numerous (Tilney and Saunders, 1983; Mulroy and Williams, 1987). Stereocilia are interconnected by lateral links (Flock et al., 1982). Most importantly, they are connected via tip-links that link the tip of the taller stereocilia to the shaft of the longer one (Pickles et al., 1984; Furness and Hackney, 1985; Kachar et al., 2000). Moreover, stereocilia are interconnected by cross-links, that are crucial as they orchestrate the whole bundle to move in unison upon stimulation (Hackney and Furness, 2013). Furthermore, it has been shown that Myosin VI is required for cuticular plate integrity in zebrafish and prevents the fusion of stereocilia, which is similar to findings in mice (Avraham et al., 1995, Self et al., 1999, Kappler et al., 2004, Seiler et al., 2004). Some hair cells express a kinocilium, which is either retained only during development, as in the mouse cochlea, or throughout life, as in zebrafish.

The mechanotransduction machinery is located in the hair bundle at the top of the cell. The hair cells mechanosensitivity is exceptional. It can detect displacements at the atomic scale (about 0.2 nm) and it is able to encode frequencies exceeding 1000 Hz by several fold. The ion-channel, that allows the mechanoelectrical transduction current (I_{Met}) to flow when the stereocilia are displaced, is unknown and the current candidates are members of the transmembrane-channel protein family (TMC1 and TMC2) (Fettiplace and Kim, 2014). However, the properties of I_{Met} are well characterised asa non-selective cation channel with fast activation and calcium-dependent adaptation (Fettiplace and Kim, 2014).

1.2.1.2 The basal pole shapes the receptor potential and releases transmitter

The basal part of hair cells contains ion channels that shape the receptor potential generated by the transducer current. The set and number of ion channels is largely dependent on the function and position of the cell and it differs between species. The synaptic machinery is located at the very base of the cell and in mammals is responsible for releasing neurotransmitter with sub-

millisecond temporal precision over a wide dynamic range (Matthews and Fuchs, 2010).

Hair cells contain a specialised presynaptic structure called the synaptic ribbon (Figure 1.5, base of cell). This ribbon is an ancient presynaptic structure that is already found in craniates (jawless fish) such as lamprey and hagfish (Holmberg, 1971; Khonsari et al., 2009). Synaptic ribbons are a speciality of sensory systems that use graded receptor potentials, e.g. auditory, vestibular and visual systems and they were first described in the 1950s (Sjostrand, 1953, 1958). Their function remains not fully understood, but they seem to be important to mediate continued exocytosis during fast and sustained stimulation (Dick et al., 2003; Heidelberger et al., 2005).

Ribbons are electron dense bodies located at the presynaptic side opposite the afferent fibre bouton and consist of the protein ribeye (Matthews and Fuchs, 2010). They tether between 20-400 vesicles (Moser et al., 2006) filled with glutamate and gather them over clusters of calcium channels (reviewed in Matthews and Fuchs, 2010; Moser et al. 2006). Each ribbon is contacted by on average one afferent bouton and the receptor on the bouton is the alphaamino-3-hydroxy-5-methyl-4-isoxazolepropionic acid (AMPA) receptor (Glowatzki and Fuchs, 2000).

The majority of calcium channels on the presynaptic side are of the L-type family, which have an unusually negative activation range, close to the V_m. In rodents and zebrafish the L-type channels ($Ca_v1.3$) present at the presynaptic zone are the main subtype (Brandt et al., 2003; Sidi et al., 2004) and they are involved in spontaneous afferent activity (Keen and Hudspeth, 2006; Li et al., 2009). Hair cells have a demand for continuous and rapidly modulated transmitter release near the V_m, which is ensured by the fact that $Ca_v1.3$ shows very little or no inactivation (*Amphibian*: Lewis and Hudspeth, 1983; Rodriguez-Contreras and Yamoah, 2001; *Mammal*: Beutner and Moser 2001, Marcotti et al. 2003; Johnson et al. 2005; Zampini et al. 2013).

1.2.2 Zebrafish lateral line hair cells

1.2.2.1 Mechanoelectrical transduction in lateral line hair cells

Zebrafish hair cells, as opposed to mammalian cochlear hair cells, contain in their stereociliary bundle a kinocilium present at mature stages. This kinocilium is involved in mechanosensitivity and important for the correct development of tip-link orientation at early stages (Kindt et al., 2012).

Similar to mammals, the mechanosensitive apparatus in fish also contains the tip link proteins protocadherin 12 (PCDH15) and cadherin 23 (CDH23) (Sakaguchi et al., 2009) and fish with null mutations show no mechanoelectrical transduction (Nicolson et al., 1998).

1.2.2.2 Basolateral membrane properties of lateral line hair cells

Up until recently, electrophysiological recordings from single zebrafish hair cells were not achievable. Therefore, a lot of knowledge stems from afferent neuron recordings that give indirect information of basolateral membrane currents. Using them, it was shown that the resting membrane potential of zebrafish hair cells is thought to be set by two distinct currents. These are the hyperpolarisation activated cation current I_h and the transducer current at rest I_{MET} (Trapani and Nicolson, 2011).

1.2.2.3 Synaptic transmission in lateral line hair cells

Similar to all other hair cells, the neurotransmitter present in the synaptic vesicles of zebrafish hair cells is glutamate and the main calcium channel is $Ca_V1.3$ (Sidi et al., 2004; Obholzer et al., 2008). The vesicles are loaded by the vesicular glutamate transporter, VGLUT3, which has been also found in hair cells of rodents and has been shown to be of great importance for proper vesicle filling in zebrafish lateral line neuromasts (Obholzer et al., 2008). The characteristic feature in zebrafish hair cells is also the ribbon body. Similar to frog and immature mouse inner hair cells (IHC) (Johnson et al., 2008) the ribbons in the zebrafish lateral line have a spherical shape. Each hair cell typically contains 3-5

ribbons, with double ribbons being rare (Sidi et al., 2004; Obholzer et al., 2008; Sheets et al., 2011).

In contrast to mammals, zebrafish have two ribeye genes, namely ribeye a and ribeye b (Wan et al., 2005). In knockdown experiments, both ribeye a and b are important for calcium channel clustering to the presynaptic side. The loss of ribeye a and b leads to severe disruption of evoked action potentials and both proteins have been associated with a role in synaptogenesis (Sheets et al., 2011).

1.2.3 Goldfish inner ear hair cells

Before the zebrafish became a popular model to study hair cells, the goldfish inner ear received a lot more attention. The sacculus has two distinct types of hair cells expressed in the rostral and caudal region. In the rostral region, hair cells are short and have ovoid or egg plant like shapes. Their resting membrane potential is – 75 mV and they show oscillatory behaviour to stimulation (damped oscillations). This resonance occurs at frequencies of 40 to 200 Hz, but resonance is of poor quality compared to that in the turtle cochlea or frog sacculus. The rostral region of the goldfish sacculus is sensitive to frequencies of up to 4000 Hz (Smith et al., 2011).

In the caudal region hair cells are longer and cylindrical and have an extraordinarily negative V_m (~ -100 mV). These cells show full spiking behaviour of about 50 mV in amplitude. The spikes are carried mainly by sodium and calcium and the cells have a small outward current, which is a delayed rectifier, I_{KD}. The caudal region of the goldfish sacculus is sensitive to lower frequencies down to 100 Hz (Smith et al., 2011). These two types of hair cells were also present in the lagena and utricle of the goldfish (Sento and Furukawa, 1987). They are not fully segregated in terms of location and they are mixed within the organ.

Furthermore, there are two types (S1 and S2) of afferent neurons contacting goldfish saccular hair cells. The S1 fibres contact rostral hair cells (oscillatory type, I_{KCa}) and have a large synapse. S1 do not show spontaneous spiking and

have a low sensitivity to sound, adapt quickly and show vigorous phase-locking to higher frequency sound.

S2 fibres make connections to the oscillatory and spike like (I_{KD}) hair cells. S2 do show spontaneous spiking, they are very sensitive to low frequency sound with slow adaptation. There are two further subtypes for the S2 fibres with one showing burst-like spontaneous firing and the other shows irregular spiking. The burst like may receive input from the spike type hair cells. The irregular spiking ones may receive input from the oscillatory hair cells in the rostral region.

1.2.4 Vestibular hair cells in mammals

Vestibular hair cells in the mammal translate information on head movement as well as head tilt and therefore fulfil the same roles as in the zebrafish. Vestibular input is crucial for motor reflexes, eye movement and head and body position. There are type I and type II hair cells in the vestibular organs of vertebrates.

1.2.4.1 Potassium currents of vestibular hair cells

In the 1950s, it was discovered that there are two types of vestibular hair cell, which are distinguished by their postsynaptic contacts. Type II hair cells receive rounded, bouton like contacts from the afferent fibres. This is the same kind of contact all auditory hair cells and vestibular hair cells in fish and amphibians receive (Figure 1.6). Type I hair cell synapses are different and they have a cupped ending or '*calyx*' shape (Figure 1.6). Even though fish and amphibians do show larger afferent endings, a fully hugging calyx is only found in amniotes. This late arrival of the calyx in evolution, suggests a distinct role for vestibular processing in amniotes.

The basolateral membrane properties, especially the set of potassium channels expressed, are the most striking difference between type II and type I hair cells as illustrated in Figure 1.6 (Eatock et al., 1998; Eatock and Songer, 2011). For type II hair cells, this set is dependent on the region of the cell, whereas for type I this is unknown.

In Type II hair cells, the outward K^+ channels show low open probability at the resting membrane potential. Potassium channels for outward currents include the rapidly activating and inactivating A-type current (I_A) and slowly inactivating delayed rectifier ($I_{K,DR}$) that activates positive to – 55mV. The A-type current varies in size between cells, but is always smaller than the delayed rectifier.

Type I hair cells also express two outwardly rectifying K^+ currents. The delayed rectifier ($I_{K,DR}$) activates positive to – 55mV but is much larger in size than one in type II hair cells. The other delayed rectifier, $I_{K,L}$, generates a large current with a very negative activation range (-90 to – 60 mV), slow activation and inactivation, and is calcium independent (Rüsch and Eatock, 1996). $I_{K,L}$ is also active at rest, making the input resistence very low (around 40 MΩ in type I hair cells). $I_{K,L}$ is carried by the KCNQ family of ion channels and may play a role in K^+ clearance from the extracellular space (Kharkovets et al., 2000). Type I hair cells have more negative resting potentials and smaller input resistances than their type II counterparts (Bao et al., 2003).

Both type II and I also express inward currents. I_h is an hyperpolarisation-activated current in type I and II hair cells (Holt and Eatock, 1995). Type II hair cells also express a fast I_{K1} that is active below – 40 mV (Masetto et al., 1994; Holt and Eatock, 1995; Sugihara and Furukawa, 1996; Rüsch et al., 1998).

Figure 1.6 Schematic of type I and type II hair cells in the mammalian utricle.

Type I and II hair cells in the utricular macula. Type I are mainly found in the striolar region, whereas type II hair cells are mainly found in the extrastriolar region. The afferent contact morphology varies between types, with the majority of cells receiving dimorphic contacts but some receiving either bouton (type II) or calyx (type I) only. Modified from Eatock and Songer 2011.

1.2.4.2 Synaptic transmission in vestibular hair cells

In most hair cells, the majority of the calcium current is carried by the L-type channel family member $Ca_v1.3$ (Brandt et al., 2003). In the vestibular system, the picture is more diverse. Other classes of calcium channels are L, N, P, Q, R and T. For example frog saccular hair cells seem to express the L- but also the N-type channels (Rodriguez-Contreras and Yamoah, 2001). In frog crista there is also the R-type additional to the L-type (Martini et al., 2000). Both mammalian type I and type II hair cells express the L-types (Almanza et al., 2003; Bao et al., 2003; Dou et al., 2004). However, since knockout mice for L-type calcium channels still show a large I_{Ca}, this suggests that different families are involved (Platzer et al., 2000; Dou et al., 2004). These different types of calcium channels are presumably associated with different functions, such as transmitter release or afferent fibre firing (Perin et al., 2000).

1.2.5 Hair cells of other lower vertebrates as an example for electrical tuning

Some hair cells are specially adapted to follow different frequencies. This frequency–filtering, also known as electrical tuning, occurs, for example, in the turtle and chicken, and is entirely intrinsic. Stimulation will drive the I_{Met} equally across a range of frequencies. The amplitude and shape of the receptor potential is modulated by different sets of voltage-gated ion channels that change along the length of the papilla and give it a tonotopic organisation. The turtle papilla contains about 1000 hair cells along 1 mm of sensing epithelium and senses frequencies of 30-600 Hz (Sneary, 1988; Hackney et al., 1993).

Electrical tuning (see Figure 1.7) is established by the interplay between calcium and potassium currents. When hair cells are stimulated continuously, in each cycle, the I_{Met} depolarises the cells, which opens voltage gated calcium channels, thereby increasing the intracellular calcium concentration. This in turn activates large-conductance K^+ (BK) channels which hyperpolarise the cell. During hyperpolarisation, the calcium channels close again and the BK-channel will be less activated due to a decrease in calcium.. This is the first cycle. Due to

continued stimulation via the I_{Met}, the membrane will depolarise again which initiates the next cycle (Fettiplace and Fuchs, 1999).

Figure 1.7 Electrical tuning in the turtle auditory cell.

Schematic drawing of two hair cells from the turtle basilar papilla, with resonant frequencies (Fo) of 75 and 300 Hz. The low-frequency cell has a longer hair bundle, and a lower density of calcium-activated K^+ ($I_{K,Ca}$) channels. The number of channel complexes increases with (Fo). The timing of the extrinsic current is shown above the voltage records. Modified from Fettiplace and Fuchs, 1999; Art and Fettiplace, 1987 and Art et al., 1995.

Membrane potential oscillations can be modified to adequately represent their best frequency by altering the BK channel density and kinetics, i.e. open and relaxation time (Art et al., 1995). The calcium sensitivity and conductance is unchanged between cells of different frequencies. The illustration in Figure 1.7

shows that hair cells with higher BK-channel densities can mediate higher frequencies sounds better. BK channels require a high calcium concentration in order to be activated, making a close association between the two channels necessary (Roberts et al., 1990; Wu et al., 1995).

1.3 Lateral line afferent neurons contacting hair cells

1.3.1 Organisation of lateral line afferent neurons

The cell bodies of the afferent neurons that contact the neuromasts, are gathered into a single ganglion (Alexandre and Ghysen, 1999). For the anterior lateral line, this ganglion is situated anterior to the ear and for the posterior lateral line, this ganglion is situated behind the ear (Alexandre and Ghysen, 1999). Neurons from both ganglia project to the hindbrain, but at different levels. They branch and send extensions into the anterior (for ALL) and posterior parts (for PLL) of the hindbrain (Alexandre and Ghysen, 1999).

The posterior lateral line ganglion (pllG) contains around 50 neurons at 5 dpf (Liao, 2010). At this time the lateral line consists of 8 primary and 2-3 secondary neuromasts and 1-2 dorsal neuromasts, this means that there are 4 times more neurons than hair cells (Liao, 2010). In turn each neuromast receives between 4 – 6 afferent contacts (Liao, 2010). The contacts on hair cells by afferent fibres are predominantly bouton-like (Nicolson, 2015).

The afferent fibres in the lateral line exclusively contact hair cells from the same polarity (Nagiel et al., 2008). They mainly branch once and contact hair cells in two different neuromasts (Ma and Raible, 2009). This suggests that each group of neuromasts (around 5-10 hair cells) receives contacts from around 8 neurons, indicating a high degree of convergence. Two sets of efferents project to the posterior lateral line organ and modulate its activity. Set 1 is cholinergic, originates in the hindbrain and is responsible for feedback or feed forward. Set 2 is dopaminergic, serves in excitatory modulation and comes from the forebrain (Ma and Raible, 2009). There are only two efferent, dopaminergic neurons, one for each side of the fish body. They branch several times and innervate all neuromasts (Nagiel et al., 2008; Faucherre et al., 2009).

1.3.2 The lateral line ganglion shows somatotopic organisation

The somatotopic organisation of the lateral line is represented within the ganglion (Alexandre and Ghysen, 1999). The afferents contacting the first primary neuromast enter the ganglion in the most anterior-dorsal region. The last primary neuromasts enter in the most posterior and ventral portion of the pllG (Alexandre and Ghysen, 1999). This somatotopic representation persists at the next level of integration. In the hindbrain, the most posterior or tail neuromast neurons project to the dorsal parts of the hindbrain whereas the anterior neuromasts of the lateral line project to more ventral parts (Alexandre and Ghysen, 1999; Ghysen and Dambly-Chaudiere, 2004).

1.3.3 Physiology of lateral line afferents

The lateral line afferents show two different cell types: one with large cell bodies and the other with smaller ones (Haehnel et al., 2012). These types presumably emerge at different time points of embryonic and larval development (Haehnel et al., 2012).

Large cells develop earlier than small ones, have a lower input resistance combined with a low spontaneous firing rate of < 15 Hz. These contact mainly multiple primary neuromasts and particularly the tail neuromasts (Haehnel et al., 2012). The smaller neurons emerge after the large ones and have higher input resistence paired with higher spontaneous rate of > 30 Hz. These tend to contact the dorsal neuromasts and the secondary lateral line (Haehnel et al., 2012).

Even though, details of this remain to be investigated, it seems likely that the two populations mediate different kinds of stimuli. Depending on the presynaptic side of the neuron, the small and high-spontaneous activity neurons could mediate phasic stimuli. On the contrary, the large and low-spontaneous activity neurons could be involved in transferring tonic stimuli.

1.4 Aims

The aim of this PhD was to investigate the biophysical properties of zebrafish hair cells both in the lateral line and the inner ear. Single cell electrophysiology was employed to study the conductances and the membrane behaviour of hair cells. This is important in order to use the full potential of the zebrafish as model to study hair cell function.

Aim 1: Establish the technical approach to access zebrafish hair cells

In order to perform electrophysiological experiments, the tissues that contain the hair cells had to be prepared and dissected in a physiological way. For the lateral line, this meant finding means to immobilise the fish and to access the hair cells.

For the inner ear, this meant establishing a physiological dissection for all macular tissues, leaving as much of the epithelium and cells intact and also accessing the hair cells.

Aim 2: Determine the ionic conductances present in zebrafish hair cells and how they affect the membrane behaviour.

Single cell electrophysiology was used to assess the potassium currents expressed on both lateral line and inner ear hair cells. It was also investigated, how they are reflected in the membrane behaviour and what their gain and speed properties are.

Aim 3: Investigate the development of the biophysical properties in zebrafish hair cells

In the mouse inner ear, hair cells undergo developmental changes until they are fully mature (Corns et al., 2014). The lateral line hair cells are assumed to be mature by 5 dpf (Ghysen and Dambly-Chaudiere, 2004), but the electrophysiological phenotype of the mature lateral line hair cell is unknown. Moreover, it is unknown, whether the lateral line hair cells develop beyond 5 dpf, which is the cut-off point for most researchers, because fish are protected

animals after this point and experiments are more regulated then (Straehle et al., 2012).

For the zebrafish inner ear, it is known that the number of hair cells increases during development (Bang et al., 2001; Higgs et al., 2002) and that hearing becomes more sensitive to sound at later stages (Lu and DeSmidt, 2013). However, it is not clear whether these morphological and functional changes with age are accompanied by changes in the biophysical properties of the hair cells.

Aim 4: Study details of the synaptic machinery of hair cells.

The main focus was on the lateral line hair cells, as they have been widely used to study hair cell synaptic transmission using imaging techniques. I have investigated their calcium current and transmitter release.

Aim 5: Establish an approach to study hair cell physiology in older fish.

Zebrafish are protected after 5.2 dpf, which is the point of independent feeding. After this point experiments with fish are regulated and must conform with the local animal and welfare regulations. Studying the biophysical properties of lateral line hair cells in older fish requires an approach that involves anaesthesia and maintenance of blood oxygenation in order to block nociception and keeping the fish alive.

Chapter 2 General Methods

2.1 Ethics statement

All zebrafish studies were licensed by the UK Home Office under the Animals (Scientific Procedures) Act 1986 and were approved by the University of Sheffield Ethical Review Committee. Every effort was made to minimise the number of animals used and their suffering.

2.2 Animals and animal husbandry

The predominant breed of animal used within this study was the zebrafish AB wildtype, which was chosen due to their success in breeding. These fish were acquired from the in-house aquarium facility at the University of Sheffield. At this facility the fish lived in a 14 hour light-10 hour dark cycle and were provided with food (Artemia) twice a day. For some experiments, myo6-rib-GFP transgenic fish from the laboratory of Dr. Katie Kindt were imported from Bethesda, USA.

For experiments using the lateral line, larval zebrafish were raised in Embryo medium (E3 Table 2.1). To stop fungal growth at larval stages, ~ 3 drops of the 0.5% methylene blue was added to the E3 medium.

Table 2.1 Composition of embryo medium.

	Final concentration (mM)
	Embryo medium E3
NaCl	4.9
KCl	0.174
$CaCl_2.2H_2O$	0.432
$MgSO_4.7H_2O$	0.332

Components and final concentration of the Embryo medium, in which fish were raised in until 5.2 dpf.

2.2.1 Zebrafish husbandry <5.2 dpf

Fertilised eggs were collected, washed in E3 and transferred to Petri dishes, which contained a maximum 50 eggs each. Unfertilised eggs were recognized by

their lack of epiboly at 5 hours post fertilisation (hpf) and discarded. Fertilised eggs were raised at 28.5 °C in the incubator (SLS, Hessle, UK) until 5.2 dpf and then destroyed in bleach. Larvae were checked on a daily basis and medium was changed.

2.2.2 Zebrafish husbandry >5.2 dpf

For experiments using >5.2 dpf zebrafish, fish were also initially raised in E3 medium and after 5.2 dpf transferred to the aquarium system. The aquarium water was taken from the main systems water and was free from ammonia and nitrite (<60 mg/L nitrate, conductivity of 300 mS, temperature of 28.5 °C and a pH of 7.5).

2.2.3 Euthanasia of zebrafish

Zebrafish older than 5.2 dpf were euthanized by an overdose of the anaesthetic tricaine methanesulfonate (MS-222). Solution for schedule 1 procedure on fish was prepared as follows: stock solutions of MS-222 was received ready-made from the aquarium facility in a 0.4 % solution dissolved in water and buffered with Tris buffer to pH 7. Fish were immersed in 100 ml of 0.017 % MS-222 and either decapitated using a scalpel upon sedation or after complete cessation of circulation (Schedule 1 method).

Other anaesthetics have also been used, including tri-bromo-ethanol (TBE, Sigma-Aldrich Co. Ltd, Gillingham, UK), which was prepared at 4 mg/L in water and benzocaine (Sigma-Aldrich Co. Ltd, Gillingham, UK) that was prepared at 20 g/L in 100% ethanol and kept in the fridge until used.

2.2.4 Tissue preparation

Hair cells from different stages of the lateral line and inner ear were investigated. This tissue preparation of both lateral line and inner ear hair cells is described in Chapter 3.

Paralysing larval fish by α - bungarotoxin injection

Larvae were paralysed by an injection of 125 μM α-bungarotoxin (α-Btx; Tocris Bioscience, Bristol, UK) into the heart (Trapani and Nicolson, 2010). α-Btx stock solution was prepared in water to 500 μM aliquots and frozen at – 20 °C. On the day of the experiment, 7.5 μl phenolred (0.5 % in DPBS, Sigma-Aldrich Co. Ltd, Gillingham, UK) was added to the 2.5 μl α-Btx stock (500 μM) which helped to visualize the injection site. Injection pipettes were pulled from borosillicate glass that had a filament inside (O.D. 1 mm; I.D. 0.5 mm, Harvard Apparatus Kent, UK) using a Narishige puller (Model PP-830; Narishige Japan) to a tip sizes of around 1-3 μm and back filled with the α-Btx. Injections into the heart were performed with an Eppendorf Femtojet injection system (Eppendorf Stevenage, UK). The filled injection pipette was advanced towards the heart of the fish which is superficial and close to the head, and was then pressed gently against the skin until it penetrated. A bolus injection of α-Btx resulted in a visible expansion of the heart cavity and the heart and circulation could be visualised by the phenolred dye.

2.3 Experimental solutions

2.3.1 FM1-43 labelling

Hair cells can be identified with a styryl dye called FM1-43 (N-(3-Triethylammoniumpropyl)-4-(4-(Dibutylamino) Styryl) Pyridinium Dibromide) (Molecular Probes), which is a permeant blocker of the mechanoelectrical transducer channel, i.e. it enters the cell through the MET channel (Gale et al., 2001). FM1-43 was prepared in water at a stock concentration of 3 mM. The entire larvae was briefly superfused with extracellular solution containing 6 μM FM1-43. Hair cells within each neuromast were viewed with an upright microscope equipped with epifluorescence optics and FITC filters (excitation 488 nm, emission 520 nm) using the optics described above. Images were captured using a CCD camera (Spot Jr;Toronto Surplus&Scientific, Inc., North York, ON, Canada). These experiments were performed at room temperature (20-24ºC).

2.3.2 Extracellular Solution

Hair cells of all tissues were continuously perfused by extracellular solution and depending on the experimental target, three different solutions were used (Table 2.2). For standard current and voltage clamp experiments, the normal extracellular solution was used. This solution contained the typical set of ions thought to be present in the native environment (Wangemann and Schacht, 1996) of murine hair cells and was similar to that used for zebrafish (Trapani et al., 2009). Note that the extracellular solution resembles that present around the basolateral membrane in murine hair cells. The apical part of mouse hair cells is bathed in the high K^+ and low Ca^{2+} solution that is required to establish the endocochlear potential. In the vestibular system and the frog lateral line, this potential difference is much smaller or even absent with 0- 10 mV (Russell and Sellick, 1976). Therefore, using the standard low K^+ extracellular solution described seems to be sufficient to study the basic properties of zebrafish lateral line hair cells.

At the moment, the details of the potential between the zebrafish cupula and hair cell are unknown and, if it is present, it could provide the cells with a bigger and faster inward MET current that would attenuate their voltage responses.

For experiments to investigate synaptic transmission, a high-calcium extracellular was used (Table 2.2), in order to emphasize the calcium current. For afferent fibre recordings, a slightly simpler solution was used (Table 2.2).

Table 2.2 Composition of extracellular solution for hair cell recordings.

Component	Final concentration (mM)	
	Normal extracellular	High calcium extracellular
NaCl	135	132.8
$CaCl_2$	1.3	2.8
KCl	5.8	5.8
$MgCl_2$	0.9	0.9
Hepes	10	10
Glucose	5.6	5.6
NaH_2PO_4	0.7	0.7
NaPyruvate	2	2

The pH was adjusted to 7.5 with NaOH. The osmolality was 308 mOsm/Kg. For the normal extracellular and high calcium solutions, MEM amino acids solution (50X, without L-Glutamine) and MEM vitamins solution (100X) were added from concentrates (Fisher Scientific, UK).

2.3.3 Intracellular solutions

The intracellular solution contained in the pipette was modified according to the type of experiment. For K^+ and V_m recordings a KCl-based solution was used (See Table 2.4).

Table 2.3 KCl-based intracellular solution.

Component	Final concentration (mM)
	KCl
KCl	131
Na_2Phosphocreatine	10
$MgCl_2$	3
EGTA-KOH	1
Na_2ATP	5
Hepes	5

Components and final concentrations of the potassium-based intracellular solutions. The pH was adjusted to 7.28 with KOH. The osmolality was 293 mOsm/Kg and the liquid junction potential was +4 mV.

Calcium current (I_{ca}) and induced changes in membrane capacitance (ΔC_m), which are normally used as an indication of synaptic transmission, in zebrafish hair cells was investigated using the intracellular solution described in Table 2.4. I_{ca} was isolated from the total membrane current by blocking the K^+ currents by adding 4-AP and TEA (Sigma-Aldrich Co. Ltd, Gillingham, UK) to the caesium-based intracellular solution (Table 2.4).

Table 2.4 Caesium-glutamic acid based intracellular solution.

Component	Final concentration (mM)
L-Glutamic Acid	85.0
CsCl	20.0
Na_2Phosphocreatine	10.0
4-AP	15.0
TEACl	20.0
$MgCl_2$	3.0
EGTA-CsOH	1.0
Na_2ATP	5.0
Hepes	5.0
GTP	0.3

Components and final concentrations of the caesium-based intracellular solutions. The pH was adjusted to 7.28 with CsCl (Sigma-Aldrich Co. Ltd, Gillingham, UK). The osmolality was 293 mOsm/Kg and the liquid junction potential was + 9 mV.

2.3.4 Solutions for extracellular superfusion

To investigate the identity of the different K^+ currents present in hair cells or the effects of anaesthetics on cell physiology, the various compounds were added to the standard extracellular solution. Generally, experiments that required the use of superfusion included recordings before, during and after the application of the compound to be tested.

In order to check the presence of the Ca^{2+}-activated K^+ current ($I_{K,Ca}$), a calcium-free extracellular solution containing 0.5 mM EGTA was used. To assess whether

the small conductance Ca^{2+}-activated K^+ current SK2 was present, 300 nM of the K^+ channel blocker apamin (Tocris Bioscience, Bristol, UK) was superfused. Apamin was kept in aliquots of 1 mM stock concentration.

Also a zero-calcium solution was perfused onto the cell, to assess whether any K^+ currents were calcium-dependent. The composition of this solution was as follows: 142 mM NaCl, 3.9 mM $MgCl_2$, 5.8 mM KCl, 10.0 mM Hepes, 5.6 mM glucose, 0.7 mM NaH_2PO_4, 0.5 mM NaEGTA. The pH was 7.48 and the osmolality was 306 mOsm.

The presence of the h-type current (I_h) was assessed by using 5 mM $BaCl_2$ (Sigma-Aldrich Co. Ltd, Gillingham, UK) in the extracellular solution (Sugihara and Furukawa, 1989). $BaCl_2$ was kept in a 10 mM stock solution.

Dihydrostreptomycin (DHS) (0.1 mM or 1mM; Sigma-Aldrich Co. Ltd, Gillingham, UK) was used to test whether the resting mechanoelectrical transducer current (Marcotti et al., 2005) contributes to the hair cell resting membrane potential (Johnson et al., 2012). DHS was kept in aliquots of 100 mM stock concentration.

MS-222 (0.01%) was also locally applied to hair cells to investigate its possible side-effects of the anaesthetic on hair cell membrane currents.

Solutions containing drugs were applied through a multi-barrelled pipette, which was gravity fed and positioned close to the preparation (Figure 2.1).

2.4 Electrophysiology

2.4.1 Glass microelectrode preparation

A Narishige PP-83 (Narishige international limited, London, UK) micropipette puller was used to pull glass capillaries with a resistence of 3-5 MΩ and tip diameter approximately 1-3 μm. Patch pipettes were made from soda glass capillary (inside diameter 0.94 mm, outside diameter 1.2 mm, Warner Instruments, USA). Capacitative properties of soda glass were reduced by applying surfboard wax to the pipette shaft (Mr. Zog's SexWax, Inc., Carpinteria, CA, USA).

2.4.2 Experimental set-up and drug application

Zebrafish hair cells from either from the lateral line or the inner ear were immobilised using a custom made recording chamber. The chamber was perfused with normal extracellular solution at a steady flow (~9 ml/min) using a peristaltic pump (Cole-Palmer, IL, USA), which was also sucking solution out from the chamber that was subsequently discarded. The solution was kept at room temperature and for some experiments, the solution in the chamber was heated using a peltier-element built in the stage. The ambient temperature was measured with a thermometer. Once the chamber was fixed onto the stage of an upright microscope, (Olympus BX51WI, Olympus, Japan), several other elements were positioned before commencing the experiments. For experiments performed at the zebrafish holding temperature (28.5°C), a thermocouple was positioned into the chamber using a micromanipulator. A home-designed multibarreled pipette connected to 10 ml syringes via silicon tubes was also positioned into the chamber, which allowed solutions containing the different compounds to be perfused by gravity (Figure 2.1) The recording pipette filled with intracellular solution was connected to an electrode holder that had a side port to allow the application of positive and negative pressure to the electrode tip. The recording pipette holder was attached to the headstage of the patch clamp amplifier. A short glass pipette filled with extracellular solution was placed in the recording chamber to act as a reference electrode. Both the recording electrode and the reference electrode were connected to the headstage as detailed in Figure 2.1. A micromanipulator (PatchStar, Scientifica, UK) was used to hold the headstage to allow the course and fine control of the microelectrode as it was positioned in the recording chamber.

Signals from the recording electrode were pre-amplified by the headstage, filtered by a Bessel low pass filter set at 2-5 kHz, passed through the Optopatch amplifier (Cairn Research Ltd, Faversham, UK). The signal was then converted from an analogue to a digital signal by the Digidata 1322A (Molecular Devices, LLC, Sunnyvale, CA, USA) before being captured by the Clampex 9.2 or 10.3 software (Molecular Devices). Recordings were sampled at 5 kHz or 100 kHz, low

pass filtered at 2.5 kHz or 10 kHz (8-pole Bessel) and stored on computer for offline analysis.

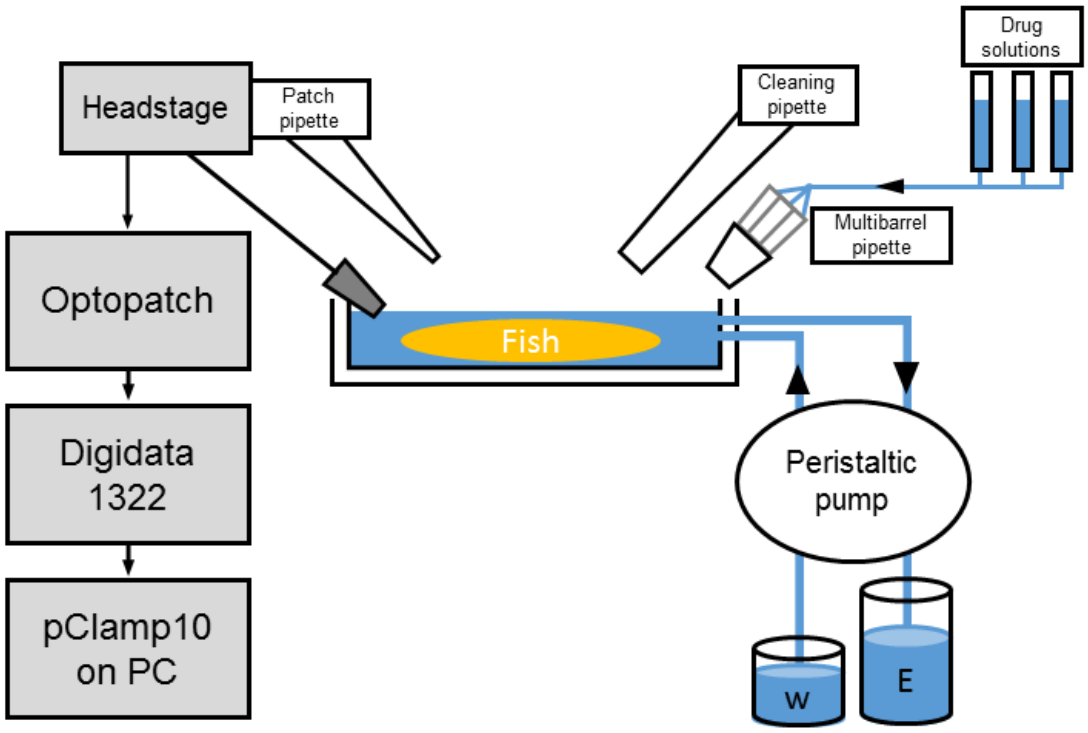

Figure 2.1 Schematic of experimental set-up.

Cartoon showing the main pieces of electrical (grey boxes) and other equipment (not to scale).

2.4.3 Electrophysiological recordings in hair cells

Electrical properties of hair cells from both the lateral line and inner ear of zebrafish (n = 248) were investigated using the whole-cell patch clamp technique (Hamill et al., 1981).

Electrophysiological recordings in current and voltage clamp mode were performed to investigate the basolateral membrane properties of hair cells. Voltage clamp were used to assess the current profiles of hair cells, whereas current clamp to study the functional implications of the basolateral current

profile, which included the resting membrane potential and assess the change in membrane potential in response to current injections.

Whole-cell patch clamp recordings were primarily performed at room temperature (21–24°C). Calcium current recordings, measurements of exocytosis and some of the voltage responses were conducted at the temperature at which zebrafish are kept (28.5°C).

Membrane potentials in voltage clamp were corrected for the voltage drop across the uncompensated residual series resistance (Rs: 3.4 ± 0.1 MΩ, n = 248) and for a liquid junction potential, measured between electrode and bath solutions, of −4mV for the KCl intracellular solution and −9 mV for Cs-glutamate. Current responses are referred to a holding potential of −84 mV or −79 mV unless specified, and are set to 0-current for comparison between individual hair cells.

Whole-cell patch clamp recordings

An upright Olympus microscope with differential interference contrast (DIC) and an objective with x60 magnification was used to view the neuromast and viable hair cells. Hair cells were easily identified by their location along the horizontal axis, size and characteristic shape (Chapter 3). During the patch process, additional magnification of x1.5 or x2 before the x15 eyepieces (all from Olympus) was used to visualise details of the cell membrane.

At the beginning of the experiments, a +10 mV command voltage was applied to the recording patch pipette using the pClamp software, which was used to assess the pipette resistence, seal formation and generation of whole cell configuration. Positive pressure was applied through the electrode after lowering it into the recording chamber solution. The resistence of the pipette was confirmed on the oscilloscope. At this point, fast capacitive transients caused by the build-up of charge on the patch-pipette during a +10mV test pulse, were cancelled out using the fast capacitance cancelling circuitry of the Optopatch amplifier.

In voltage clamp mode the pipette offset was compensated using the amplifier's offset dial. The tip of the electrode was brought into the centre of the field of view

and lowered close to the neuromast using the course control of the manipulator. Then, using the fine control it was advanced to the target hair cell until the positive pressure caused a dimple to appear in the cell membrane. The positive pressure was released and the seal formation was observed by monitoring the current response changing to zero. A seal was considered to be good with resistances of ≥ 3 GΩ. During the sealing process the holding potential was decreased to a nominal value of –80 mV by an external calibrator. The holding potential was set using an external calibrator that applied a known dc voltage shift to the cell. The whole-cell configuration was achieved by a little suction and could be confirmed by the current response getting larger and by the appearance of slow membrane transients in response to the + 10 mV test voltage step. For lateral line hair cells, the cell resistance was usually in the order of one GΩ, so that a successful whole-cell configuration could sometimes be linked to the appearance of capacitative transients only due to the hair cell membrane properties. These transients were measured using the slow capacitance cancelling circuitry of the Optopatch amplifier. Measuring the slow capacitive transients allowed measurement of the capacitance of the cells membrane surface area. The series resistance was measured with the series-resistence dial of the patch-clamp configuration, important for calculating the voltage drop of the command voltage applied to the cell. For cells with a large capacitance a compensatory circuit (RS-comp) was enabled that directly altered the membrane time constant to overcome the filter properties of cells. This was rarely used in zebrafish hair cells, which are small and have a small time constant and therefore high cut off frequencies. Then the + 10 mV test-voltage step was switched off and the desired protocol was run.

Voltage Clamp

The procedure described above was already in voltage clamp, so current recordings were performed straight away using the protocols described in the results in Chapters 4 to 6.

Current Clamp

For current clamp experiments, after reaching the whole-cell configuration, the amplifier was switched from big-cell (configuration under whole-cell) to small cell mode. Simultaneously, the amplifier was switched from voltage clamp mode to I-0 (no current injection) to current clamp mode. At this point, any compensatory current injections would be reduced or disabled by the amplifier to ensure that the cell is not overstimulated. Since the holding potential was set using an external calibrator, under current clamp conditions the calibrator was used to zero the voltage trace. This gave an indication of the hair cell's resting membrane potential. The calibrator had no direct effect on the cell's voltage responses in current clamp mode.

Capacitance recordings

Measurements of exocytosis are indirectly done by measuring changes in cell capacitance. This reflects the surface area of cells and when enough vesicles fuse with the membrane, this can be detected by a change in capacitance (ΔCm).

Capacitance measurement are carried out in "track-in" mode of the Optopatch amplifier (Johnson et al., 2002). The 'track in' technique is an extension on the 'lock in' technique that is used for piece-wise-linear capacitance measurements and utilises phase-sensitive lock-in amplifier to measure the passive properties of cell membranes (Lindau and Neher, 1988). The piece-wise-linear technique is popular for cells with large capacitance changes. However, hair cells are expected to have smaller changes, therefore 'track in' was developed (Johnson et al., 2002).

Capacitance measurements start in voltage clamp mode in the whole cell configuration. After switching off the + 10 mV voltage step used during the establishment of the whole-cell configuration, the amplifier switched to track-in mode. A 2.5 – 4 kHz sine wave command potential was applied to the voltage clamped hair cell from the holding potential of -81 mV. The amplitude of the sine wave was 13 mV RMS (37 mV peak-to-peak). The command sine wave was interrupted for the duration of the voltage steps. This allowed recording of the inward I_{Ca} that triggered the ΔCm.

Membrane capacitance and series resistance signals were amplified by the Optopatch (×50 and ×5, respectively). They were sampled at 5 kHz, filtered at 150 Hz (two-pole bessel) with additional 8-pole Bessel filtering at 250 Hz.

2.5 Data acquisition and analysis

Offline analysis was carried out using Clampfit software (Molecular Devices) to quantify holding currents, peak currents and leak conductances. OriginPro software (Origin lab, USA) was used to calculate the actual command voltages by correcting them for the voltage drop across the uncompensated series resistance. This was done using Ohm's law $V = R \times I$, where V is the voltage, R is the resistence and I is the current. Steady state currents were measured in OriginPro. Average results are presented as mean ±S.E.M.

Changes in membrane capacitance (ΔCm) were calculated by subtracting the mean capacitance calculated over a 100-200 ms period after the voltage step from the mean prepulse capacitance.

Calculation of calcium channel number

The number of calcium channels can be calculated with the following equation:

$$N = \frac{I_{Ca}}{iP_O}$$

Equation 1 Calculating the total number of calcium channels.

N – total number of channels, I_{Ca} – size of calcium current at peak [I_{Ca} = -11pA at peak], i – single channels conductance [i=−0.34 pA], P_o – channel open probability [Po = 0.21 pA](Zampini et al., 2013).

Statistics

Statistical comparisons were made using the two-tailed Student's *t* test or, for multiple comparisons, one-way ANOVA followed by a Bonferroni *post hoc* test.

Values are mean ± S.E.M. A *P*-value of < 0.05 indicates statistical significance. In some of the figures statistical significance is indicated by asterisks.

Chapter 3 Establishing Methods for Hair Cell Recordings in Zebrafish

Introduction for lateral line and inner ear

The main aim of this project was to utilize the zebrafish as a model to study hair cell physiology *in vivo*. The most accurate read-out of single cell activity is patch-clamp electrophysiology. However, this technique has never been successfully applied to the hair cells of the zebrafish because of several technical limitations, including the ability to make a stable contact between the patch electrode and the very small surface area of these sensory cells. Therefore, the successful implementation of single cell electrophysiology in zebrafish required the development of a novel experimental approach able to provide a controlled, repeatable and physiological method to probe hair cell activity.

3.1 Methods for the zebrafish lateral line

3.1.1 Identifying the stage of zebrafish development

In order to investigate the functional development of the hair cells, I used zebrafish from larval to adult stages. Staging zebrafish larvae up to 5.2 dpf according to their age in hours is the most common and precise method (Kimmel et al., 1995). However, this staging method becomes unreliable for older fish (> 5.2 dpf) because their size and level of maturation seem to depend largely on the housing conditions, which normally vary quite substantially among zebrafish aquarium facilities. Therefore, zebrafish older than 5.2 dpf are normally staged according to their length in cm (Parichy et al., 2009). The average lengths of larvae and juvenile zebrafish in the Sheffield zebrafish facility are shown in Figure 3.1.

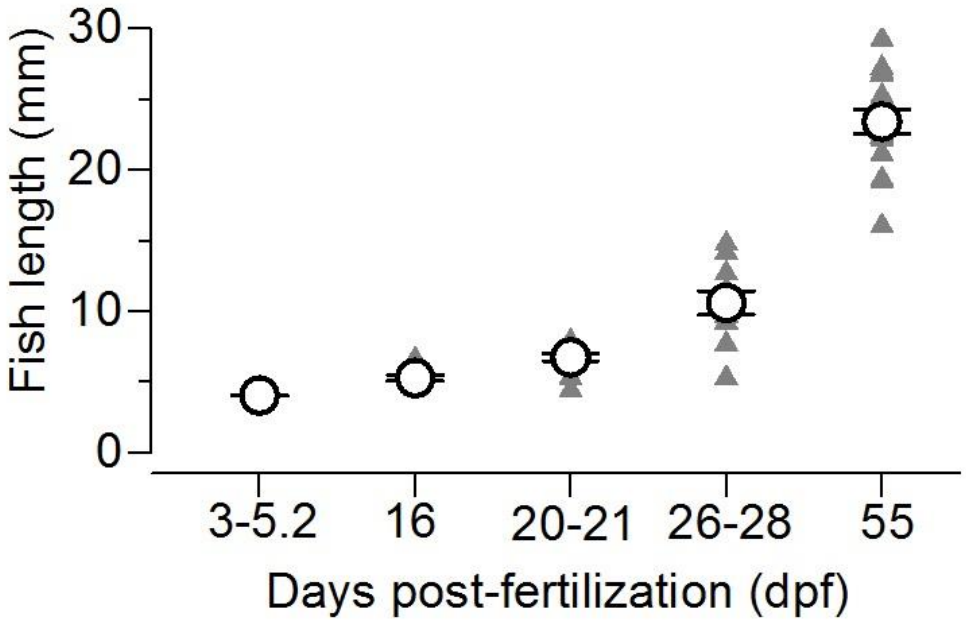

Figure 3.1 Zebrafish length development.

A, Growth of the zebrafish (*Danio rerio*) during the first 55 days post-fertilization (dpf) under the husbandry conditions used at the University of Sheffield. Numbers of zebrafish measured at each age were 44, 10, 14, 11 and 16, respectively (Olt et al., 2014).

Under the husbandry conditions in place at the University of Sheffield and using information from previous studies, where characteristic features of larval and adult stages are correlated to fish length (Kimmel et al., 1995; Parichy et al., 2009), the stage of zebrafish development was classified as follows:

1) Larval stages: from 3 dpf to 2 weeks post fertilization (wpf)

2) Juvenile stages: from 2 wpf to the point at which zebrafish become sexually mature (3–6 months)

3) Adult stages: from 6 months onwards, when fish are sexually mature

3.1.2 Hair cell growth in the lateral line

While the fish is growing in size, the number of hair cells per neuromast in the lateral line increases (Pujol-Marti and Lopez-Schier, 2013). I have assessed the number of hair cells per neuromast at different stages and found that in larval fish, the newly formed neuromasts contain about 6 to 12 hair cells and this increases to about 20–30 cells by the juvenile stage (Figure 3.2).

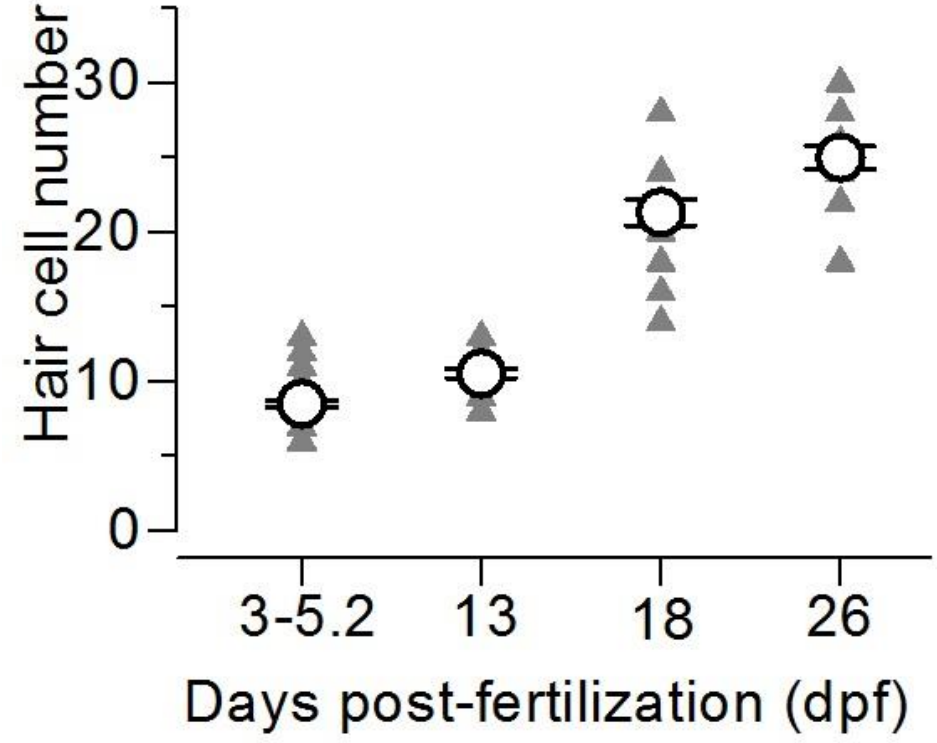

Figure 3.2 Developmental increase in zebrafish hair cell number.

Number of hair cells in each neuromast during the first 26 dpf of zebrafish development, which is within the age range at which electrophysiological recordings were obtained in the lateral line. Numbers of neuromasts investigated at each age were 66, 20, 24 and 20, respectively (Olt et al., 2014)

Each neuromast is normally composed of hair cells with different degrees of functional development. Newly differentiating cells are thought to be present towards the edges of the neuromast (Williams and Holder, 2000; Lopez-Schier

and Hudspeth, 2007; Kindt et al., 2012). The small numbers of hair cells in the neuromast of larval zebrafish, compared to juveniles, made the distinction between the central (older hair cells) and edge (new hair cells) regions very difficult (Figure 3.3), and was only possible to do in a few cases. However, the stage of maturation of a given hair cell is unlikely to be linked to the age in dpf of the zebrafish (larval or juvenile) because new hair cells are being continually added within each neuromast throughout development and at adult stages for regeneration (Corwin and Oberholtzer, 1997; Lopez-Schier and Hudspeth, 2007; Kindt et al., 2012). Differences in the electrophysiological properties of hair cells in the edge and central regions within the neuromast were investigated and are described in Chapter 4 and Chapter 5.

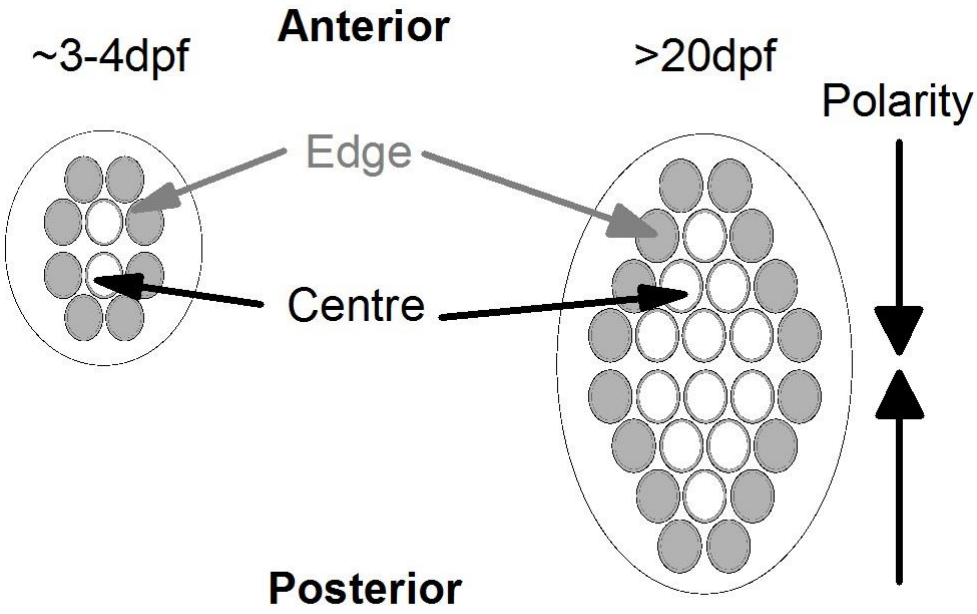

Figure 3.3 Morphological characteristics of the developing zebrafish lateral line.

Diagram of neuromast structure showing the increase in hair cell number according to the degree of differentiation, with new hair cells emerging at the edge (grey) and older hair cells being present in the centre (white). Note that each neuromast is believed to contain hair cells at different degrees of functional development (Williams and Holder, 2000; Lopez-Schier and Hudspeth, 2007). The polarity of hair cells is indicated with the black arrows (left).

3.1.3 Tissue preparation of the lateral line

3.1.3.1 Posterior lateral line preparation

In the lateral line, all recordings were performed from the primary neuromasts (L1–L4) originating from the first primordium (primI) (Pujol-Marti and Lopez-Schier, 2013). The primary neuromasts show planar polarity along the anterior-posterior axis. Each neuromast contains two compartments, with the anterior compartment being responsive to stimuli from the anterior-posterior direction and the posterior part responding to stimuli from the opposite direction, which is also shown in Figure 3.3 (right) (Nicolson et al., 1998; Lopez-Schier et al., 2004). Therefore, the fish was orientated perpendicular to the patch-pipette so that both polarities were accessible and could be studied.

The *in vivo* larval preparation

For *in vivo* hair cell recordings, larvae (3.0 dpf – 2 wpf) were briefly (10-30 seconds) anaesthetised in a petri dish containing 0.017 % MS-222 (Henry Schein, Inc., Dumfries, UK) in normal extracellular solution and then transferred to the recording chamber.

The recording chamber contained a microscope cover slide that was coated with ~ 0.5 mm of the silicone elastomer, Sylgard (Dow Corning, Seneffe, Belgium). Sylgard was ideal due to its relative optical clarity and elasticity and the cover slides were prepared in advance and only used for one experimental day.

Under a stereo microscope (MZ16, Leica Microsystems GmbH, Germany) zebrafish were pinned down onto the Sylgard using fine tungsten wire (0.015 mm diameter, Advent Research Materials Ltd, Oxford, UK) through a region between their heart, inner ear and mouth (anterior pin) and their notochord close to the anal exit (posterior pin) (Figure 3.4). This approach was modified after (Trapani and Nicolson, 2010).

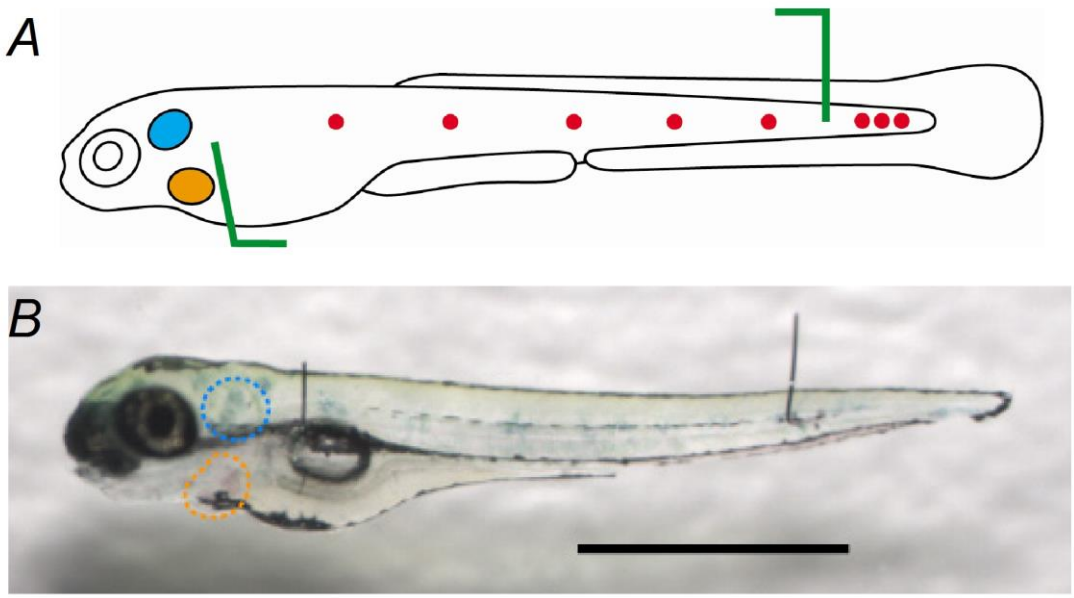

Figure 3.4 Schematic drawing and image of a pinned down zebrafish larvae.

A, Cartoon drawing showing the approximate locations of tungsten pins (green) used to pin the larva to a Sylgard-lined cover slide in the recording chamber. One pin is inserted close to the head, just posterior to the inner ear (blue circle) and above the heart (orange circle) and the second pin is inserted into the notochord toward the distal end of the tail. *B*, Image of 5 dpf zebrafish with pins in place and inner ear (blue dashed circle) and heart (orange dashed circle) indicated. Scale bar: 1 mm. Cartoon in *A* modified from Olt et al., (2014).

Larval zebrafish were subsequently paralysed by an injection of 125 µM α-bungarotoxin as described in Chapter 2. The recording chamber with the pinned and paralysed larvae was then moved to the electrophysiological set-up and placed on a stage that allows 360° rotation, which permitted recordings to be made from hair cells in any position of the neuromast. The recording chamber was connected to a peristaltic pump (Masterflex L/S, Cole Palmer, London, UK) and the solution in the chamber containing MS-222 from the pinning and injection process was washed off immediately with normal extracellular solution. At this stage, the zebrafish was only paralysed by the α-Btx.

The *in vitro* juvenile preparation

Injections of α-Btx could not be performed after 5.2 dpf as zebrafish become protected animals according to ASPA 1986. This means that experiments on > 5.2 dpf zebrafish had to be performed *in vitro/in situ*.

Therefore, juvenile zebrafish were anaesthetized with 0.017 % MS-222, decapitated with a scalpel and the digestive tract was carefully removed using fine forceps. The digestive tract had to be removed as it contains enzymes targeting proteins and fats, which would diffuse into the extracellular solution and damage the hair cells present on the surface of the fish. Zebrafish were then immediately washed from the anaesthetic with normal extracellular solution, transferred to a microscope chamber and immobilized onto a thin layer of Sylgard using fine tungsten wires with a diameter of 0.025 or 0.050 mm. Four pins were inserted into the fish, two in the tail fin and one in the dorsal and ventral fin (Figure 3.5). Occasionally, a pin was inserted through the neck for extra stability. The juvenile preparation was also continuously perfused with extracellular solution using the peristaltic. At juvenile stages, the primary neuromasts migrate slightly ventrally, which is shown in Figure 3.5.

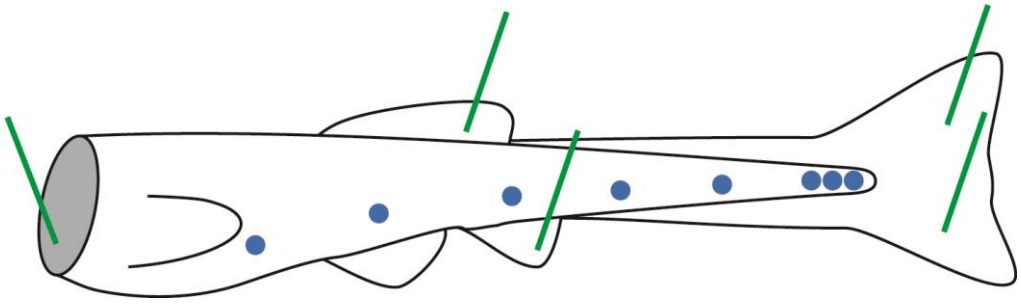

Figure 3.5 Schematic drawing and DIC of juvenile hair cells patch.

Cartoon drawing showing the approximate locations of tungsten pins (green) used to pin the decapitated juveniles to a Sylgard-lined cover slide in the recording chamber. One to two pins are inserted in the skin where the head was cut off, the other pins are inserted into the back, ventral and tail fin.

The juvenile preparation – *in vivo* intubation

Since the main aim of this study was to use the zebrafish as an *in vivo* model to study hair cell physiology, I had to develop an approach to perform *in vivo* experiments in older fish. This involved a search for an appropriate anaesthetic and will be described in depth in Chapter 5, Section 5.3.2.

The anaesthetic was prepared as described in Chapter 2 and added to the normal extracellular solution. Young zebrafish (5.2 – 21 dpf) are small enough to maintain their oxygenation through their skin, therefore bathing them in normal extracellular solution with anaesthetic was sufficient to keep blood oxygenation high. However, zebrafish older than 21 dpf are much larger and mainly use their gills for oxygenation. So for *in vivo* experiments I had to develop a way to maintain oxygenation via the gills. I considered several methods of doing this (Chapter 5, Section 5.3.2) and found that intubating the fish provided the most reliable results. After brief anaesthesia in MS-222, zebrafish were intubated with a thin (0.2-0.3 mm diameter) plastic tube that was inserted carefully ~ 3 mm into the mouth without damaging the gills (Figure 3.6). The intubation cannula was fed by a gravity driven system and the level of the anaesthetics container could be adjusted to regulate the flow. The flowrate of the solution through the tube and gills was ~ 1 ml/min which was within an accepted physiological level (communication with Veterinarian at the University of Sheffield). The zebrafish was bathed in normal extracellular solution, whereas the solution flowing through the intubation tube contained the anaesthetic. All juvenile fish where pinned down through their dorsal and ventral fins and two pins were inserted through their tail fin (Figure 3.6).

Figure 3.6 Intubation of juvenile zebrafish.

Image showing a 34 dpf old zebrafish that is intubated under anaesthesia using 50 mg/L Benzocaine and pinned to a Sylgard-lined cover slide in the recording chamber. Scale bar is 1 cm.

3.1.3.2 Identifying hair cells and the approach for patch clamping

Approaching lateral line hair cells for patch-clamp experiments was achieved in the same way for hair cell across all ages. Hair cells were visualized using a 60× water immersion objective with additional magnification of 1.5x or 2x and a 15x eyepieces (all from Olympus).

Neuromast structure

The neuromast is the functional unit in which hair cells are grouped together with a uniform structure along the fish body. The hair cells are defined by the stereociliary hair bundle, together with the kinocilium, that projects from their apical surface into the cupula (Chapter 1, Section 1.1.1). The basal pole of the cell is where the contacts with afferent neurons are located. Each kinocilium originates from a single hair cell and can therefore be used to count the hair cell numbers within the neuromast. In the example shown in Figure 3.7 *A* the neuromast contains 8 hair cells. The apical surface of the hair cells form the cuticular plate, which are joined together in neuromasts, giving a total circumference of ~8 μm that is surrounded by a ring of skin cells (Figure 3.7 *A*, symbol (+)). Further down inside the neuromast, the outlines of the tear-drop

shaped hair cells are recognizable in the most central part (Figure 3.7 *B*, symbol (*)), which are surrounded by mantle cells (Figure 3.7 *B*, symbol (-)) and supporting cells (Figure 3.7 *C*, symbol (~)). Below the neuromast the muscle fibres become apparent (Figure 3.7 *D*).

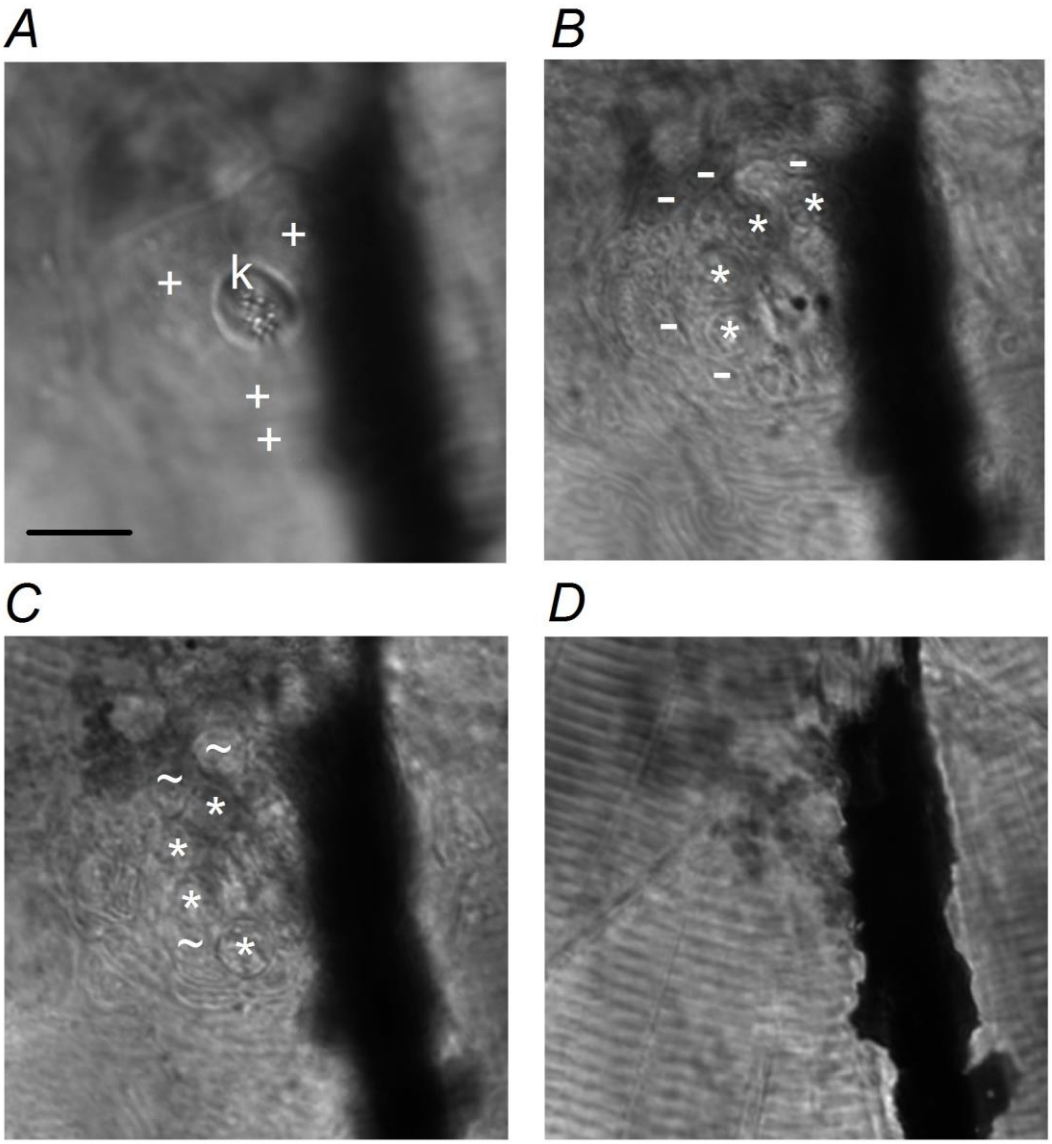

Figure 3.7 Structure of a neuromast.

A-*D*, DIC images through a neuromast from apical (*A*) to basal below the hair cells (*D*). *A*, The kinocilia (k) are visible at the top of the neuromast, rooted in the cuticular plate and surround by skin cells (+). *B*, Below the skin, the round hair cells are visible (*) which are surrounded mantle cells (-). *C*, Further inside the cell bodies of supporting cells (~) become apparent. Scalebar is 10 µm. Figure modified after Olt et al., 2016.

Hair cell approach for electrophysiological recordings

Accessing lateral line hair cells for patch-clamp experiments was performed in a series of steps which are depicted in Figure 3.8 showing DIC images at different levels of the neuromast, starting most apically where the kinocilia are visible.

In order to gain access to the lateral line hair cells, other cells surrounding the neuromast were removed using a "cleaning" glass pipette (Borosillicate, Harvard Apparatus, Cambridge, UK) with a tip diameter of ~3–4 μm. This pipette, which was connected to a syringe via a silicon tube, was filled with the same extracellular solution as that bathing the fish. The application of positive and negative pressure through the syringe allowed the selective removal of skin cells and debris in a similar manner that has been previously described to access cochlear hair cell (Marcotti et al., 2003a).

The procedure started with the removal of one or two large skin cells about 20-30 μm away from the neuromast (Figure 3.8 *A, B*), just outside the ring of skin cells surrounding the cuticular plate. The aim of this approach was to avoid damage to the cupula and the embedded hair bundles. The damage of these structures resulted in a very short kinocilia or the bundles lying flat on the surface of the fish. Following this, the cleaning pipette was used to suck out connective tissue surrounding the neuromast. When one side of the neuromast was partially exposed, some supporting and mantle cells were removed too (Figure 3.8 *C*). The last step was to get access to part of the hair cell membrane by removing the remaining debris with gentle suction or expulsion of solution from the pipette. Once a hair cells membrane was exposed, the patch-pipette was advanced towards it (Figure 3.8 *D*). Hair cells were approached perpendicularly to the length of the zebrafish, which allowed access to cells of opposing planar polarity within individual neuromasts and current and voltage responses were recorded from each polarity.

Positive pressure was applied through the patch-pipette to prevent any debris blocking the tip. A GΩ seal was generated between the patch pipette and the cell

by gently pushing the pipette tip against the basolateral membrane, which is visible by a dimple in the cell. The pressure was then released and seals readily formed in the order of 2-10 GΩ. The whole cell configuration was achieved by gentle negative pressure on the pipette, which ruptured the patch of membrane within the tip of the patch-pipette.

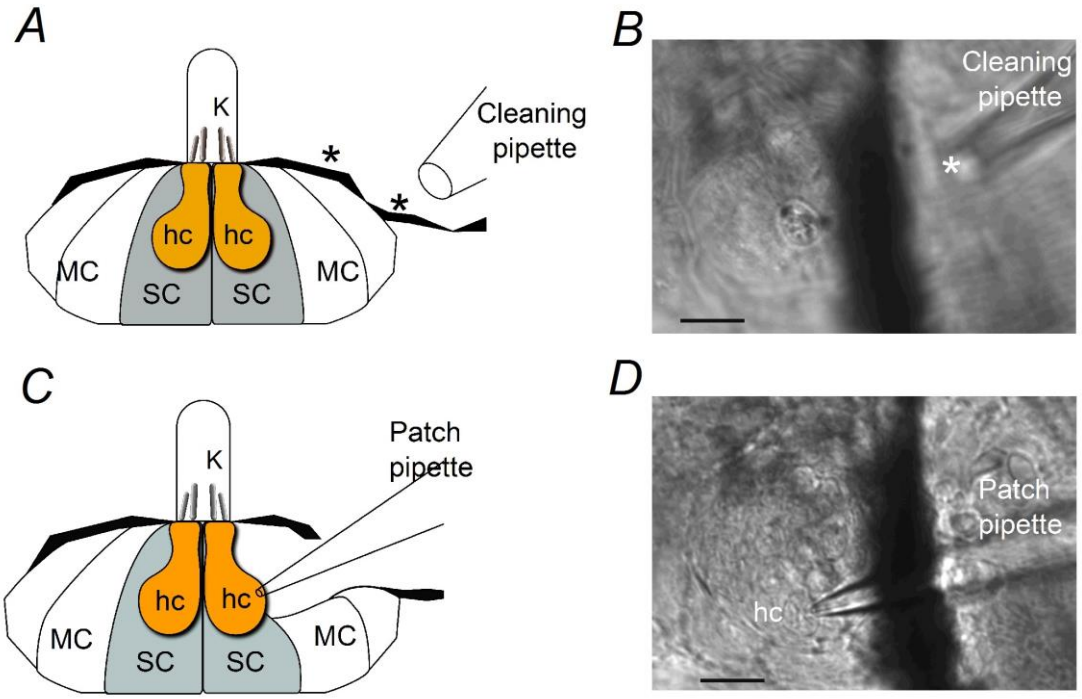

Figure 3.8 Morphological characteristics of the neuromast and hair-cell patching procedure in the larval lateral line.

A, Side view of a 3 dpf neuromast showing the hair cell kinocilia (K) projecting from its centre and surrounded by skin cells (asterisks). Mantle (MC) and supporting cells (SC) surround the hair cells (hc, orange). Note that the cleaning pipette approached the skin cells at about 20-30 µm from the hair cells, which is evident by the presence of the kinocilia seen in *B*. *B*, DIC top view of the neuromast with cleaning pipette (*) at the level of the cuticular plate and kinocilia, surrounded by skin cells. *C, D*, Diagram (*C*) and image (*D*) of the larval neuromast during the patching of a hair cell with a patch pipette. Scale bars in *B* and *D* are 10 µm. Figure modified after Olt et al., 2016.

Hair cells were identified visually by the hair bundle at the cell's apical surface. Electrophysiologically, hair cells were identified by their high input resistence, which was in the order of 1-3 GΩ, and voltage dependent current responses. Only cells of healthy appearance were used for electrophysiological recordings.

Healthy cells were defined as those with an intact hair bundle, cell membranes with a smooth surface, absence of vacuoles in the cytoplasm and lack of Brownian motion of mitochondria. Supporting cells were visually distinguished from hair cells based on their position within the neuromast, the absence of hair bundles and the deeper extension of their cell body into the neuromast. Electrophysiologically, supporting cells had a much lower input resistance (200-400 MΩ) and showed linear current responses as previously described in goldfish (Sugihara and Furukawa, 1989).

3.1.4 Methodological consideration

Pinning down the larval fish to immobilize them in the recording chamber was originally performed to study the zebrafish spinal cord and neuromuscular junction. An additional method, that is widely used to immobilize the zebrafish, is to embed them in low melting point agarose, the major advantage of which is to provide a more stable preparation than that using the pins. The agar-approach was performed during the initial stages of this project but I discovered that the agar needed to be removed to gain access to the hair cells and this damaged the hair bundles. Hence, fish were pinned down.

One of the issues I had to solve when using the pins was avoiding possible damage to the lateral line nerve. The neuromasts are innervated by several neurons that project along the horizontal midline above the notochord back to the posterior lateral line ganglion (pllG). Therefore the pin close to the head had to be inserted distal to the pllG and the inner ear to avoid damage of both the nerve and the pllG itself.

3.2 Methods for the zebrafish inner ear

Similar to the lateral line, hair cell recordings from zebrafish inner ear tissue required the development of a reliable dissection method and subsequent approach to the target hair cells.

3.2.1 Tissue preparation of the inner ear

3.2.1.1 Dissection of the zebrafish inner ear

Hair cell recordings were performed from the three otolithic organs (utricle, sacculus and lagena) of the adult zebrafish (> 1 year). In the lagena, I also investigated the juvenile stages (7–8 weeks) to provide an indication of possible developmental changes.

Zebrafish were culled by immersion in a solution containing 0.017% MS-222. Upon cessation of circulation, the fish were transferred into a petri dish containing normal extracellular solution and then decapitated using a fine scalpel. The head, which included the inner ear was then moved into a new petri dish with normal extracellular solution in order to remove any remaining blood or other unwanted tissue before commencing with the fine dissection of the inner ear (Figure 3.9). The gills were then removed using fine forceps. The bony skull was broken between the eye and gill as well as between the eye and top of the skull (Figure 3.9 *A* and *B*). Then, the head was broken in two halves and the brain was removed. At this point, the otolithic organs could be seen inside the skull (Figure 3.9 *C*). Depending on the organ of interest the next steps were adapted. The general approach is shown in Figure 3.9 *D*.

Dissection of the sacculus: the nerve fibres contacting the sacculus and lagena were cut. Because the sacculus and lagena are attached to one another, by holding the lagena and gently pulling it away from the skull, the sacculus was freed too. Then, the lagena was removed while making sure no damage was done to the sacculus. Finally, the bulla containing the saccullar macula was cut open from the anterior side and the otolith gently removed (Figure 3.9 *D*). Only the posterior part of the sacculus could be used for recordings.

Dissection of the lagena: The sacculus was held with the forceps and pulled out from the skull together with the lagena. The lagena was placed with the macular side (medial side of brain) facing upwards to avoid hair cell damage. Using very fine forceps, the membrane surrounding the otolith was cut open and the otolith was freed. On some occasions, additional nerve fibres below the sensory epithelium were removed in order to flatten the tissue.

Dissection of the utricle: The utricle contains the biggest and most anterior sensory epithelium. To dissect it, the nerve was cut distal to the tissue and the utricle was gently removed from the skull. This was followed by cutting some of the surrounding membrane in order to isolate the sensory epithelium. The sphere-like shape of the utricle was cut on one side to make the tissue sufficiently flat for the recordings.

The isolated sensory epithelium of the different inner ear organs was transferred to the microscope chamber and fixed using a nylon mesh attached to a stainless steel ring (Johnson et al., 2013). Care was taken to make sure that the mesh only touched the outer parts of the tissue in order to avoid any damage to the sensory hair cells and to allow access with the patch and cleaning pipette.

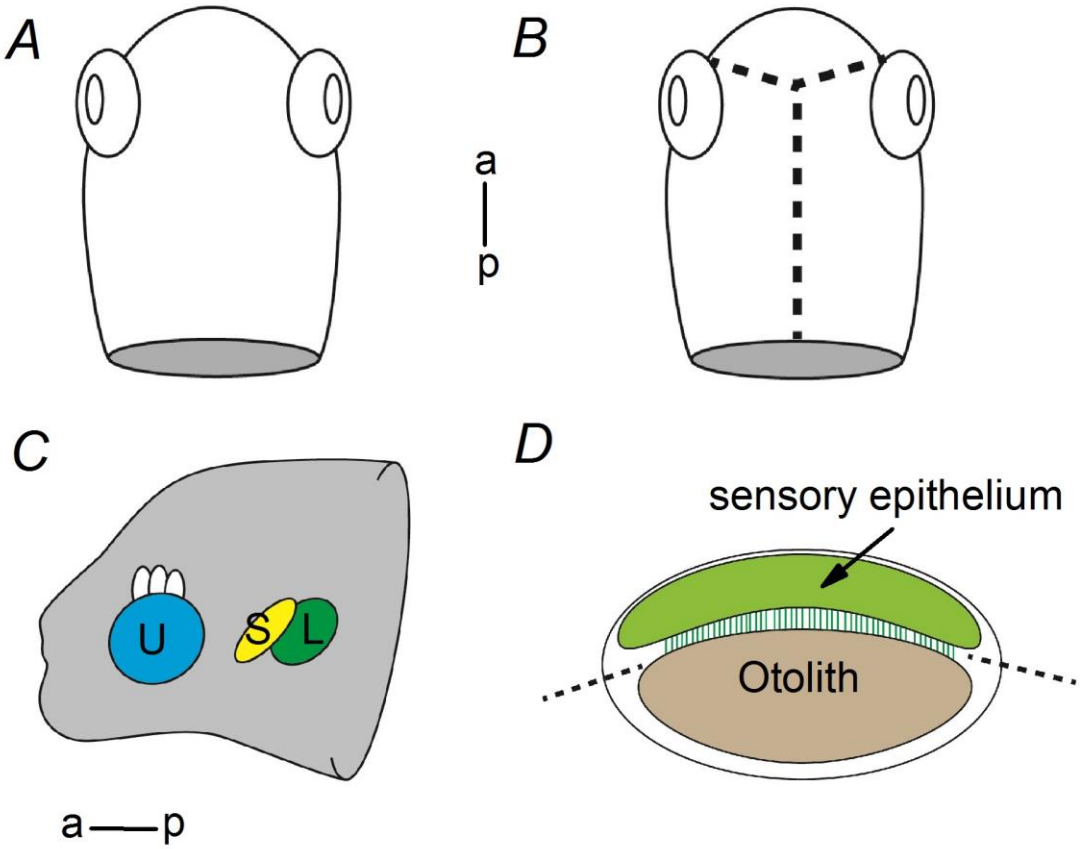

Figure 3.9 Schematic drawing of zebrafish inner ear dissection.

A, Top view of the decapitated head. *B*, The skull was cut in half and the most anterior part was removed (dashed line). *C*, Inside view of one half of the head. The three maculae are shown, utricle (blue), sacculus (yellow) and lagena (green), the semicircular canals are indicated in white. *D*, Crossection through a macula, top: otolith (brown) directly on top of the hair bundles (dark green) protruding from the sensory epithelium (light green). Note the drawing is not to scale.

3.2.1.2 Approach to inner ear hair cells

In order to successfully patch macular hair cells, their basolateral membranes needed to be "cleaned" to allow GΩ seal formation. This was done in a similar way described for the lateral line hair cells (see above) using the same cleaning-pipette set-up with a large diameter glass pipette (3–4 µm) filled with

extracellular solution and connected to a syringe allowing positive and negative pressure to be applied to the tip.

First, the cleaning pipette was used to remove a few hair cells and supporting cells in order to access the deepest part of the epithelium where the basolateral membrane of cells reside. Then, healthy looking hair cells were selected and their basolateral membrane was carefully cleaned using negative pressure. Great care was taken to minimise pressure on the hair cell membranes and especially on their stereociliary bundle. Once access to the hair cell basolateral membrane was obtained, the patch pipette was brought into position with a little positive pressure and it was pushed gently against the cell. GΩ seals with the hair cells where readily achieved upon releasing the positive pressure. Healthy hair cells were identified by their intact hair bundles, cell membranes with a smooth surface, absence of vacuoles in the cytoplasm and lack of Brownian motion of mitochondria, similar to the lateral line hair cells. This method has been used successfully to record hair cells of the mammalian cochlea (Marcotti et al., 2003a).

3.2.3 Methodological consideration

Successful electrophysiological recordings from zebrafish inner ear hair cells depended on the condition of the dissected tissue. Since hair cells are mechanosensory receptors, any mechanical stress must be avoided as this can damage the mechanoelectrical transduction apparatus and with it alter the V_m of cells, which will impact on the activity of ion channels. Also mechanical stress can lead to cell death. Intact hair bundles can be seen easily by the orientation and length of the stereocilia. Also the V_m of cells can be measured and used as a means to determine cell health. To avoid damage of the hair bundle, the epithelium could be turned upside down with the hair cells facing the top and the otolith the bottom. While the otolith was cut out with fine forceps, gravity would not push it onto the hair cells, which is the case *in vivo*. The continuous perfusion with fresh extracellular solution prolonged the lifetime of the preparation to 90 minutes. The use of enzymatic treatment is also to be avoided since it has been show to

provide a large variability in the voltage responses, which was not evident in our in situ recordings.

3.2.4 Summary

The reason to use zebrafish for this study, is that they provide the only tool at the moment that would enable direct *in vivo* investigations of hair cells. Therefore, the main aim is to establish an experimental protocol that leaves the whole fish as intact as possible.

Firstly, damage to the hair cell has to be avoided and intact hair cells can be distinguished by their shape and by the Brownian motion of intracellular particles. Crucially, the stereociliary bundle must not be damaged as the MET channel is a major contributor to the V_m. Damaged bundles can either be seen directly, when they splay, or indirectly via a very hyperpolarised V_m. The links between the stereocilia cannot be seen either, so possible damage cannot be assessed. Although great care was taken, damage to the hair cell and its bundle cannot be ruled out completely.

Crucially, the cupula, that provides a protective dome over the bundles, is not easily visible with the microscope used. It is likely, that the potential difference between the inside of the cupula and the hair cell is small, unlike in mammalian auditory hair cells. Therefore, the loss of the cupula may not significantly alter the K^+ ion concentration to which the cells are exposed (see above, Russell and Sellick, 1976).

Overall, the integrity of the mechanosensory apparatus cannot be assessed beyond doubt in the present preparation. This would be important for experiments involving direct stimulation of the bundle, which have not been carried out here.

Secondly, the hair cell itself should not be affected and its membrane was exposed gently. This cleaning process involves removing neighbouring mantle and supporting cells, which may have removed the cupula or the efferent neurons that contact the hair cell. Neither could be assessed. The efferent system mainly

functions in modulating the V_m to increase or to decrease sensitivity (Schofield, 2011). Changes in the V_m linked to the experimental approach cannot be ruled out, although they might be small.

In general, the cleaning process can compromise cell membrane integrity, making them leakier. This feature can however be directly seen and measured in the electrophysiological recordings. Moreover, the K^+ current recordings made under voltage clamp are unaffected by changes in the V_m, which was clamped to around – 80 mV.

Thirdly, larval fish were paralysed via bungarotoxin injection. Even though this blocks nAChRs, it might also bind to the mAChR and therefore block efferent feedback to hair cells. This would be important to rule out, if the feedback mechanisms of hair cells are investigated.

Overall, the presented experimental approach was designed to make a first description of the basolateral membrane properties of zebrafish hair cells in voltage clamp mode. In this way, the ion channel composition and properties can be assessed with great accuracy. This could usefully be applied to screen mutants and transgenic lines.

On the other side, a more physiological readout of these cells requires current clamp experiments, but these are largely influenced by the condition of the cell. In this case, our experimental approach may not be the most physiologically useful. Afferent neuron activity, microphonic potential recordings or calcium imaging may provide a better and less invasive approach (Trapani and Nicolson, 2010).

One very interesting aspect would be to study the MET channel in an *in vivo* setting using the fish. Several attempts have been made to do so, with little success. The orientation of the bundle is not visible, the bundle is very short, making stimulation difficult, and the recordings are generally not stable for more than a few minutes. On the few occasion recordings were made, the MET current was extremely small and the cells did not last for long enough. In any case the MET current in these delicate cells is likely to be small. Therefore, single cell

electrophysiology to study mechanoelectrical transduction in zebrafish hair cells may be of limited value.

Chapter 4 Biophysical Properties of Larval Zebrafish Lateral Line Hair Cells

4.1 Introduction

In the past two decades, zebrafish have emerged as a great genetic tool for studying hair cells *in vivo*. Several techniques have been used on normal and genetically modified zebrafish: mainly imaging (in fish with genetically encoded calcium indicators, GECI's), but also immunostaining and behavioural assays (vestibulo-ocular-reflex – VOR; Mo et al., 2010). Studies utilising these techniques have yielded a great deal of knowledge about the specification of hair cell progenitors and lateral line development as well as about genes involved in normal hair cell function (Nicolson, 2005).

However, to understand hair cell function *in vivo* it is crucial to know their electrical properties and, more importantly, how these cells detect sensory stimuli and transmit the encoded information onto the afferent fibre. In order to do this, two more specialised techniques had been developed and adapted: a) microphonics, which investigates mechanoelectrical transduction occurring at the cupula level using extracellular recordings and b) afferent fibre recordings, which elucidate details on the output of hair cells onto their neurons (Trapani and Nicolson, 2010). These two techniques have been used to describe action potential firing of the wildtype lateral line neurons and have been employed to study intracellular calcium signalling in the lateral line hair cells. Experiments using microphonics and afferent fibre recordings techniques can only provide an indirect indication of hair cell function. In order to understand the physiology at the single cell level, a more direct approach was required such as performing patch-clamp recordings.

The first aim of this part of the project was to establish a methodological approach to access and record from single hair cells from the intact larval zebrafish. Details on the methodology are given in Chapter 3. The second aim was to understand the *in vivo* physiology of these cells.

There is extensive knowledge on the properties and function of hair cells in both lower and higher vertebrates, both in the auditory and vestibular system. Bearing in mind that the lateral line functions as a low frequency sensing organ, with little

or no endocupular potential, I expect to find that zebrafish hair cells have properties that match those criteria. These cells might share great similarity with hair cells in the vestibular system of mammals or lower vertebrates. If lateral line hair cell roles extends beyond vestibular function, they will be expected to show features similar to the auditory cells of other lower vertebrates, such as the bullfrog, which would include electrical tuning.

Moreover, the larval fish responds to water vibrations with an escape response as early as 3 dpf. This suggests, that at least some of the hair cells are functional by this time, although it is unclear whether these are located in the inner ear or lateral line. Therefore, if lateral line hair cells are involved in the perception of vibrations, I expect all of them to exhibit one K^+ current phenotype.

Specifically, this part of the project is aimed at investigating whether larval zebrafish hair cells (3-5.2 dpf) have a functional mechanoelectrical transducer current, which ion channels shape their receptor potential and details on the synaptic transmission. Moreover, it will provide some details on whether the function of hair cells is affected by the use of the common anaesthetic MS-222.

4.2 Methods

For a detailed description of the Materials and Methods see Chapter 2 as well as Chapter 3 for specifics on how to record from lateral line hair cells.

Briefly, for lateral line experiments, only hair cells from the first primordium (see Figure 4.1) of 3-5.2 dpf zebrafish were investigated. The identification of the first primordium was made on the basis of the position of the primary neuromasts and their size. Zebrafish were immobilized to the bottom of the Sylgard coated recording chamber with tungsten wire pins inserted between the heart and ear (anterior) and after the anal exit (posterior).

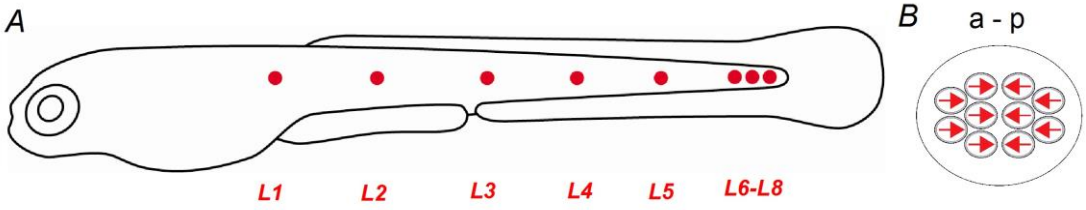

Figure 4.1 Schematic representation of the lateral line organisation at 5 dpf.

A, In red the primary lateral line consisting of 8 neuromasts including 3 terminal neuromasts (*L6-8*). *B*, Polarity of a single neuromast consisting of several hair cells: arrows indicate excitatory direction. The anterior portion is activated by stimuli from the anterior-posterior direction. The posterior portion is activated in the opposite direction.

The majority of recordings were performed with larvae injected with 125 µM α-Btx into the heart, which blocked transmission at the neuromuscular junction by binding competitively to the nicotinic acetylcholine receptor on the muscle fibre (Young et al., 2003). All recordings were performed at room temperature unless indicated otherwise for the specific experiment.

The anesthetic MS-222 was locally applied to hair cells in a concentration of 0.01 % to investigate its possible effects on membrane currents. Solutions containing drugs were applied through a multi-barrelled pipette positioned close to the preparation (Chapter 2).

4.3 Results

4.3.1 Current profiles and voltage responses of lateral line hair cells

4.3.1.1 Mechanoelectrical transduction in larval hair cells

Hair cell mechanoelectrical transduction occurs in response to movement of the stereociliary hair bundle that opens transducer channels located at the tips of the shorter stereocilia (Beurg et al., 2009). This process is extremely sensitive, detecting bundle movements of less than a nanometre, allowing the detection of sound and orientation with high sensitivity and precision. In the absence of

stimulation, when the hair bundle is in its resting position, the transducer channels are partially open (about 10%), which allows the constant influx of cations into the cells, causing their depolarization. This resting mechanotransducer current (I_{Met}) is therefore a crucial determinant of $V_{\mathbf{m}}$ (Johnson et al., 2011). The resting membrane potential of all hair cells at 3 – 5.2 dpf was -75.3 ± 0.9 mV (n = 12). To test whether the resting I_{Met} was present and functional in our *in vivo* recording conditions, two approaches were taken.

Firstly, FM1-43, a styryl dye that is a permeant blocker of the transducer channel (Gale et al., 2001) was perfused onto lateral line hair cells. FM1-43 selectively labelled unstimulated hair cells in the neuromasts (Figure 4.2 *A* bottom), confirming the presence of the resting transducer current, consistent with previous findings from mouse hair cells (Gale et al., 2001). Secondly, to evaluate the contribution of the resting I_{Met} to the cells V_m, current clamp experiments were performed (Figure 4.2 *Bi* and *C*). In control conditions hair cells had a resting membrane potential of – 59.6 ± 1.0 mV (n = 3), which was significantly (P < 0.05 and P < 0.01, respectively, one-way ANOVA) more depolarised compared to that measured when the permeant blocker of the transducer channel dihydrostreptomycin (DHS) was applied onto the hair bundles (67.00 ± 0.3 mV; n = 3; Figure 4.2 *Bii* and *C*). DHS is an effective blocker of the MET channel in mouse (Marcotti et al., 2005). The V_m returned to control values when DHS was washed out (-59.5 ± 0.4 mV, n = 3; Figure 4.2 *Biii* and *C*). This indicates that the fraction of transducer channels open at rest is directly contributing to cells V_m in larval zebrafish hair cells.

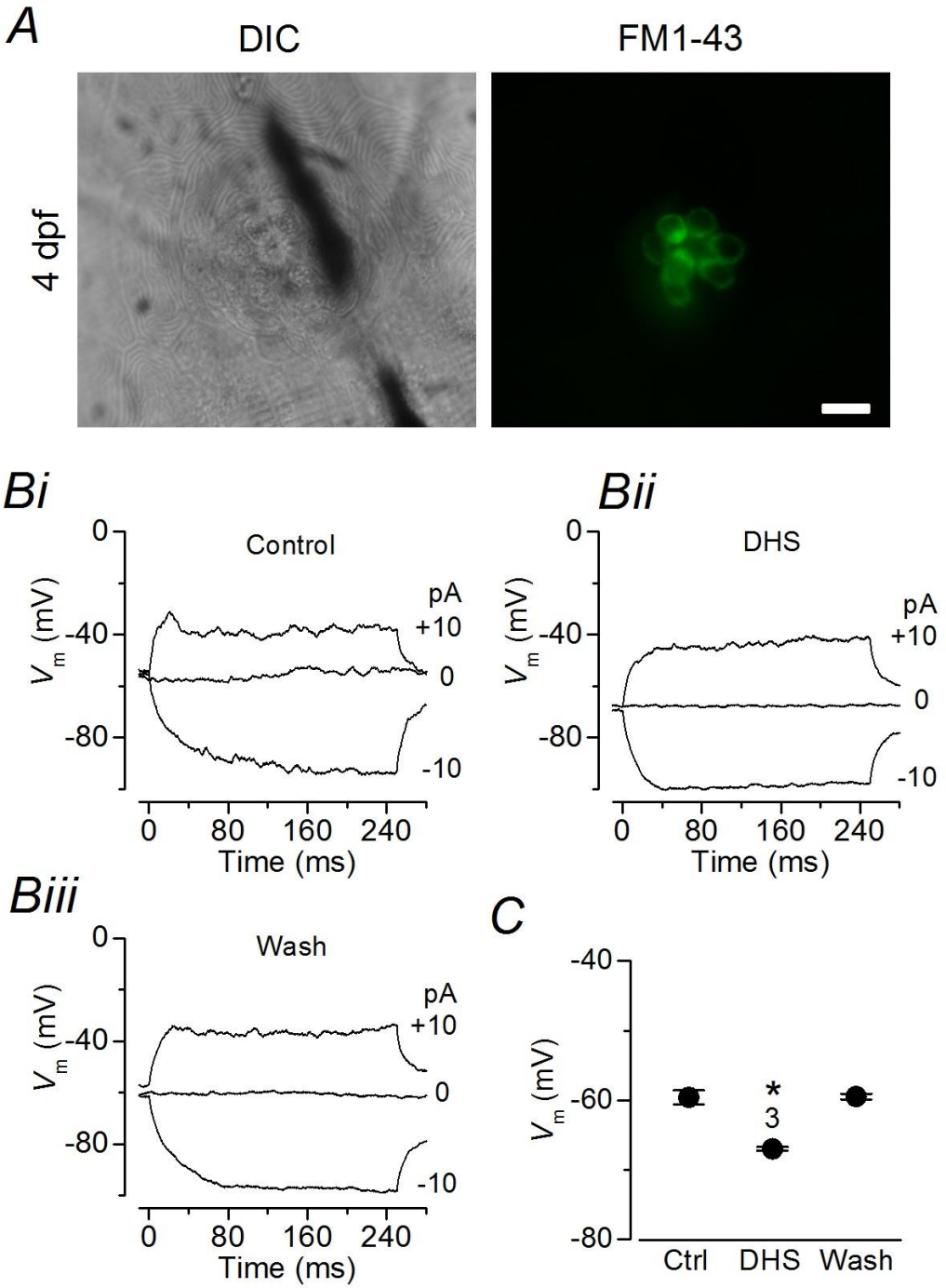

Figure 4.2 Resting mechanoelectrical transducer current in hair cells from larval zebrafish.

A, differential interference contrast (DIC) and fluorescence images from a 4 dpf larval neuromast (primI) showing that hair cells are labelled with FM1-43, indicating the presence of mechanotransducer channels open at rest, Scale bar: 10 μm. *Bi-iii*, voltage responses to current injections of –10, 0 and +10 pA from the V_m of the individual cell (3 dpf, neuromast L4), in control conditions and

exposed to 1 mM dihydrostreptomycin (DHS). Note that blocking the mechanotransducer channels with DHS hyperpolarizes the cell, which was completely reversible after washout of the drug. *C*, average V_m measured using the three different conditions described in *B* from three hair cells using 0.1 mM (two cells) or 1 mM DHS (cell in *B*). Note that recordings in *B* and *C* were performed at 28.5°C for a more physiological approach.

4.3.1.2 Pharmacological and electrical isolation of K^+ currents in zebrafish larvae

Membrane depolarization caused by I_{Met}, which is also known as receptor potential, modulates the neurotransmitter release at the cell's ribbon synapses. The time and voltage-dependence of the different ionic conductances in the basolateral membrane are crucial in shaping this receptor potential. These K^+ currents have been unknown in zebrafish hair cells and a detailed description and identification will be given below.

In order to characterise the different K^+ currents expressed in larval hair cells, voltage clamp experiments were performed. Hair cells were subjected to a series of depolarizing voltage steps from –120 mV to +70 mV in 10 mV nominal increments from the holding potential of -84 mV. The identity of the individual K^+ currents was evaluated using either voltage or pharmacological protocols.

One current type found was a rapidly activating and inactivating outward K^+ current termed I_A. This was identified using a voltage protocol as previously described (Norris et al., 1992). I_A is known to deactivate at potentials close to -40 mV. Therefore, hair cells were initially held at -84 mV and subjected to a voltage step to -14 mV (Figure 4.3 *Ai*). The protocol was then repeated in the same cells but from the holding potential of –54 mV (Figure 4.3 *Aii*). The isolated I_A was obtained by subtracting the current recorded at the holding potential of -54 mV from that obtained at -84 mV (Figure 4.3 *Aiii*).

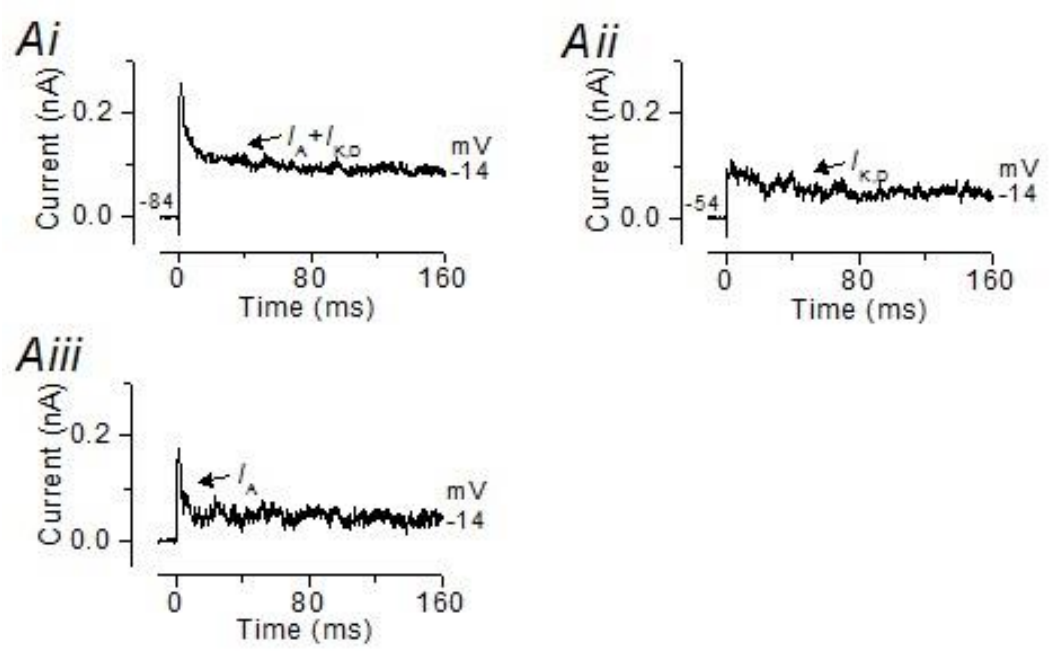

Figure 4.3 Isolation of A-type current in a lateral line hair cell.

Ai, Example of cell containing the A-type current. Currents were elicited by depolarizing steps as shown by the traces. *Aii*, Recordings from same cell but with holding potential of -54 mV, where I_A is nearly inactivated. *Aiii,* Isolated I_A obtained by subtracting the current in panel *Aii* from the control in panel *Ai*.

Another current type found was an outward Ca^{2+}-activated K^+ current ($I_{K,Ca}$), which was determined based on two main features: the characteristic N-shaped of the *I-V* curve and pharmacologically. The calcium-dependence of this outward current was assessed by perfusing the hair cells with a calcium-free extracellular solution. A typical recording from a hair cell before (Figure 4.4 *A*, black trace) and during the application of a calcium -free extracellular solution (Figure 4.4 ii*A*, blue trace). The isolated $I_{K,Ca}$, which was obtained by subtraction, is shown in the red trace of Figure 4.4 *Aii*. The *I-V* relation for the different recordings conditions described above are shown in Figure 4.4*B*.

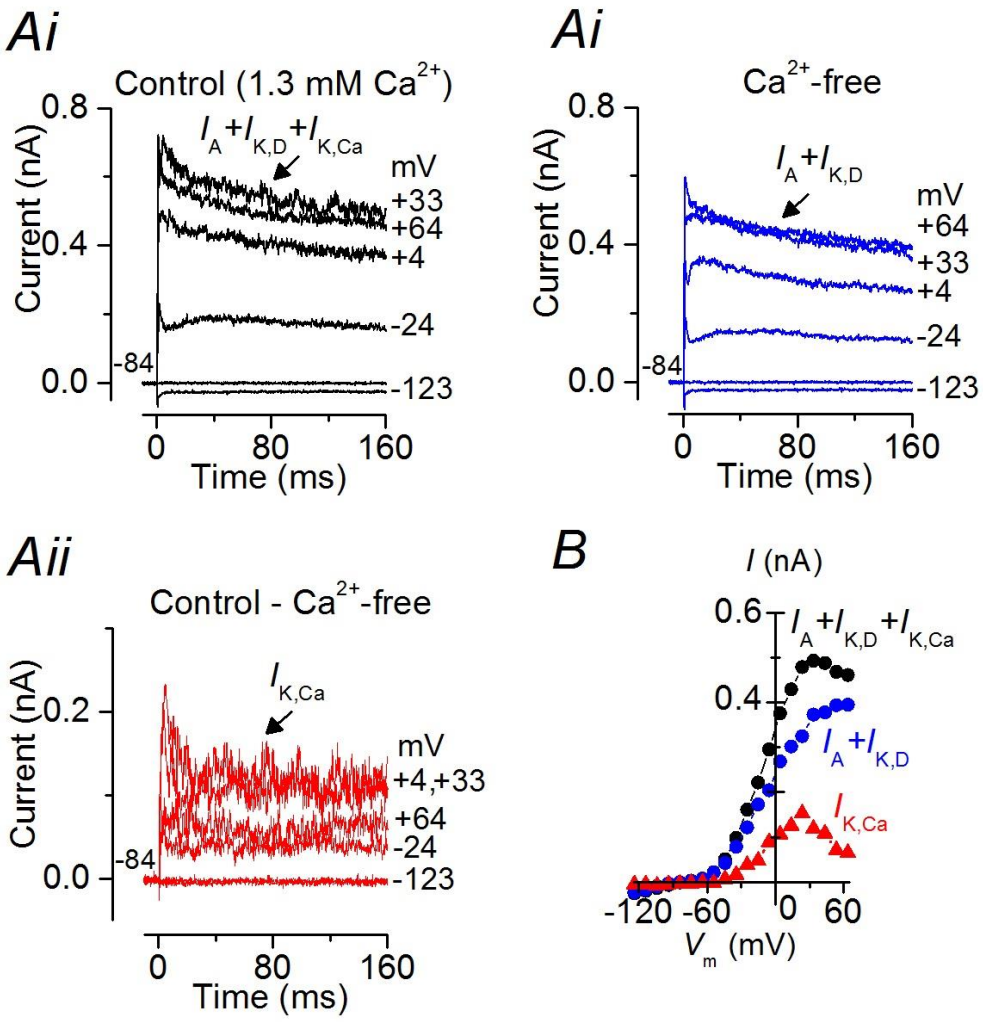

Figure 4.4 Isolation of the Ca^{2+}-activated K^+ current in a lateral line hair cell.

Ai, Example of cell containing $I_{K,Ca}$. Currents were elicited by depolarizing and hyperpolarizing voltage steps in 10 mV nominal increments from the holding potential of −84 mV to the various test potentials ranging from −124 to +64 mV. For clarity only a few test potentials are shown next to the traces. *Aii*, Blue trace: recordings from the same cell as in panel *Ai* but during the perfusion of a calcium-free extracellular solution. *Aii*, Red trace: isolated $I_{K,Ca}$ obtained by subtracting the current in panel *Ai* from the control in panel *Ai*. *B*, Steady-state (measured at 160 ms) *I-V* relationship for all three conditions shown in *Ai-Aiii*.

To identify whether $I_{K,Ca}$ was carried by small (SK) or large (BK) conductance K^+ channels, hair cells were perfused with the highly selective SK channel blocker

apamin. The current was insensitive to the perfusion of apamin confirming its identity as a BK current (Figure 4.5 *A-B*).

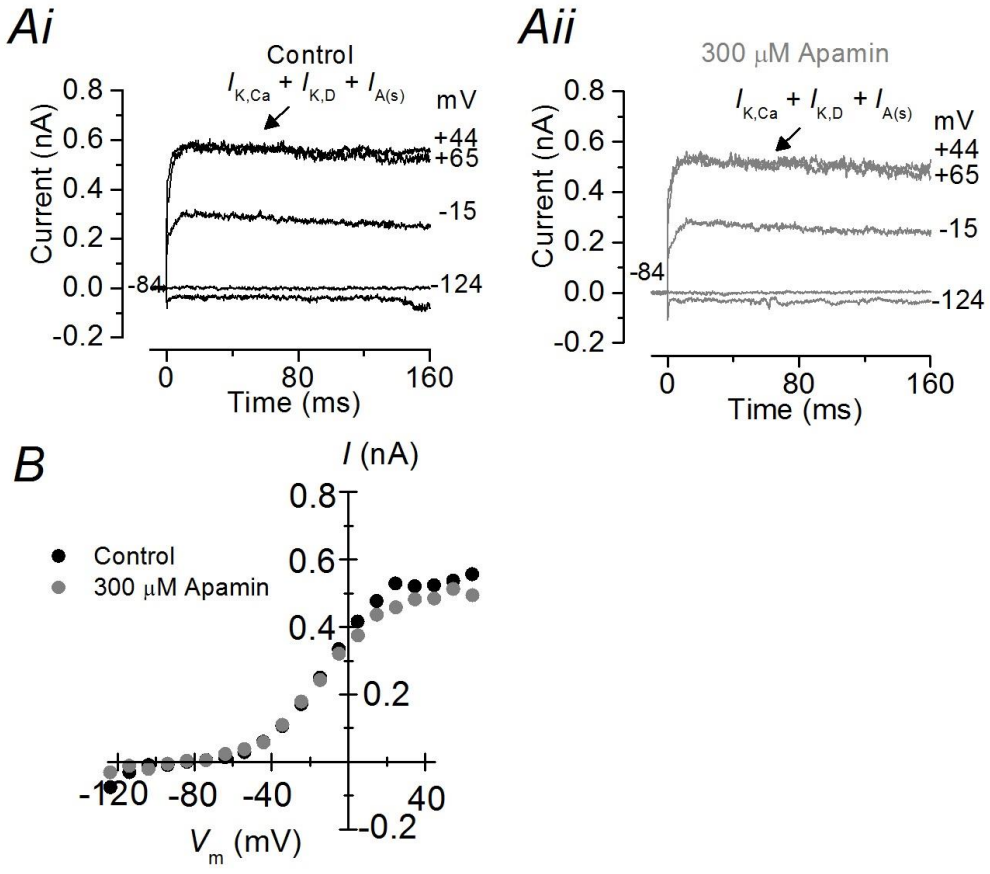

Figure 4.5 Identification of Ca^{2+}-activated K+ current in a lateral line hair cell.

Ai – ii, Example of K^+ currents recorded from a hair cell (3 dpf) before (A*i*) and during (A*ii*) the superfusion of 300 μM Apamin. Currents were elicited by depolarizing and hyperpolarizing voltage steps from the holding potential of −84 mV to the test potentials shown by some of the traces. *B*, Steady-state (measured at 160 ms) *I–V* curves obtained from the recordings shown in *Ai* and *Aii*.

Finally, a hyperpolarisation-activated K^+-Na^+ current termed I_h was found. This current is well characterised by its inward rectification, its negative activation range and very slow activation kinetics that creates a voltage sag in current clamp recordings in response to hyperpolarizing current injections (see Figure 4.8 below). The only other inward current that is found in zebrafish hair cells is the

large and fast $I_{K,1}$ in the zebrafish inner ear (see Chapter 6, Figure 6.2) or the goldfish sacculus (Sugihara and Furukawa, 1989).

Both inward current candidates can be distinguished pharmacologically. BaCl in concentrations > 1mM is a known blocker of $I_{K,1}$ (Marcotti et al., 1999) whereas I_h is known to be insensitive to its application. Figure 4.6 *A* shows that the inward current in lateral line hair cells was not affected by the perfusion of 5 mM BaCl, indicating the presence of I_h and not $I_{K,1}$. The *I-V* curves further highlight that the inward I_h is unaffected, but that the outward $I_{K,Ca}$ is blocked (Figure 4.6 *B*) when Ca^{2+} was replaced with Ba^{2+} in the extracellular solution (as also described in Figure 5 above). This indicates that the perfusion of BaCl was successful and the undetectable effect it has on I_h is real.

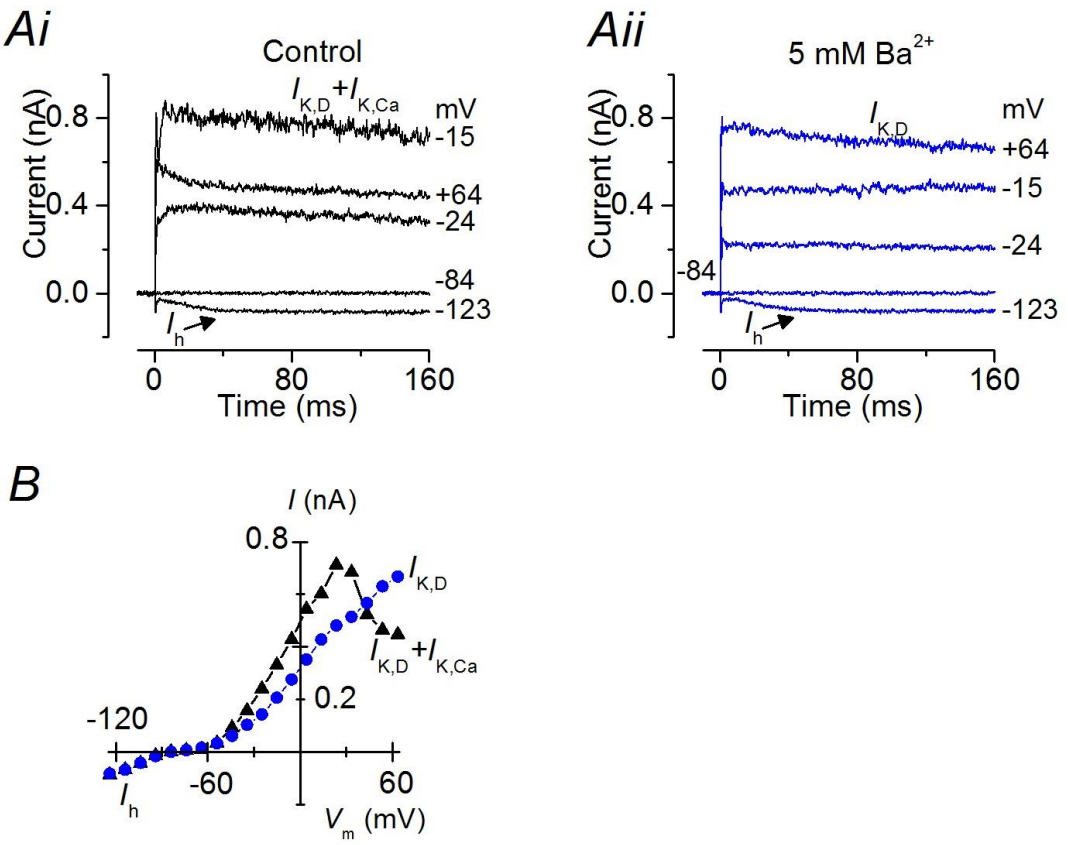

Figure 4.6 Pharmacological isolation of K⁺ currents in larval zebrafish hair cells.

Ai, Example of a cell containing both I_h and $I_{K,Ca}$ (black trace). Currents were elicited by depolarizing and hyperpolarizing voltage steps in 10 mV nominal increments from the holding potential of −84 mV to the various test potentials shown by the traces. *Aii*, Blue trace: perfusion of extracellular solution containing 5 mM BaCl. *B*, *I-V* relationship for conditions shown in *Ai* and *Aii*. Note that BaCl affects the outward current but not I_h.

4.3.1.3 Current and voltage responses of larval zebrafish hair cells in vivo

The different K⁺ currents found in hair cells were then closely investigated in terms of their time and voltage behaviour and relative expression within a neuromast.

Current responses of lateral line hair cells

The K^+ currents in larval lateral line hair cells were then investigated further using voltage clamp. Currents were elicited by applying a series of depolarizing voltage steps from −120 mV in 10 mV nominal increments from the holding potential of -84 mV. This protocol has highlighted a wide range of current phenotypes (Figure 4.7). It is important to note that there was no correlation between type of K^+ current and hair cell position within a neuromast, i.e. hair cells in the edge and centre of a neuromast express similar K^+ currents. Therefore, the hair cells within a neuromast were classified into three main profiles depending on the complement of K^+ currents they expressed:

Type 1 cells showed a rapidly activating and inactivating outward A-type current (I_A) in combination with a delayed rectifier current ($I_{K,D}$) and no or little inward current (Figure 4.7). About 14% of Type 1 cells showed an I_h. This current profile was seen in 17 % of all larvae cells investigated.

Type 2 cells showed an $I_{K,D}$ with a small I_A and no or little inward current (Figure 4.7). Around 3 % of all hair cells tested show this current profile.

Type 3 cells are mainly characterised by a Ca^{2+}-activated K^+ current ($I_{K,Ca}$) with a small contribution from an I_A and $I_{K,D}$. About 34% of Type 3 cells also showed a hyperpolarised-activated current (I_h) (Figure 4.7). About 80% of all the hair cells investigated show this profile. The capacitance of all larval hair cells was 3.6 ± 0.1 pF (n = 62).

This classification was based solely on the presence and dominance of either current, i.e. a large I_A or $I_{K,CA}$. The Type 2 cells were classed because neither current was dominantAll these current profiles have been previously described in hair cells from other lower vertebrates such as the goldfish (Sugihara and Furukawa, 1989) and frog (Masetto et al., 1994; Holt and Eatock, 1995).

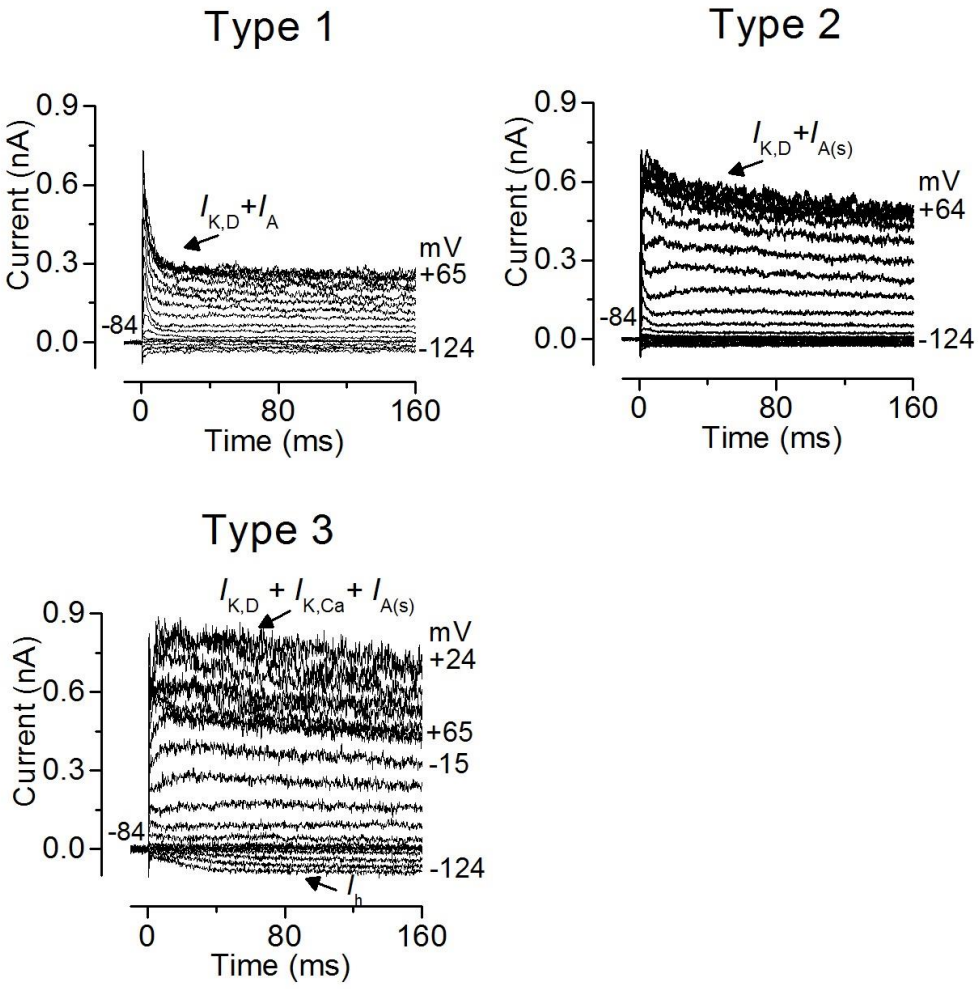

Figure 4.7 Potassium currents in hair cells from the larval zebrafish lateral line.

Examples of K^+ current recordings from hair cells in different neuromasts (L2–L4) when fish were paralysed with α-Btx. Note that the three different current phenotypes were seen in hair cells within each neuromast from larval zebrafish. Currents were elicited by depolarizing and hyperpolarizing voltage steps in 10 mV nominal increments from the holding potential of −84 mV to the various test potentials shown by the traces.

Voltage responses of larval hair cells

Next, I performed current clamp experiments, which reveal the contribution of the different conductances to the overall membrane potential behaviour.

As described above, the complement of K^+ currents varied among hair cells, indicating a possible variation of voltage responses. In both Type 1 and 2 cells,

hyperpolarizing current injection caused large negative sustained voltage responses, which reflects the absence or very small contribution of an inward K^+ current at these negative membrane potentials (Figure 4.8, top and middle right). Type 3 cells responded to hyperpolarising current injections with a characteristic voltage sag that matched the activation of the I_h at hyperpolarised potentials (Figure 4.8, bottom left).

Depolarizing current injections elicited voltage responses that reflected the time course of the different outward K^+ current components. The largest voltage change to positive current injections was seen in Type 1 cells. These cells showed a slow time-dependent depolarisation (Figure 4.8, top right), which reflected the presence of the fast inactivating I_A. The larger overall depolarization in these cells is due to the smaller sustained $I_{K,D}$ compared to the other cell types (Figure 4.8, top). Type 2 cells showed a faster, but smaller voltage change to positive currents injections (Figure 4.8, middle right) due to their larger sustained $I_{K,D}$. Type 3 cells had the largest K^+ currents and showed the smallest but fastest voltage changes to positive current injections (Figure 4.8, bottom right). Membrane oscillations during positive current injection, which was seen in hair cells of the inner ear (see Chapter 6, Figure 6.3), was absent in all recorded cells from the neuromast.

The average resting membrane potential (V_m) was similar in all hair cells investigated between 3.0–5.2 dpf and was −71.4 ± 1.7 mV (n = 27).

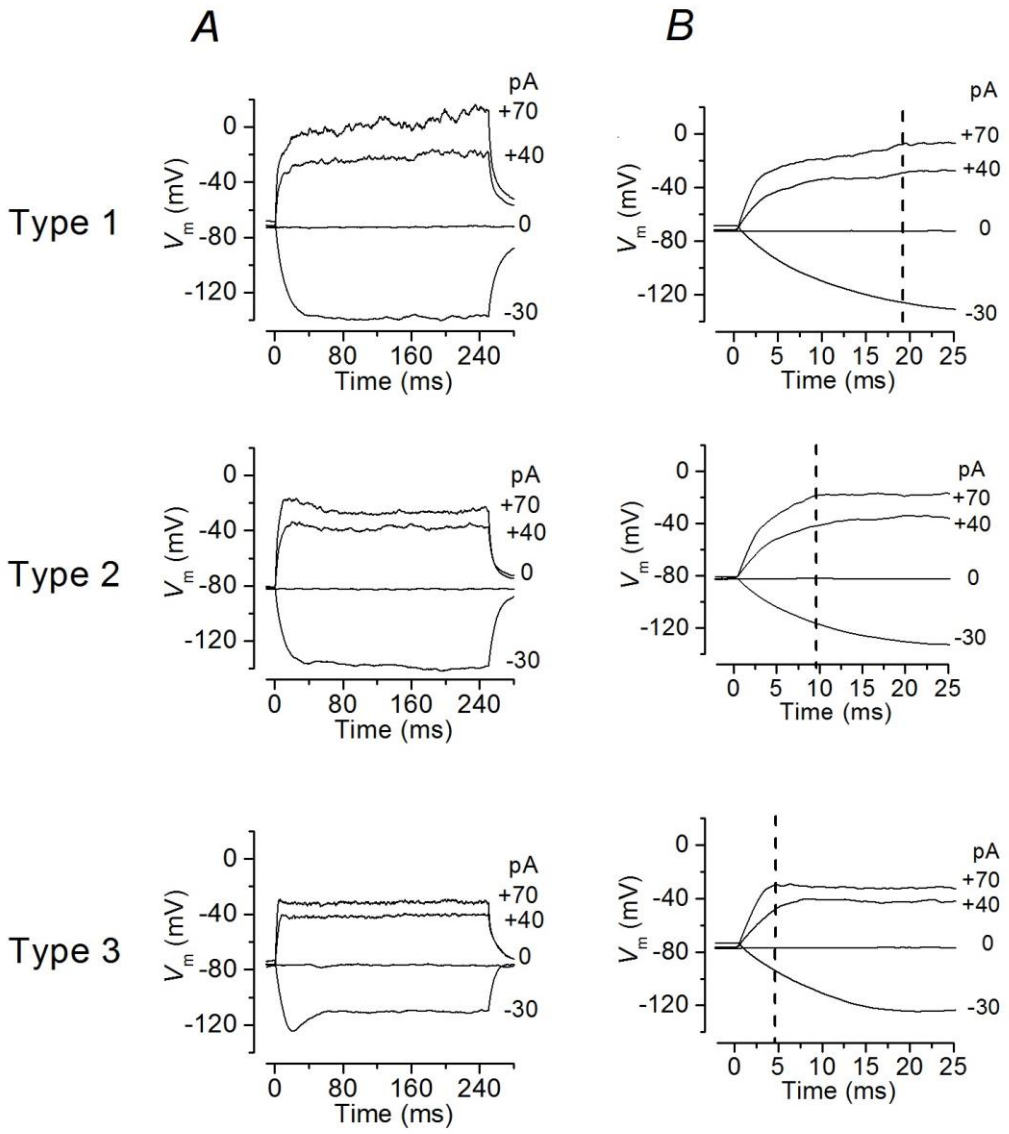

Figure 4.8 Voltage responses in hair cells from the larval zebrafish lateral line.

Left, Voltage responses to current injections of –30, 0, + 40 and + 70 pA from the V_m of the three types of hair cells. Voltage responses are from hair cells shown in Figure 4.7. *Right,* Inset of the first 25 ms of the recordings from left, note the dashed line indicates the time until the voltage change reached a first plateau.

4.3.1.4 Effect of MS-222 on larval hair cell K^+ currents

Larval zebrafish are commonly paralysed with an injection of α-Btx into the heart to stop movement. α-Btx is then distributed via the blood stream and binds reversibly to the nicotinic acetylcholine receptor on the muscle fibre and therefore blocks neurotransmission (Young et al., 2003). The anaesthetic MS-222 is used to cull zebrafish but also sometimes to perform both *in vitro* and *in vivo* studies on zebrafish hair cells. Even though MS-222 is a known K^+ channel blocker, its possible effect on the hair cell basolateral membrane physiology has never been assessed. Figure 4.9 shows that in the presence of MS-222 hair cells exhibit a similar combination of K^+ currents, namely type 1, 2 and 3, to that reported in the absence of the anaesthetic.

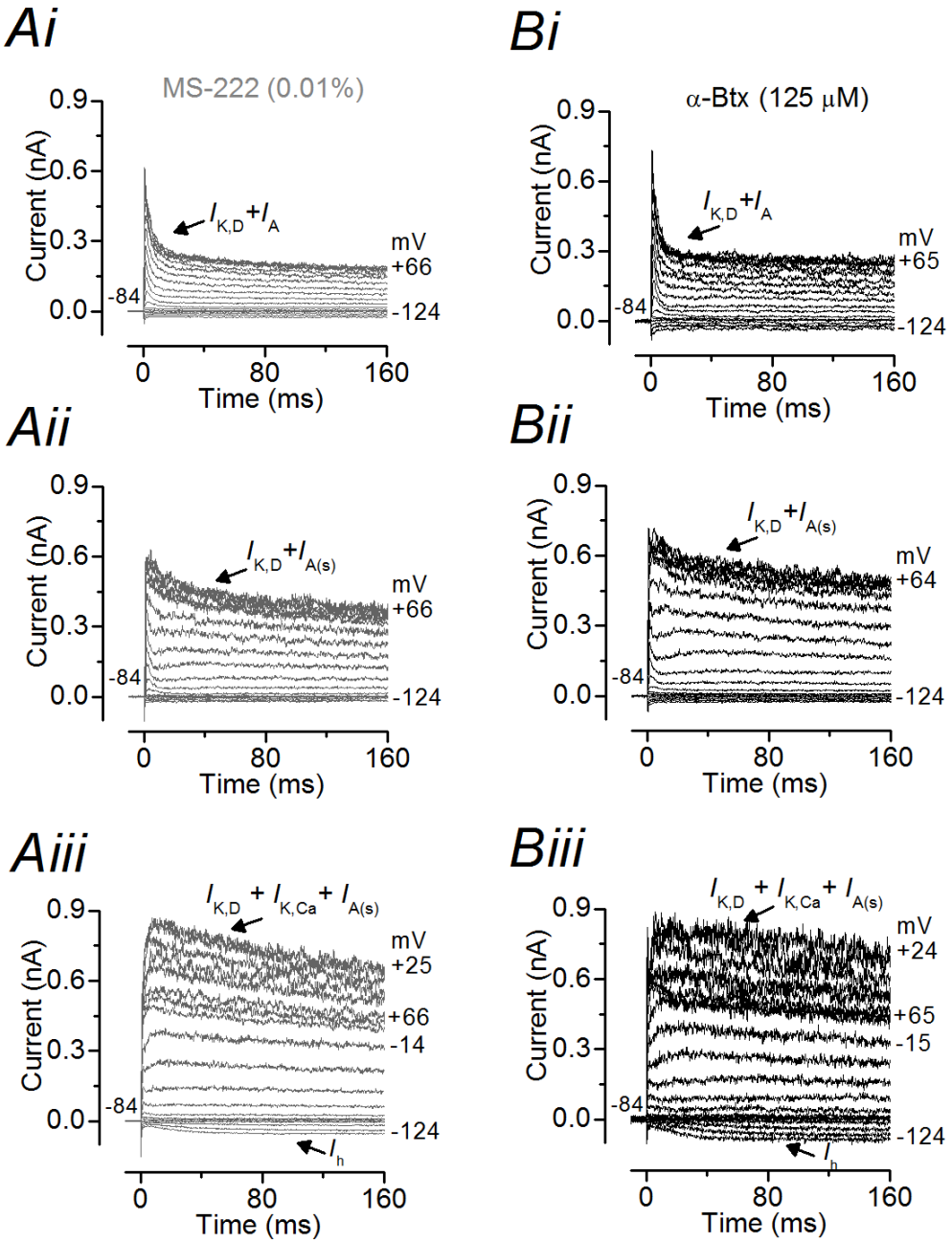

Figure 4.9 Examples of larval hair cells recorded in the presence and absence of MS-222.

A, examples of hair cells of the larval zebrafish neuromast (3.0–5.2 dpf) in the presence of 0.01 % MS-222. Currents were elicited by depolarizing and hyperpolarizing voltage steps in 10 mV nominal increments from the holding potential of −84 mV to the various test potentials shown by the traces. *B,* examples of hair cells of the larval zebrafish neuromast (3.0–5.2 dpf) without MS-

222. Note that all larvae used haven been injected with α-Btx (*B*) and in (*A*) the MS-222 was contained in the extracellular solution.

Even though the variety of K^+ conductances found with and without MS-222 in the extracellular solution did not differ, it was unclear whether there were subtle alterations. Therefore, the possible interference of the anaesthetic on single hair cells was verified by locally superfusing hair cells with MS-222. One example of a type 2 hair cell recorded from a 4 dpf hair cell before and during the superfusion of 0.01% MS-222 is shown in Figure 4.10 *Ai* and *Aii*. The steady-state values of the K^+ currents (Figure 4.10 *B*) were used to generate *I–V* curves and did not differ between control and MS-222 perfusion. The similar peak and steady-state amplitudes (Figure 4.10 *C*) of the outward K^+ current indicate that MS-222 does not influence the current profile observed in hair cells from larval zebrafish. Therefore, it can be concluded that MS-222 is an appropriate anaesthetic to use on larval zebrafish (3-5.2 dpf).

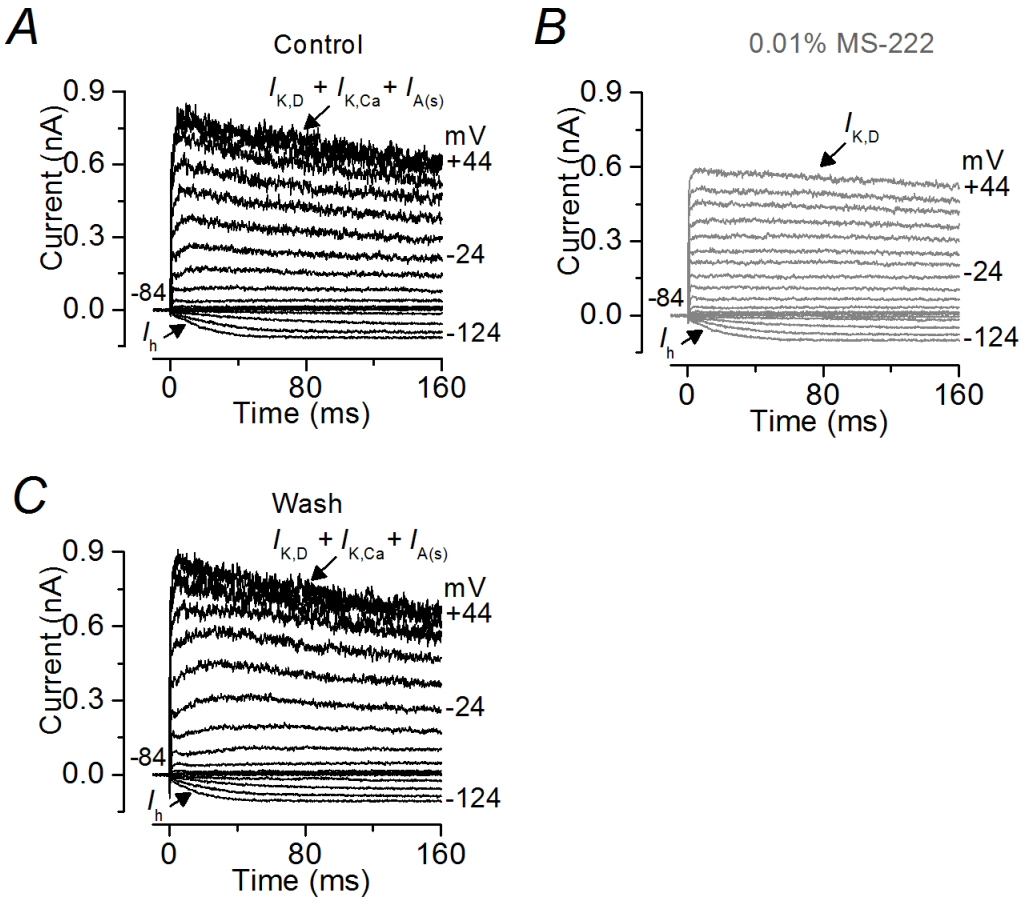

Figure 4.10 Effect of MS-222 on potassium currents from larval lateral line hair cells.

Ai – ii, Examples of K^+ currents recorded from a hair cell (4 dpf) before (*Ai*) and during (*Aii*) the superfusion of 0.01% MS-222. Currents were elicited by depolarizing and hyperpolarizing voltage steps in 10 mV nominal increments from the holding potential of −84 mV to the various test potentials ranging from – 123 to + 66 mV. *B*, steady-state (measured at 160 ms) *I–V* curves obtained from the recordings shown in *Ai* and *Aii*. *C*, average peak and steady-state amplitude of the K^+ current at 0 mV, including those shown in *Ai* and *Aii*.

4.3.1.5 K^+ current in early developing hair cells from different neuromasts

In the first few days of development (<5.2 dpf) the posterior lateral line undergoes dramatic and quick morphological changes. Hence, it was investigated whether the current profiles identified above also changed within this small age range. The results showed that the set of K^+ current types does not seem to differ

as a function of age (3, 4 or 5 dpf) as shown by the similar peak current size at 0 mV (3 dpf: 466 ± 26 pA, *n* = 15; 4 dpf: 456 ± 23 pA, *n* =22; 5 dpf: 541 ± 41 pA, *n* = 4 (Figure 4.11 *A*). The steady-state currents at 0 mV were also not significantly different with 3 dpf: 311 ± 29 pA, *n* = 15; 4 dpf: 339 ± 22 pA, *n* =22; 5 dpf: 408 ± 86 pA, *n* = 4 (Figure 4.11 *A*).

The PLL shows somatotopic organisation, with the most anterior neuromasts being most ventrally organised in the lateral line ganglion and the most posterior neuromasts being innervated by neurons from the ventral parts of the ganglion (Alexandre and Ghysen, 1999). Consequently, it was also tested whether there are differences in the occurrence of K^+ current along the body axis of the fish. Figure 4.11 *A* shows that there is no significant difference in the peak and steady-state values of the inward and outward currents between different neuromasts. Additionally, recordings from the three neuromasts were pooled to generate *I-V* relationships (Figure 4.11 *C*). The three *I–V* curves showed similar overall amplitude and voltage dependence, indicating that the current profiles of hair cells within each neuromast showed similar levels of variability.

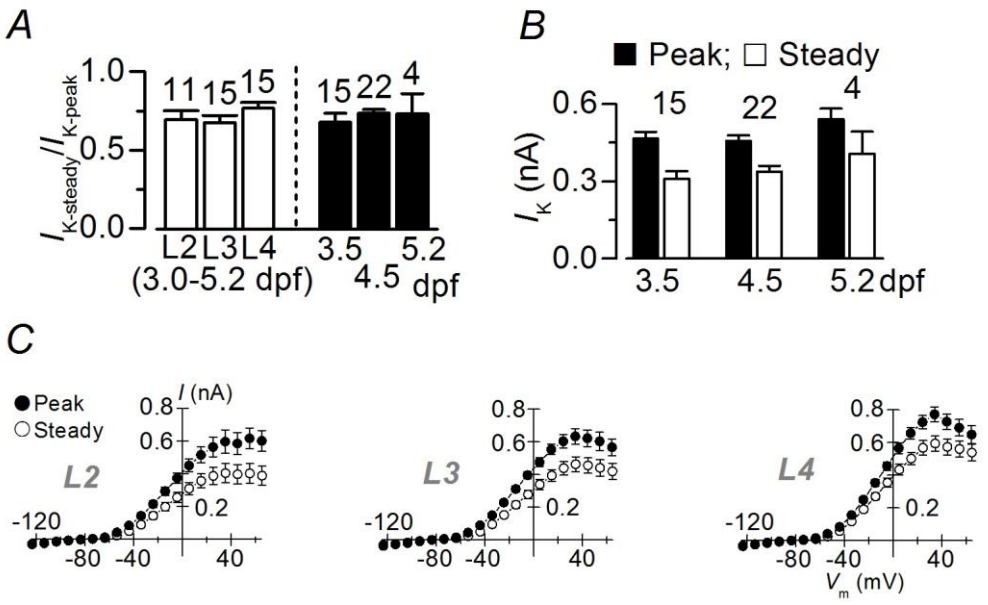

Figure 4.11 Hair cell K⁺ current abundance depending on larval stage and neuromast location.

A, Average peak and steady-state amplitudes for the outward K⁺ current at 0 mV recorded from hair cells as a function of age in all neuromasts. *B*, Average steady-state : peak amplitude ratio for the outward K⁺ current at 0 mV recorded from hair cells in the three neuromasts (open bars) or as a function of age in all neuromasts (filled bars). *C*, Average peak and steady-state (measured at 160 ms) *I–V* curves from hair cells in neuromasts L2–L4. *I–V* curves include all recordings (with MS-222 and α-Btx) obtained in each of the three neuromasts investigated.

Another important morphological aspect in this sensory organ refers to the position of hair cells within a neuromast. New hair cells are born at the apical and basal poles of the neuromast and migrate around the periphery/edge so that the whole neuromasts grow from the outside to the inside (Lopez-Schier and Hudspeth, 2007). However, at this stage of development, larval neuromasts only contain about 10 hair cells, which makes it impossible to distinguish between the edge and centre of the organ. In those very few experiments (n = 12) where the exact location of larval hair cells within a neuromast could be determined, I found a similar current profile between centre and edge: all six cells in the edge and four of six hair cells in the centre showed Type 3 cells - $I_{K,Ca}$, $I_{K,D}$, and $I_{A(s)}$. Two cells from the centre exhibited Type 1, where $I_{K,Ca}$ was missing and only $I_{K,D}$ + $I_{A(s)}$

remained. However, considering the large variety of K^+ phenotypes the findings based on 12 cells are inconclusive and it appears that all three types occur throughout the neuromast.

This indicates that at early larval stages, the different basolateral current profiles of newly formed hair cells are present within and across the different neuromasts and as a function of age.

4.3.2 Synaptic Transmission in lateral line hair cells

The receptor potential generated by I_{Met} and shaped by the basolateral membrane currents causes the opening of voltage gated calcium channels of the $Ca_v1.3$ subtype that are part of the L-type family (Moser and Beutner, 2000; Sidi et al., 2004). Details about the properties of I_{Ca} and transmitter release are crucial to understand how zebrafish hair cells are able to function. The biophysical properties of I_{Ca} in lateral line hair cells were investigated using voltage clamp experiments. Figure 4.12 *A* shows a typical example of I_{Ca} recorded from a larval hair cells. Current traces from six hair cells were used to generate the *I*-*V* relation (Figure 4.12 *B*), which revealed the characteristic bell shape of this current. At potentials positive to –70 mV the channel started to open and peaked near – 31 mV with a maximum size of **−**12.3 **±** 1.1 pA (3.0–4.5 dpf). This *I*-*V* curve was fitted using Equation 2.

$$I = \frac{g_{max}(V - V_{rev})}{1 + \exp(\frac{V_{1/2} - V}{S})}$$

Equation 2 Calcium current fit.

Parameters are: I is the current, g_{max} is the maximum chord conductance, V is the membrane potential, V_{rev} is the reversal potential of the current, $V_{1/2}$ is the potential at which the conductance is half activated, and S is the slope factor that defines the voltage sensitivity of current activation. Fitting parameters for are larvae (for 3.0–4.5 dpf) g_{max} = 0.2 nS, V_{rev} = 17 mV, $V_{½}$ = −48.2 mV and S = 6.6 mV.

The calcium current leads to the fusion of vesicles at the presynaptic membrane. Exocytosis was estimated by measuring changes in cell surface, which are reflected in its membrane capacitance (ΔCm) following depolarizing voltage step to the peak of the I_{Ca} at –31 mV. This is generally interpreted as a sign of neurotransmitter release from presynaptic cells (Moser and Beutner, 2000; Johnson et al., 2008; Johnson et al., 2013). An example of ΔCm recorded in response to a 1 s depolarizing voltage step from a larval hair cells is shown in Figure 4.12 *C*. On average, ΔCm in larval zebrafish was 2.3 ± 0.5 fF (n = 6). Assuming each vesicle is on average 37 aF (Lenzi et al., 1999), around 62 vesicles fused with the membrane after a 1s depolarizing step.

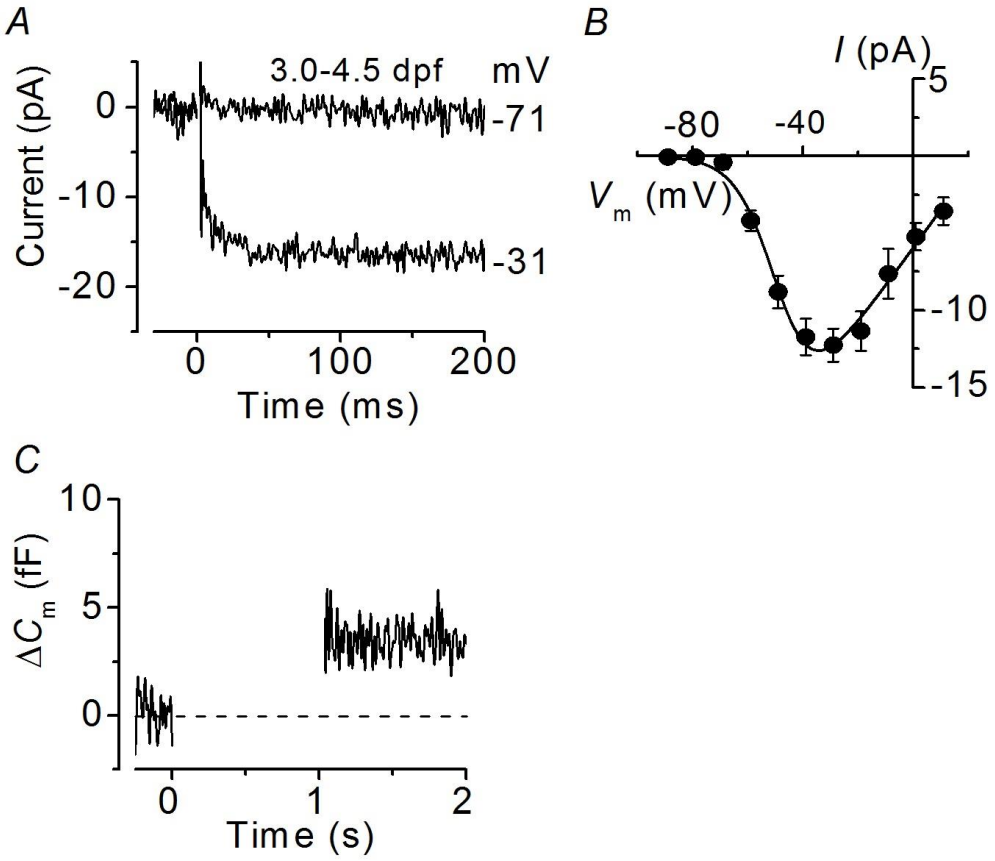

Figure 4.12 Calcium currents and neurotransmitter release in lateral line hair cells.

A, Calcium currents (I_{Ca}) recorded from hair cells of the larval (3.0–4.5 dpf) zebrafish lateral line. Currents were elicited by depolarizing voltage steps (200 ms in duration) from the holding potential of −79 mV to the potentials shown by the traces. For clarity only the traces at the holding potential and near the peak of I_{Ca} (−31 mV) are shown. *B*, average peak calcium current *I–V* curves from 3.0–4.5 dpf (black) hair cells (n = 6), including the one shown in *A*. *C*, changes in membrane capacitance (ΔCm) recorded from hair cells of larval (3.0–4.5 dpf) zebrafish. Recordings were obtained in response to 1 s voltage steps from the holding potential of −79 mV to −31 mV. Recordings were obtained at 28 °C.

4.4 Summary

The zebrafish lateral line has been used as a model for studying the genetics of hair cells in recent years. Yet, little was known about the electrical properties of the sensory cells in the neuromasts. This chapter provides a thorough description of the biophysical properties of larval hair cells. They were subdivided in three main subtypes, based on their current profile.

Type 1 hair cells show an I_A in combination with $I_{K,D}$ and no or little inward current. They respond with large voltage changes, both negative and positive to hyperpolarising and depolarising current injections.

Type 2 hair cells have an $I_{K,D}$ with a small I_A and no or little inward current. They show a similar voltage change to type 1, but slightly smaller and faster.

Type 3 hair cells exhibit $I_{K,Ca}$ with a small contribution of I_A and $I_{K,D}$, sometimes with I_h. They prevent the membrane potential from large hyper- or depolarisation and mediate the fastest changes out of all three types.

4.5 Discussion

Lateral line hair cell function

This chapter provides a more detailed insight into the electrical properties of the basolateral membrane of larval hair cells in the lateral line.

Previously, it has been shown that all hair cells have a functional MET channel, as indicated by FM1-43 labelling and imaging studies (Kindt et al., 2012). This could be further tested with electrophysiological techniques, such as direct bundle stimulation with a water-jet device (Trapani and Nicolson 2010) and would allow more detailed investigation of the properties (e.g. size, I_{Met} at rest, adaptation) of the MET machinery in lateral line hair cells. Unfortunately, this is technically very challenging and could not be successfully performed.

However, an experiment that could be performed, was measuring the V_m with and without the MET channel blocker DHS, which revealed that the I_{Met} was

indeed open at rest. In a number of other experiments the V_m was measured and averaged at about -75 mV, which is in contrast to the DHS experiments, where it was -60 mV. This discrepancy could have several origins: firstly, the sample size for the DHS experiment was low and only the more depolarised cells were measured. From previous studies, it is expected that the I_{Met} channel is not homogenously functional throughout the neuromast, despite all hair cells labelling with FM1-43 (Kindt et al., 2012), and it could have different sizes of current active at rest. The overall V_m measured is relatively negative but it is still away from the K^+ reversal potential of about -80 mV, which indicates that there is a cation influx at rest, albeit a small one.

Secondly, this discrepancy could be, at least in part, due to destruction of the tip links, where the MET channel is located. This would abolish cation influx and hyperpolarise the cell. The V_m with broken tip-links is unknown, therefore it cannot be compared to my findings. It is likely to be in the order of -80 or -90 mV, which is close to the K^+ reversal potential. Even though great care was taken to limit damage to the hair bundle, it cannot be completely ruled out.

The overall finding that zebrafish lateral line hair cells show three K^+ phenotypes is very surprising. These different K^+ currents are found in a number of mechanosensory organs, but not in this combination.

Initially, it was assumed that the hair cells in the lateral line would resemble those in the vestibular system. The latter comprises two cell types, one with an A-type current (Type II) and the other with a large K^+ current ($I_{K,L}$, Type I) but only the Type 1 in the fish (I_A) resembles Type II of the vestibular system. A-type currents are found in various non-sensory cells to, where they function to modulate spiking latency (Norris et al., 1992). The function in vestibular hair cells and the lateral line could also be different.

The A-type current mediates the slowest, largest voltage response in the cells investigated. In the intact system, where the bundle is deflected, it will clamp the membrane potential quickly after the MET channel is opened. During continued stimulation, the current through the MET channel will get smaller (slow adaptation). This coincides with inactivation of the A-type current, thus allowing

the depolarising response to be constant. This is important to signal constant stimulation of the lateral line. A second role of the Type 1 hair cells might lie in velocity or intensity detection. In contrast to type 2 and type 3 lateral line hair cells, it has the biggest gain. During continued stimulation, this will allow these cells to be gradually more depolarised the more the bundle is pushed as the fish swims faster or when it engages in shoaling behaviour. Type 1 cells in the fish are potentially limited to sensing low frequencies as they are similar to vestibular hair cells sensing up to a few Hz.

In contrast, Type 3 ($I_{K,D}$ and $I_{K,Ca}$) as well as Type 2 ($I_{K,D}$ and $I_{A(s)}$) hair cells in the fish show currents found in the auditory hair cells of the bullfrog sacculus as well as turtle cochlea (Fettiplace and Fuchs, 1999). Both types mediate faster, smaller voltage changes than Type 1. Interestingly, neither the Type 3 nor Type 2 hair cells show electrical tuning, albeit they have the appropriate channels. The main reason for this is that the calcium current is most likely too small and neither channel is localised in close proximity. From a functional perspective, this almost rules out an auditory function of these cells.

Even though BK channels are not found in vestibular hair cells (Eatock et al., 1998), as these are associated with the need for electrical tuning above 50 Hz, they could still carry vestibular function for linear acceleration in the lateral line. In the intact fish, water stimulation of the neuromast will lead to a fast voltage change in the type 2 and 3 cells and quick transmitter release. This makes these cells ideal for escape responses, where the fish needs to integrate sudden stimuli quickly. During continued stimulation, Type 2 and Type 3 cells are most likely less sensitive than Type 1, because they have a smaller gain. Other functions of BK channels in non-neuronal cell types include regulation of cell excitability. This seems less likely in zebrafish hair cells, as the calcium current is very small and excitability of these cells is more likely mediated by the efferent system (Toro et al., 2015).

The types of potassium currents described above do not reveal much of their function without detailed knowledge of the synaptic machinery of the cell and the afferent neuron that contacts it. Measurements of the size of the calcium

current in zebrafish lateral line hair cells show that it is on average 10 times smaller than in the mature mammalian IHC (Marcotti et al., 2003b) and two to three times smaller than in rat vestibular hair cells (Eatock and Hutzler, 1992); Bao et al., 2003). Even when the cell surface area is taken into consideration, with mammalian IHC being around 10 pF and rat vestibular hair cells 5 pF in size, the size of the calcium current in the lateral line is still considerably smaller. The size of the calcium current has been associated with increasing the precision of the synapse (Li et al., 2014) the bigger the current, the more accurate the postsynaptic response. This leads to the conclusion that zebrafish hair cell synapses are not as accurate as their auditory counterparts and that precision is achieved by incorporating the responses of several synapses of the same or different hair cells. Indeed, one neuromast is contacted by on average 4-6 neurons that branch extensively (Liao 2010; Haehnel et al., 2012 and 2014). In this fashion, transmission of signal intensity can be achieved by subsequently recruiting more hair cells and increasing afferent nerve firing.

In the vestibular system, differences between Type I and II extend beyond their K^+ current set in ways that affect their gain and filtering properties (Songer and Eatock, 2011). As for the filter properties, this does not seem to be the case in lateral line hair cells. None of the three hair cell types seem to differ in terms of cell capacitance and they do not have any current at rest, which would influence the cell resistence and impact on the membrane time constant (τ). τ is directly associated with the cut-off or roll-off frequency, which indicates the point where a low-pass RC circuit can no longer follow a frequency. This means, that all three cell types are most likely equal in terms of their ability to change their membrane voltage. However, this would need further investigation of their cell resistance, whereas in this study only the series resistance was measured. Moreover, experiments applying a sinewave current to the cell and measuring the membrane voltage change, will shed light on details of the filtering properties.

As for the gain, this is indeed different in the different types, with Type 1 cells showing the largest gain, while Type 2 and 3 can be about a third smaller. This indicates, that Type 1 cells have a larger dynamic range, which could be in line with them transmitting velocity or intensity during swimming.

However, in this experiment, the stimulation was a square current. This is most likely different to the physiological shape of the MET current, that will adapt and become smaller over time. This can be adjusted with the experimental design and the injected current can be mimicking the *in vivo* MET current.

Lateral line hair cell development

It is perhaps surprising, that at these early larval stages the number of types or channels expressed does not differ either as a function of age (3 to 5 dpf) or as a function of distance along the fish body. However, the rapid development of zebrafish cannot be underestimated. By the time they hatch (2-3 dpf), fish have near complete sensory systems, which allow them to escape, shoal, smell and catch prey by 5 dpf (Straehle et al., 2012). Therefore, it is little surprise that the hair cells in larval fish are fully functional. However, the question remains as to why there are so many types present and whether this changes during adulthood. It has been shown in the vestibular system that a large proportion of immature hair cells show a delayed rectifier current between p 0 and p 3 (Rüsch et al., 1998) and then gradually develop their characteristic features such as I_A (Type II) or $I_{K,L}$ (Type I). This means that some cells are immature, despite the animal being perfectly capable in terms of the righting reflex. Similarly, neuromast hair cells seem to undergo morphological changes up to at least 5 dpf, where the kinocilium and bundle height increase as well as more stereocilia being added to the apical surface (Kindt et al., 2012). This is accompanied by a refinement in the polarity of the transducer. All these changes occur in cells that are already present and apparently functional at 5 dpf. Unfortunately, our knowledge about this does not extend beyond 5 dpf, after which the fish are protected.

In the time between hatching and adulthood, which is marked by reaching sexual maturity, the sensory systems do refine and adapt to new tasks. As the fish behaviour changes from slow, burst like swimming to faster, undulating swimming, the hair cell types might adapt to match the task. Therefore, in the next chapter I have investigated juvenile lateral line hair cells to shed more light

on the questions which hair cell type has which role and whether this changes over time as more hair cells are added to the neuromast.

Chapter 5 Biophysical Properties of Juvenile Zebrafish Lateral Line Hair Cells

5.1 Introduction

Hair cells in the larval (< 5.2 dpf) zebrafish lateral line organ show K^+ currents that I have grouped into three types based on their channel identity and current size (see Chapter 4). This finding was surprising as fewer types were initially expected. The reason for this variety in the current profiles could be related to differences in function or developmental stages. In the vestibular system of higher and lower vertebrates two distinct cell types are present, each assigned with a different function in transmitting stimuli. On the other hand, in higher vertebrates, such as mice, it is well documented that the basolateral membrane currents largely change from immature to adult stages (Corns et al., 2014).

Therefore, I investigated hair cells of juvenile zebrafish, which are around 4 weeks older. If the three larval K^+ types relate to developmental changes, this would lead to the juvenile fish showing a smaller number of current profiles. However, if they are related to function, the same phenotypes should be present throughout all ages. Potentially, the number of K^+ profiles could even increase as the demands on sensory transduction change from larvae to juvenile fish. Moreover, the synaptic machinery will be investigated at older stages to assess whether its properties change over time.

Experiments on juvenile or young adult zebrafish were performed under two main conditions: *In vitro* using decapitated animals and *in vivo* using zebrafish under non-recovery anaesthesia (Benzocaine). These results will be described in detail in the two main sections of this chapter.

5.2 Methods

For a detailed description of the general methods used to prepare the zebrafish for electrophysiological experiments see the Methods in Chapters 2 and 3. All recordings were performed at room temperature unless otherwise indicated. Calcium currents were investigated both in decapitated and *in vivo* juveniles. They were isolated from the total membrane current by blocking the K^+ currents with 4-AP and TEA in the caesium-based intracellular solution (see main

Methods in Chapter 2). In the decapitated fish, MS-222 was added to the extracellular solution to stop involuntary muscle movement of the tail.

The anesthetics MS-222 and Benzocaine were locally applied to hair cells to investigate possible effects on membrane currents. Solutions containing the drugs were applied through a multi-barreled pipette positioned close to the preparation (see main Methods in chapter 2). The stock solution of MS-222 (0.4 % in water, see main Methods in Chapter 2) was prepared by the aquarium facility. The stock solution of Benzocaine was prepared at 20 g/L in 100% ethanol and kept in the fridge.

Juvenile zebrafish have larger neuromasts than the larvae (>10 hair cells), which allowed us to determine whether hair cells were located either at the edge or at the centre of the organ (37 of 42 hair cells tested).

Hair cells from juvenile zebrafish had a cell membrane capacitance of 3.2 ± 0.1 pF (n = 132).

5.3 Results

5.3.1 *In Vitro* properties of juvenile lateral line hair cells

5.3.1.1 Current and voltage responses from juvenile lateral line hair cells

The K^+ currents of juvenile lateral line hair cells were investigated by applying depolarizing voltage step in 10 mV nominal increments (200 ms in duration) from –124 mV to + 66 mV starting from a holding potential of –84 mV. This set of experiments revealed a similar variability of K^+ current profiles in juvenile hair cells, but only Type 1 and 3 are shown as examples, as that seen in larval fish. The four currents expressed in juvenile hair cells, I_h, $I_{K,D}$, I_A and $I_{K,Ca}$, are normally expressed in the two main combinations shown in Figure 5.1.

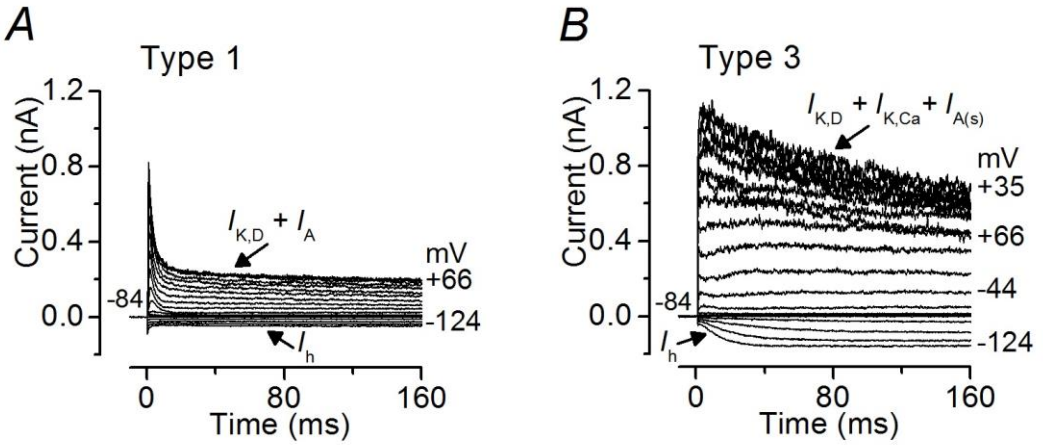

Figure 5.1 Current responses in juvenile hair cells.

A, B, Characteristic K^+ currents recorded from lateral line hair cells (*A*; 29 dpf, *B*; 28 dpf) in the neuromast. *A*, Hair cell expressing a prominent I_A and the small I_h. *B*, Hair cell expressing the $I_{K,Ca}$ with a larger I_h. Currents were elicited as described in the text.

In order to determine how the two different current profiles of juvenile hair cells shape their voltage responses, I performed current clamp experiments, in which cells were injected with currents ranging from -30 pA to +70 pA in 10 pA nominal increments from the V_m of the individual cell (Figure 5.2).

In hair cells that mainly showed a large I_A (Type 1, Figure 5.2 *A*), hyperpolarising current injections led to a large membrane hyperpolarisation of about 40 mV, indicating that inward currents (possibly I_h) were either not present or very small. Positive current injections led to large and slowly (~20 ms) developing membrane depolarization, which reflects the rapid activation and inactivation of I_A (Type 3, Figure 5.2 *A*). In the cells expressing $I_{K,Ca}$, hyperpolarizing current injections caused a voltage sag of ~-15 mV characteristic of the presence of I_h, which activates slowly and drives cations into the cell to prevent further hyperpolarisation. Large depolarising current injections led to small but fast (~2 ms) voltage changes due to the large $I_{K,Ca}$ that allows substantial cation efflux (Figure 5.2 *B*). None of the hair cells responded with membrane oscillations as seen in hair cells of the inner ear (Chapter 6).

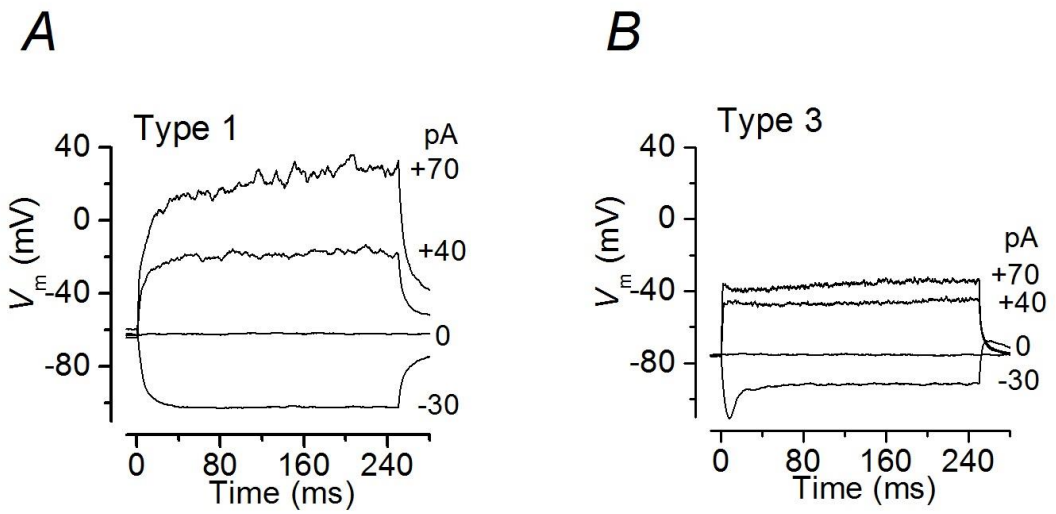

Figure 5.2 Voltage responses in hair cells from the juvenile zebrafish lateral line.

Examples of voltage responses from cells in the centre (*A*) and edge (*B*) of the juvenile neuromasts. Voltage responses to current injections of –30, 0, + 40 and +70 pA from the V_m of the individual juvenile hair cells. Voltage responses are from the same hair cells as those shown in Figure 5.1 *A* and *B*.

5.3.1.2 Development of potassium currents at juvenile stages

As mentioned above, mammalian hair cells undergo dramatic developmental changes before the onset of hearing (Corns et al., 2014). Similarly, vestibular hair cells acquire their mature profile after around p 3 (Eatock et al., 1998). In zebrafish, it is unclear whether the lateral line hair cells undergo similar developmental changes and if yes, whether this was reflected in the different K^+ current profiles. One hint that this indeed might have been the case comes from the fact that juvenile neuromasts contain more hair cells than their larval counterparts, and that newly formed hair cells originate at the periphery of the epithelium (Lopez-Schier and Hudspeth, 2007).

Therefore, I investigated whether the variability in K^+ current profiles was due to hair cells at different developmental stages within a neuromast, depending on the cells position within it, and whether these differences are the same between

larval and juvenile fish. All hair cells recorded were pooled according to position within a neuromast and age as follows: 3-5.2 dpf, 20-23 dpf and 26-29 dpf.

Different current profiles in hair cells as a function of developmental stages

Even though juvenile hair cells showed the same variability in current profiles as their young counterparts, the relative proportions of each type was unclear. Therefore, I investigated the numbers of each K^+ profile found in the different age groups. In order to do this I counted the occurrence of the inward (I_h) and outward currents ($I_{K,D}$, $I_{K,Ca}$, I_A) found in lateral line hair cells.

The common feature at every age was the expression of the delayed rectifier ($I_{K,D}$), which was found in all hair cells from all ages (Figure 5.3). The hyperpolarisation-activated current I_h is the only inward K^+ current found in lateral line hair cells. At larval stages (3-5.2 dpf) it is expressed in around a third of hair cells. Later on, about 70 % and 40 % of hair cells expressed I_h at 20-23 dpf and 26-29 dpf respectively. These differences are not significant, suggesting that I_h is equally expressed throughout development (Figure 5.3).

By contrast, the outward K^+ currents ($I_{K,Ca}$ and I_A) observed in lateral line hair cells are not homogenously expressed throughout development.

$I_{K,Ca}$ is the most prominent current in larval (3-5.2 dpf) hair cells with 80 % of them expressing this current (Figure 5.3). This current remains prevalent at early juvenile stages (20-23 dpf) with 85 % of cells expressing it. However, after 26 dpf only a quarter (26 %) of hair cells expressed $I_{K,Ca}$ (Figure 5.3).

The A-Type current (I_A) was found in 17 % of larval hair cells. Its abundance slightly increased at early juvenile stages (20-23 dpf) to 21 %. However, after 26 dpf the occurrence increased dramatically and 52 % of all 26-29 dpf hair cells express this fast current (Figure 5.3).

Overall it can be noted that the I_A is the main current expressed by hair cells older than 26 dpf whereas $I_{K,Ca}$ is mostly found at larval stages.

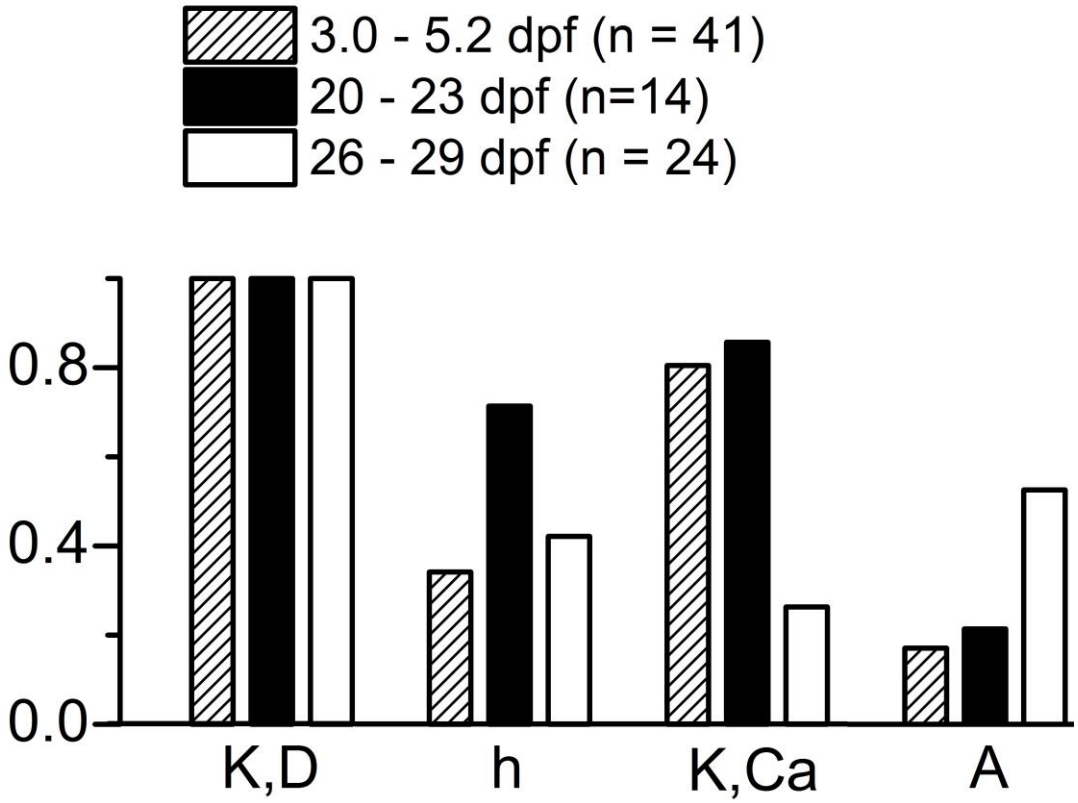

Figure 5.3 Abundance of potassium currents during development.

Fraction of hair cells expressing different currents at three stages of zebrafish development, which are larval (3-5.2 dpf, striped), early (20-23 dpf, black) and late (26-29 dpf, white) juvenile.

Potassium currents in different locations of the neuromast

Following the notion that newly originating hair cells develop at the edge of the neuromast (Lopez-Schier and Hudspeth, 2007), I have classed all hair cells depending on their position in the centre and edge and assessed which currents they express at the different ages.

For larval neuromasts (3-5.2 dpf), a clear distinction between centre and edge was difficult due to their small size, and was only determined for 12 cells. From these cells I found a similar current profile between cells in the centre and edge: 100 % of cells in the edge (n = 6) and 70 % of cells in the centre (n = 6) showed

an $I_{K,Ca}$, $I_{K,D}$, and $I_{A(s)}$. In 30 % of cells from the centre $I_{K,Ca}$ was missing and only $I_{K,D}$ + $I_{A(s)}$ remained (n = 6).

Throughout all juvenile age groups, the $I_{K,D}$ was present in every hair cell and consequently equally distributed between centre and edge. The same was also true for the I_h which also had no preferred position (Figure 5.4). For early juveniles (23-26 dpf) I_h was found in 85 % of cells in the centre (n = 7) and 60 % in the edge (n = 7). After 26 dpf about 45 % expressed this current in the centre (n = 11) and 40 % in the edge (n = 8).

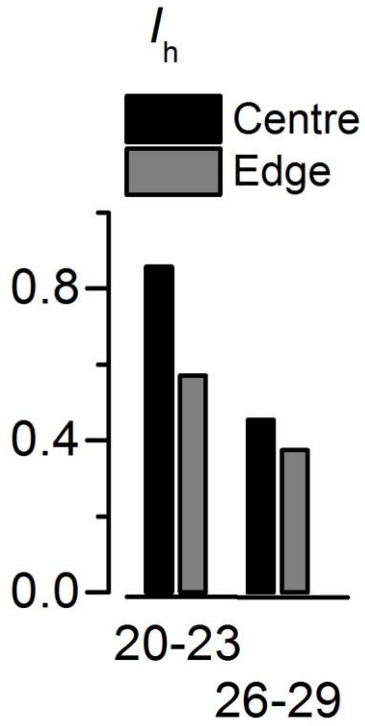

Figure 5.4 Abundance and position dependence of the hyperpolarisation-activated current during development.

Fraction of hair cells in the centre and at the edge of a juvenile neuromast expressing I_h currents (left: 20–23 dpf; right: 26–29 dpf).

When looking at the presence of $I_{K,Ca}$ in juvenile hair cells it was apparent that it was expressed widely in 20-23 dpf fish being in 85 % of cells in the centre (n = 7) and 85 % in the edge (n = 7) (Figure 5.5 *A*). However, at later juvenile stages after

26 dpf the $I_{K,Ca}$ was hardly found in the centre (10 %, n = 11) but stayed prominent in the edge (50 %, n = 8) (Figure 5.5 *A*).

As for the fast I_A in early juveniles (20-23 dpf), it was present in cells in the centre (40 %, n = 7) but was not found at all in those in the edge (n= 7) (Figure 5.5 *B*). At later juvenile stages (26-29 dpf) there was a large increase in its occurrence in cells in the centre with about 80 % expressing I_A (n = 11) (Figure 5.5 *B*). However, it was still only seen in a small proportion of cells in the edge with only 12 % showing its presence (n = 8) (Figure 5.5 *B*).

It should be noted that the segregation of the A-type current between cells in the centre or edge is much stronger than that found for the $I_{K,Ca}$, especially considering there was no segregation for $I_{K,Ca}$ in early juveniles. The segregation of I_A and $I_{K,Ca}$ in late juveniles showed a pattern with I_A in the centre and $I_{K,Ca}$ in the edge.

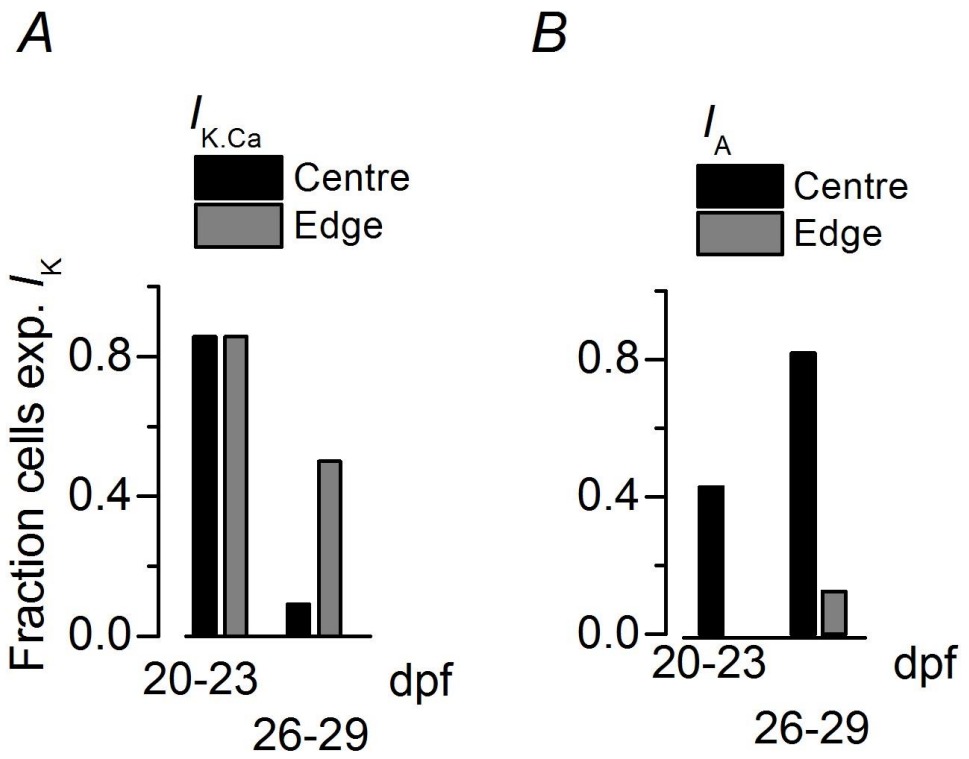

Figure 5.5 Abundance and position dependence of the Ca^{2+}- activated K^+ current and A-type current during development.

Fraction of hair cells in the centre and edge of a juvenile neuromast expressing I_{KCa} (*A*) and I_A (*B*) currents (left: 20–23 dpf; right: 26–29 dpf).

Overall, I found that at larval stages, the current profiles in hair cells is variable throughout neuromasts. However, the location of each type could not be specified due to its small size. After 26 dpf they seem to segregate with I_A being dominant in the centre and $I_{K,Ca}$ in the edge of the tissue. This coincides with the fact that new hair cells are formed at the periphery of the neuromast and suggests that the presence of $I_{K,Ca}$ is an indication of a younger cell, whereas the expression of I_A is a sign of an older hair cell, which is predominant in the centre of the neuromast.

Finally, I have compared the resting membrane potential of cells in the edge and centre of juvenile neuromast. The different K^+ current phenotypes could be reflected in differences in the V_m of cells, if these currents are active around the resting membrane potential. However, this is not the case since the average V_m

values were comparable between hair cells (26–29 dpf) in the centre (−69.9 ± 2.5 mV, n = 10) and edge (−68.3 ± 4.0 mV, n = 7).

Size of potassium currents at different stages

I measured the size of the outward K^+ current at 0 mV to check possible differences in the current availability over development (Figure 5.6). From larval throughout to later juveniles stages, the current size was similar for both the peak, ranging from around 340 to 510 pA, and the steady-state current size, ranging from around 240 to 370 pA (Figure 5.6), indicating a similar level of channel expression at different ages.

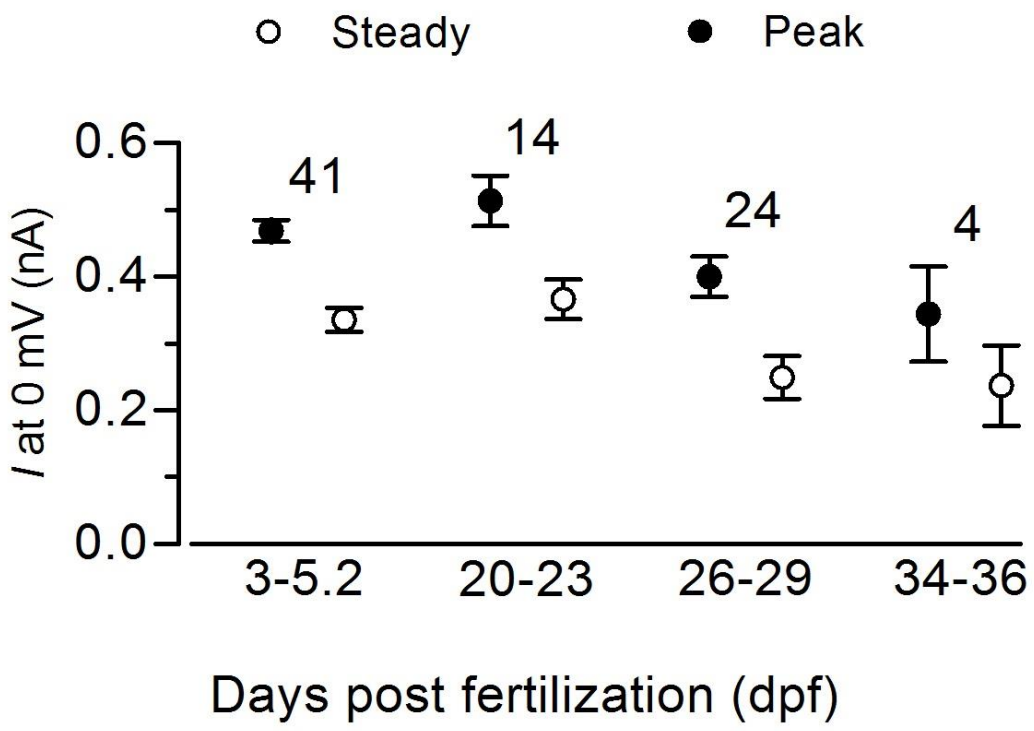

Figure 5.6 Potassium current size during development.

Average peak and steady-state outward K^+ current, extrapolated at 0 mV from the *I–V* curves, measured from hair cells as a function of age. The number of cells investigated is given above the data. Note that all recordings after 5.2 dpf have been performed in decapitated fish.

5.3.1.3 Synaptic Transmission in juvenile lateral line hair cells

As described above, the K^+ channels in the basolateral membrane of hair cells shape the receptor potential generated by the MET channel. This membrane potential change will lead to the opening of calcium channels and transmitter release. Similar to the larval hair cells, I have also investigated details of the synaptic transmission.

A typical example of I_{Ca} from a juvenile (29–34 dpf) zebrafish hair cell is shown in Figure 5.7 *A*. This was recorded in the presence of 2.8 mM extracellular calcium at the physiological temperature for the zebrafish (28.5°C). For clarity, only 2 traces are shown at -71 mV and – 31 mV. The average I_{Ca}-voltage relation (Figure 5.7 *B*) was fitted using Equation 2 (Chapter 4).

The *I-V* curve generated for I_{Ca} from six juvenile hair cells shows the current's characteristic bell shape and reveals that it activates at around −70 mV (defined as 5% of g_{max}). At potentials positive to -30 mV the current gets smaller again when approaching the calcium reversal potential and reverses at around 15 mV. The maximum size of I_{Ca} in hair cells measured near −30 mV was found to be similar between early juvenile (−13.0 ± 2.9 pA, n = 5, 17-22 dpf) and later juvenile zebrafish (−10.5 ± 2.7 pA, n = 6, 29–34 dpf).

The calcium current triggers the release of transmitter filled vesicles from the presynaptic membrane. Exocytosis was estimated by measuring changes in cell membrane capacitance (ΔCm) following depolarizing voltage steps, which is generally interpreted as a sign of neurotransmitter release from presynaptic cells (Moser and Beutner, 2000; Johnson et al., 2008; Johnson et al., 2013). An example of ΔCm recorded in response to a 1 s depolarizing voltage step to -31 mV (near the peak of the I_{Ca}) from a juvenile hair cell is shown in Figure 5.7 *C*. Juvenile hair cells of 17-22 dpf showed a ΔCm of 7.7 ± 2.3 fF (n = 4) which did not differ significantly from that measured at later juvenile stages 6.6 ± 0.6 fF (29-34 dpf, n = 5).

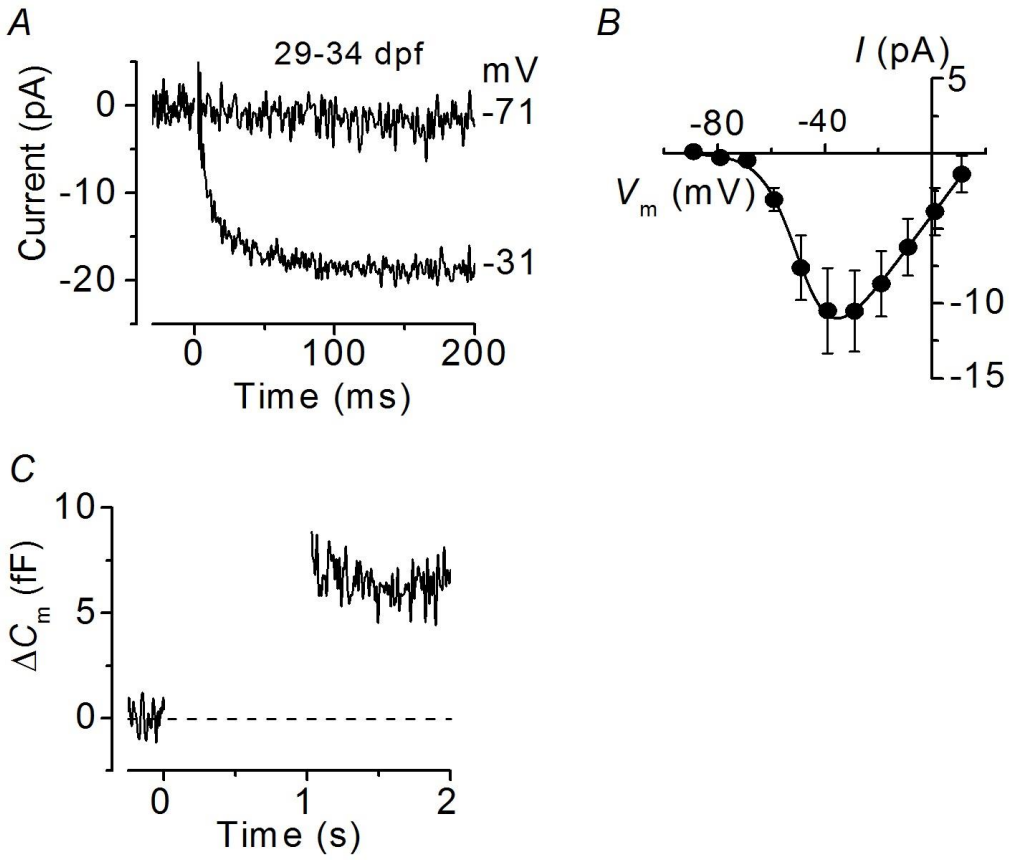

Figure 5.7 Calcium currents and neurotransmitter release in juvenile lateral line hair cells.

A, Calcium currents (I_{Ca}) recorded from hair cells of the juvenile (29–34 dpf) zebrafish lateral line. Currents were elicited by depolarizing voltage steps (200 ms in duration) from the holding potential of −79 mV to the potential as shown by the traces. For clarity only two of the traces are shown. *B*, Average peak calcium current I–V curve from 29–34 dpf hair cells (n = 6), including those shown in *A.* The fitting parameters for the I_{Ca} in juveniles (29–34 dpf) are g_{max} = 0.2 nS, V_{rev} = 24 mV, $V_{½}$ = −48.3 mV and S = 7.1 mV. *C*, change in membrane capacitance (ΔCm) recorded from a hair cells of a juvenile (29–34 dpf) zebrafish. The recording was obtained in response to a 1 s voltage step from the holding potential of −79 mV to near the peak of I_{Ca} (near −30 mV). Recordings were obtained at 28 °C.

I then investigated whether the sizes of the calcium current and synaptic transmission in lateral line hair cell change during development. Larval hair cells (3.0-5.2 dpf) showed a maximal I_{Ca} of −12.3 ± 1.1 pA (n = 6) which was not significantly different from that recorded in early juvenile hair cells (−13.0 ± 2.9 pA, n = 5; 17-22 dpf) or at later juvenile stages (−10.5 ± 2.7 pA, n = 6; 29-34 dpf). Although I observed no change in the size of I_{Ca} size with development, the corresponding ΔCm did increase. In larval hair cells ΔCm was 2.3 ± 0.5 fF (n = 6) in response to 1 s voltage steps. By early juvenile stages (17-22 dpf) this significantly increased to 7.7 ± 2.3 fF (n = 4, significant at $P < 0.05$, two-tailed Student's t test) and remained at around this value at later juvenile stages (29-34 dpf) with a ΔCm of 6.6 ± 0.6 fF (n = 5, significant at $P < 0.001$ compared to larval cells, two-tailed Student's t test).

This reveals that although the calcium current remained the same size throughout development, the synaptic machinery becomes more efficient at juvenile stages eliciting the release of more synaptic vesicles for the same amount of calcium entry.

5.3.1.4 Supporting cells

In addition to hair cells, each neuromast also contains supporting cells that are positioned below the hair cell body (Chapter 1 and 3). Supporting cells of larval to juvenile hair cells (4-27 dpf) had a cell membrane capacitance of 4.1 ± 0.3 pF (4 – 27 dpf, n = 5) and did not show any voltage dependent currents in their basolateral membrane (Figure 5.8 *A*). The lack of membrane ion channels meant that the supporting cell voltage responses in current clamp were large and passive as shown in Figure 5.8 *B*. This profile did not differ in supporting cells between larval or juvenile stages. The average *I-V* curves measured in supporting cell from both larval and juvenile stages (4-27 dpf) are shown in Figure 5.8 *C*, showing an almost linear relation. Together, these results reflect the absence of voltage-gated ion channels.

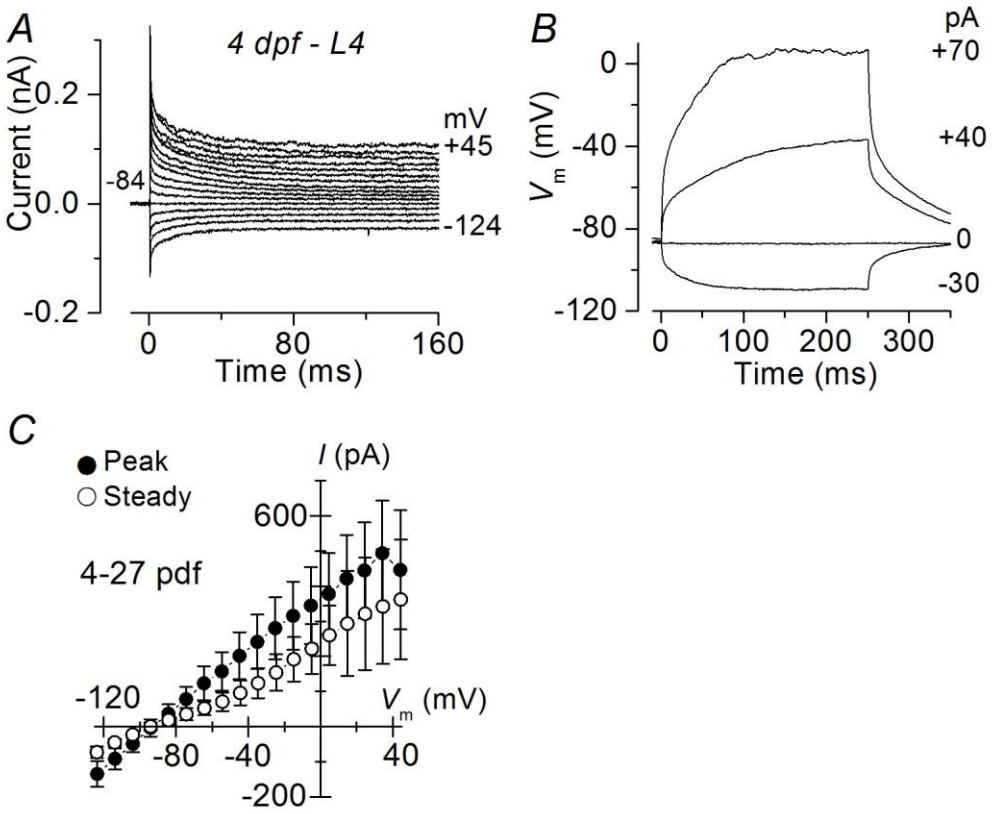

Figure 5.8 Current and voltage recordings from supporting cells in the neuromast of the larval and juvenile zebrafish lateral line.

A, Example of membrane currents recorded from a supporting cell (4 dpf) in neuromast L4. Currents were elicited by depolarizing and hyperpolarizing voltage steps from -124 to + 45 mV in 10 mV nominal increments from the holding potential of −84 mV to the various test potentials ranging from −124 to +45 mV. *B*, Voltage responses to current injections of −30, 0, +40 and +70 pA from the V_m of the individual juvenile supporting cell shown in *A. C*, Average peak and steady-state *I–V* curves from five supporting cells (4–27 dpf), including that shown in *A*.

5.3.1.5 Effect of MS-222 on juvenile hair cells in vitro

Although larval hair cells were not affected by MS-222 (Chapter 4), it has been shown using behavioural experiments that the zebrafish become more sensitive to MS-222 as they get older (Rombough, 2007). In MS-222, cessation of circulation and movement occurs earlier in adult compared to larval zebrafish (Rombough, 2007). Therefore, I decided to investigate whether MS-222 affects

the normal physiology of juvenile hair cells. Zebrafish below 5.2 dpf were injected with α-Btx into the heart to paralyse them. This approach was not possible for juveniles as they are protected animals so they were decapitated (see Chapter 2).

Hair cells in juvenile zebrafish (21-26 dpf) were studied using voltage clamp experiments and subjected to a series of voltage steps in 10 mV nominal increments (200 ms in duration) from –124 mV to + 44 mV starting from a holding potential of –84 mV. Recordings were obtained before, during and after perfusing hair cells with extracellular solution containing 0.01 % MS-222 (Figure 5.9). In the presence of MS-222 the outward current was partially reduced in size, and $I_{K,Ca}$ seemed the most affected (Figure 5.9 *B*), but this was fully reversed upon washout (Figure 5.9 *C*).

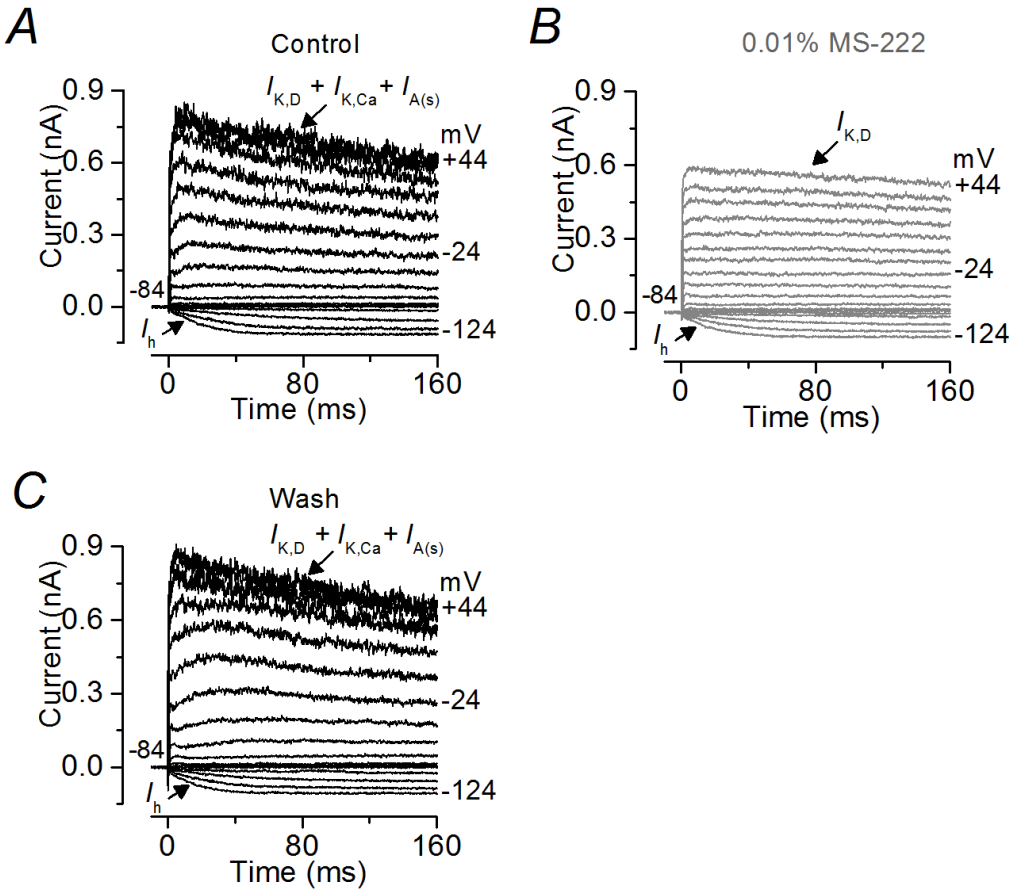

Figure 5.9 Current recordings from hair cells of the juvenile lateral line before and during local application of MS-222.

A–*C*, examples of K+ currents recorded from hair cells at 21 dpf before (*A*), during (*B*) and after (*C*) local superfusion of 0.01% MS-222. Note that MS-222 mainly blocks the Ca^{2+}-activated K^+ current $I_{K,Ca}$ and the small A-type K^+ current $I_{A(s)}$. I_h was not affected by the anaesthetic. Currents were elicited as described in the text.

The average *I-V* curves derived from 4 cells in control conditions (Figure 5.10 *A*) and in the presence of MS-222 (Figure 5.10 *B*), show that MS-222 largely reduced the size of the outward component (Figure 5.10 *B*). The peak outward K^+ current appeared to be most sensitive to the anaesthetic ($P < 0.05$, two-tailed Student's *t* test) which is shown in Figure 5.10 *C*. Therefore it should be concluded that MS-222 is not a suitable anesthetic for juvenile fish, since it affects the physiology and consequently the function of hair cells.

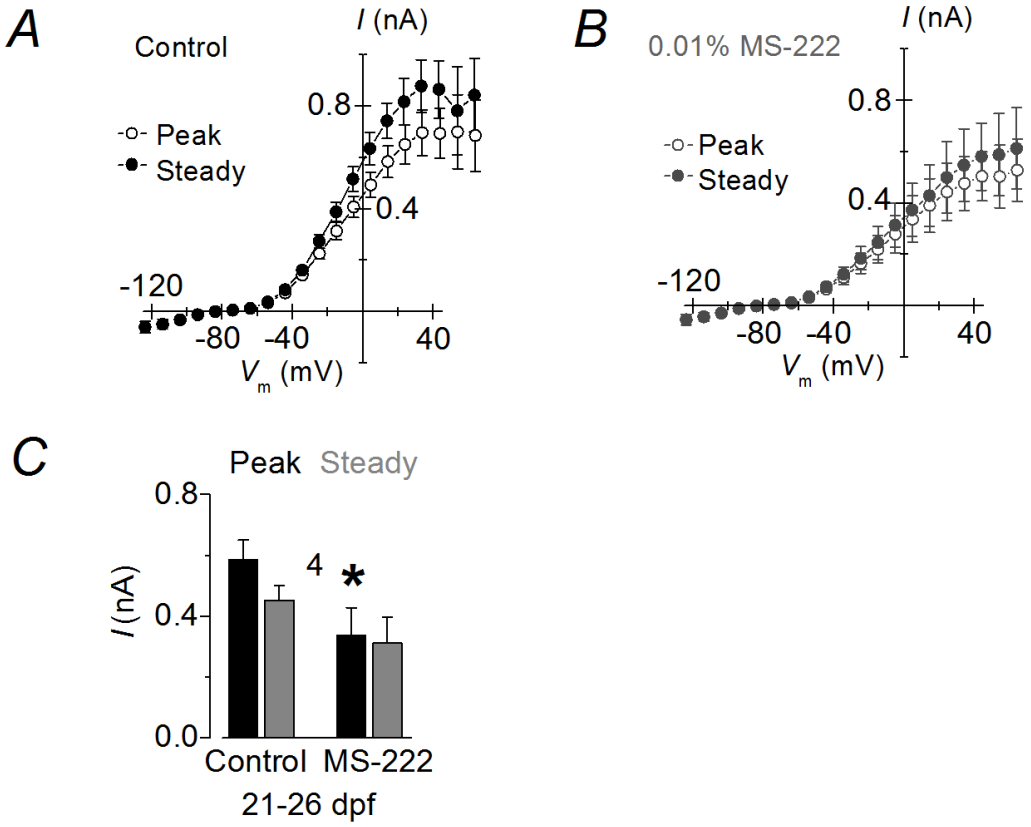

Figure 5.10 *I-V* relationship for recordings from hair cells of the juvenile lateral line before and during local application of MS-222.

A, B, Average peak and steady-state *I–V* curves for the K+ currents recorded before (*A*) and during (*B*) the perfusion of 0.01% MS-222 in four hair cells of 21–26 dpf zebrafish, including the recording shown in Figure 5.9. *C*, Peak and steady-state currents extrapolated at 0 mV before (control, black bar) and during the superfusion of MS-222 (grey bar) in the same four cells. Note that the peak current was significantly reduced in MS-222. Asterisk indicates significance at $P < 0.05$, two-tailed Student's *t* test.

5.3.2 *In Vivo* properties of juvenile zebrafish hair cells

5.3.2.1 Anaesthesia is required to study lateral line hair cells in vivo after 5.2 dpf

The main aim of this part of the project was to use the zebrafish to study the properties of lateral line hair cells *in vivo*. Using decapitated zebrafish, I found that the abundance of K^+ profiles of lateral line hair cells changes at juvenile

stages. Therefore, in order to study the mature function of hair cells *in vivo* a new experimental approach involving an appropriate anaesthetic for older zebrafish had to be developed.

Effect of different anaesthetics on zebrafish behaviour

According to the regulations detailed in the Animals (Scientific Procedures) Act 1986, zebrafish become protected after 5.2 dpf. After this point, experimental work with living zebrafish is tightly regulated and an anaesthetic has to be used. Other than MS-222, which I showed to be unsuitable for studying the function of juvenile hair cells due to its effect on the ion channels, there is a large number of anaesthetics available and a pre-selection was made on the basis of a study focusing on their behavioural effect (Readman et al., 2013). The anaesthetics listed in Table 5.1 below have been selected due to their low aversive properties, i.e. at 50% of the published effective dose they were not detected by the fish, which is required to minimise the stress levels of the animals during anaesthesia (Readman et al., 2013). This pre-selection is compared to MS-222 in Table 5.1 purely because this is the standard anaesthetic for zebrafish.

Table 5.1 Comparison of different anaesthetic agents.

Comparison of different features of three candidate anaesthetics (MS-222, Benzocaine and TBE).

	MS-222	**Benzocaine**	**Tri-bromo-ethanol (TBE)**
Effective dose published	100 mg/L (Carter et al., 2011; Pelkowski et al., 2011)	100 mg/L (Pelkowski et al., 2011)	4 mg/L (Pelkowski et al., 2011)
Target	K^+ channels (Rombough, 2007)	Voltage-gated Na^+ channels (Scholz, 2002)	Generalised CNS depression, target unknown (Posner and Burns, 2009)
Nociception	NA	Yes (Zahl et al., 2012)	unknown
Solubility	In water	In Ethanol	In water
Price per 1 g	£ 2.95	£ 0.28	£ 4.08
Application	Immersion	Immersion	Injection and immersion
Used for fish before?	Yes, mainly trout (Weber, 2011)	Yes, Salmon (Weber, 2011)	Mainly for rodents, as an injectant (Posner and Burns, 2009)

According to the literature, the effective anaesthetic dose of Benzocaine is 100 mg/L (Weber, 2011) and 4 mg/L for TBE. In a pilot-experiment, two adult fish were exposed to each of the anaesthetics using the above doses and, while they became quickly sedated in Benzocaine, TBE had no noticeable effect and fish were culled using a Schedule 1 technique. This finding was not surprising since TBE is an injectable anaesthetic typically used for rodents (Posner and Burns, 2009). In the Readman study it was used via immersion (Readman et al., 2013), but the lack of effect in my findings could be explained by it not being effective at all.

After this trial, only the potency of Benzocaine was further tested using different concentrations (see Table 5.2). The aim was to rapidly induce deep anaesthesia with simultaneous relaxation of muscle tone but keeping the heart beat (for review on stages of anaesthesia in fish see (Sneddon, 2012)).

A concentration of 50 mg/L was deemed optimal, as the zebrafish became sedated within minutes, while the heart was still beating for nearly one hour and yet the dose was terminal.

Table 5.2 Behavioural trial with Benzocaine.

Zebrafish stages of sedation in different concentrations of Benzocaine. For each concentration, three adult (> 1 year) fish were immersed. The anaesthetic was dissolved from the stock in aquarium systems water.

Concentration	N	Time				
		< 2 Min	< 6 Min	< 20 Min	< 40 Min	< 60 Min
10 mg/L	3	No detectable reaction				
30 mg/L	3	Slowed swimming	Drop to bottom of tank, responsive to touch	Still responsive to touch, experiment abandoned		
50 mg/L	3	Drop to bottom of tank, gills moving	Gill movement stopped	Heart still beating (72-102 bpm)	Heart still beating (49-85 bpm)	Cessation of circulation for 2/3 zebrafish used
75mg/L	3	Drop to bottom of tank	Cessation of circulation			

Maintaining gill oxygenation during *in vivo* experiments

The anaesthetics abolish muscle activity, which includes the gill movement. At around 21 dpf zebrafish start using their gills to oxygenate their blood. This means that merely bathing the fish in oxygenated solution is not sufficient to maintain their blood oxygen levels.

In order to overcome this, I decided to saturate the extracellular bathing solution by continuously bubbling it with a carbogen mixture of 95% O_2 and 5% CO_2 gas. However, this had the undesired side effect of filling the swimming bladder with excessive oxygen which made the zebrafish float and impossible to pin it down in the recording chamber. Therefore, zebrafish blood oxygenation was achieved by intubation and delivery of ambient oxygenated extracellular solution (for details see Chapter 3).

5.3.2.2 Possible effect of Benzocaine on hair cell physiological properties

Following the identification of Benzocaine as the ideal anaesthetic for *in vivo* recordings, I tested whether, like MS-222, it affected the physiology of hair cells.

Possible effect of Benzocaine on potassium currents

First of all, I investigated whether Benzocaine affected the K^+ currents present in the hair cell basolateral membrane. This was done by locally superfusing benzocaine onto the hair cell during voltage clamp experiments (Figure 5.11). Hair cells were exposed to double the ideal dose for analgesia described above. K^+ currents were recorded in normal extracellular solution and then with the addition of 100 mg/L Benzocaine. Two examples are given in Figure 5.11 *Ai* and *Bi*. This shows that the current size and kinetics were unaltered when Benzocaine is perfused onto hair cells (Figure 5.11 *Aii* and *Bii*). Both previously described hair cell phenotypes, those expressing $I_{K,Ca}$ and I_A, were not affected.

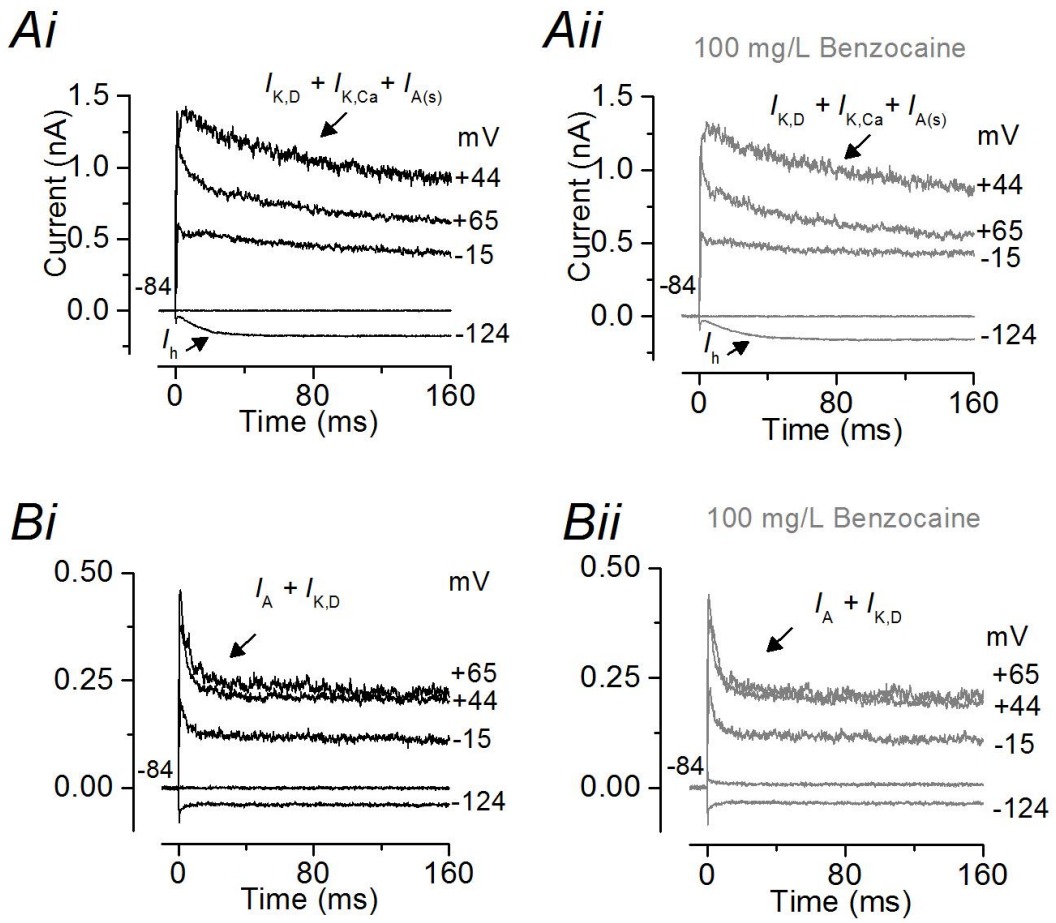

Figure 5.11 Current recordings from juvenile hair cells before and during local application of 100 mg/L Benzocaine.

A–B, Examples of two main types of K^+ currents recorded from hair cells at 25 dpf before (*Ai and Bi*) and during (*Aii* and *Bii*) local superfusion with benzocaine (n = 5). Currents were elicited by voltage steps as shown by the traces from the holding potential of −84 mV.

To gain an overview on the effect of all recorded hair cells, they were pooled to generate *I-V* curves and compared between those in control conditions and those in the presence of Benzocaine (Figure 5.12). The average *I-V* curves contain data from cells with a variety of K^+ phenotypes and are a good measure to assess an overall effect of the anaesthetic. The curves show that 100 mg/L Benzocaine did not change the size of the currents expressed (Figure 5.12 *B*).

I have also tested the effect of 50 mg/L, which was the ideal dose from a behavioural point of view. This did not change the size of the currents in the cells studied, which is shown in *I-V* curves in Figure 5.12 *A*. Lastly, the highest concentration of 300 mg/L did not have any effect on K^+ currents, which can be seen in the *I-V* relationship in Figure 5.12 *C*.

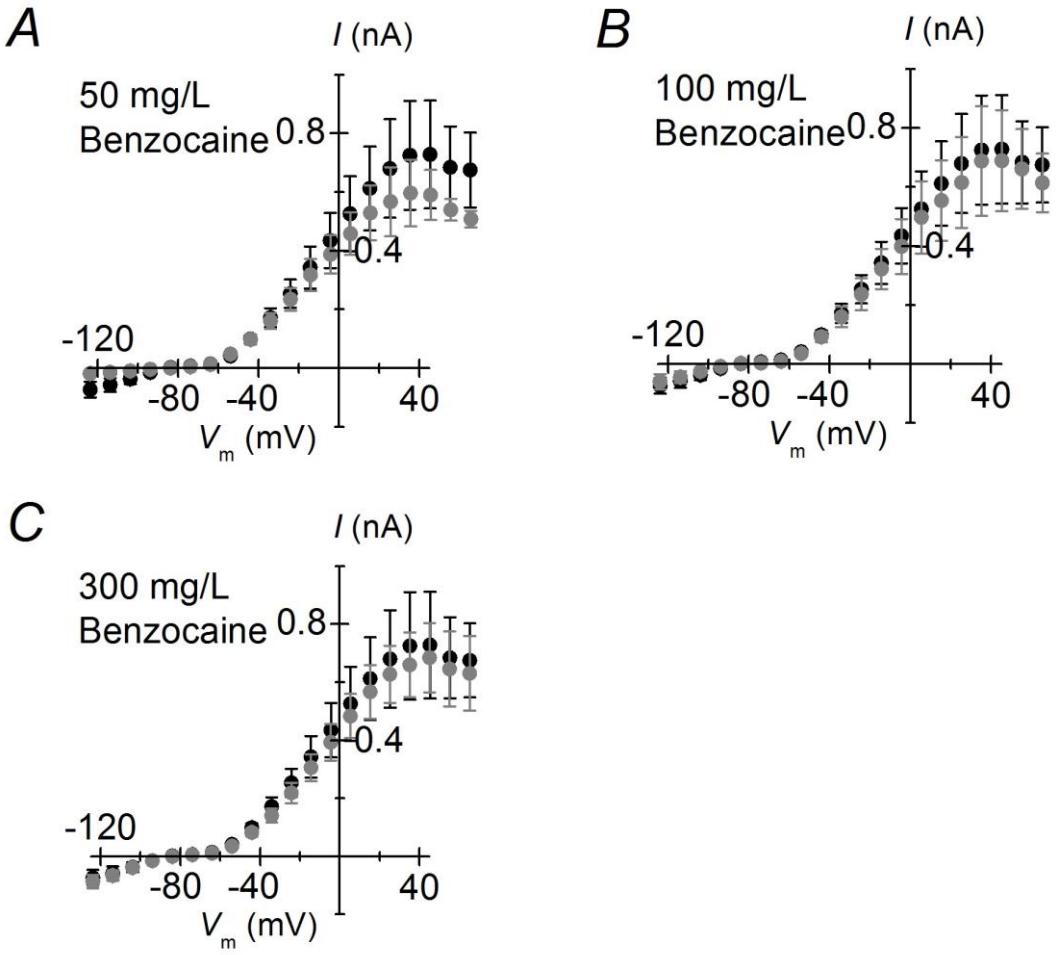

Figure 5.12 *I-V* relationship for hair cells from juvenile zebrafish during the perfusion of different concentrations of Benzocaine.

Average peak *I–V* curves from primary hair cells in the three groups investigated: 50 mg/L Benzocaine, $n = 2$ (*A*), 100 mg/L Benzocaine, $n = 5$ (*B*), and 300 mg/L, $n = 7$ (*C*). *I–V* curves include all recordings shown in Figure 5.11. The peak current is shown in control (black trace) and under 50mg, 100mg or 300 mg/L Benzocaine perfusion (grey trace).

Possible effect of Benzocaine on hair cell synaptic transmission

After confirming that Benzocaine did not alter the basolateral K^+ currents, I tested whether the anaesthetic affected synaptic transmission.

The calcium current was studied using voltage clamp protocols as described earlier (Chapter 4). An example of I_{Ca} in control conditions and in the presence of 100 mg/L Benzocaine is shown in Figure 5.13 *A* and *B* and reveals that it does not alter the size of the current at the peak (Figure 5.13 *C*).

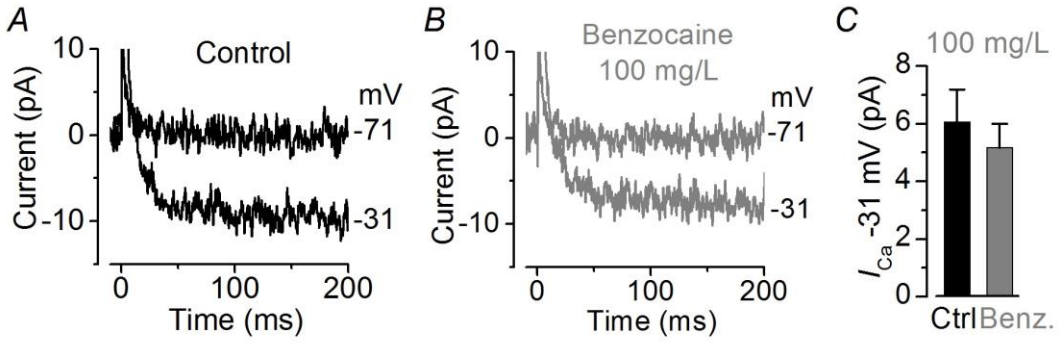

Figure 5.13 Calcium current recording from juvenile hair cells before and during Benzocaine perfusion.

A, B, Example of calcium currents (I_{Ca}) recorded from hair cells of the juvenile (34 dpf) zebrafish lateral line before (black) and during (grey) the local perfusion of 100 mg/L Benzocaine. Currents were elicited by depolarizing voltage steps of 10 mV increments (200 ms in duration) from the holding potential of −79 mV. For clarity only the traces at the holding potential and near the peak of I_{Ca} (−31 mV) are shown. *C*, Average size of the calcium current at its peak (~ -31 mV), before (black) and during (grey) the perfusion of 100 mg/L Benzocaine, n = 7. Recordings were performed at 28 °C.

I then investigated whether the synaptic vesicle release that is induced by I_{Ca} was altered. Hair cells were depolarised for 1 sec to near the peak of the I_{Ca} and the induced exocytosis (ΔCm) was measured. An example is given in Figure 5.14 and shows that the size of the ΔCm is similar in control (*A*) and in the presence of

benzocaine (*B*). Average ΔCm (n= 4) further confirmed that benzocaine does not affect vesicle release (Figure 5.14 *C*).

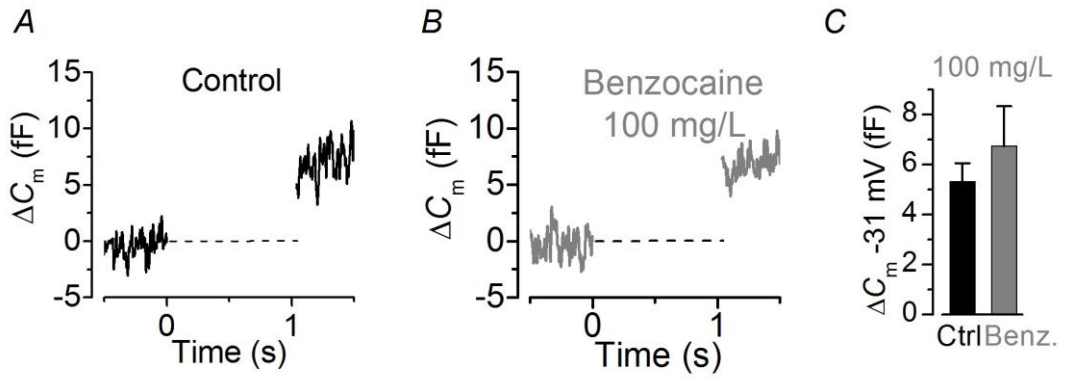

Figure 5.14 Capacitance changes recorded from juvenile hair cells before and during the perfusion of 100 mg/L Benzocaine

A, *B*, Examples of ΔCm recorded from hair cells of 31 dpf zebrafish before (*A*) and during (*B* grey) the perfusion of 100 mg/L Benzocaine. Recordings were obtained in response to 1 s voltage steps from the holding potential of −79 mV to near the peak of I_{Ca} (near −30 mV). *C,* Average ΔCm size from 4 hair cells before (black bar) and during (grey bar) the perfusion of 100 mg/L Benzocaine. Recordings were obtained at 28 °C.

5.3.2.3 In vivo properties of juvenile zebrafish hair cells

This new *in vivo* approach was then used to assess the basolateral membrane properties of lateral line hair cells in a fully intact adult zebrafish and compared to those obtained from *in vivo* recordings from larval hair cells.

Juvenile zebrafish were intubated using a cannula (Chapter 3) and hair cells from 34 to 48 dpf fish were voltage clamped. Two examples of the currents (Type 1 and 3) recorded are given below (Figure 5.15). They show the I_A with little or no inward current (I_h) (Figure 5.15 *A*) and the $I_{K,Ca}$ with a small I_h (Figure 5.15 *B*). These current profiles have been found throughout all developmental stages.

I then measured the size of the outward current at 0 mV for peak and steady-state. These were compared by *in vivo* recordings of larval and juvenile zebrafish

and were significantly smaller in juveniles. (Figure 5.15 *C,* significant at $P < 0.05$, two-tailed Student's *t* test).

This further strengthens my previous finding that larval and juvenile hair cells have different proportions of K^+ current types from larval to juvenile stages, even though the types of K^+ current profiles expressed are similar.

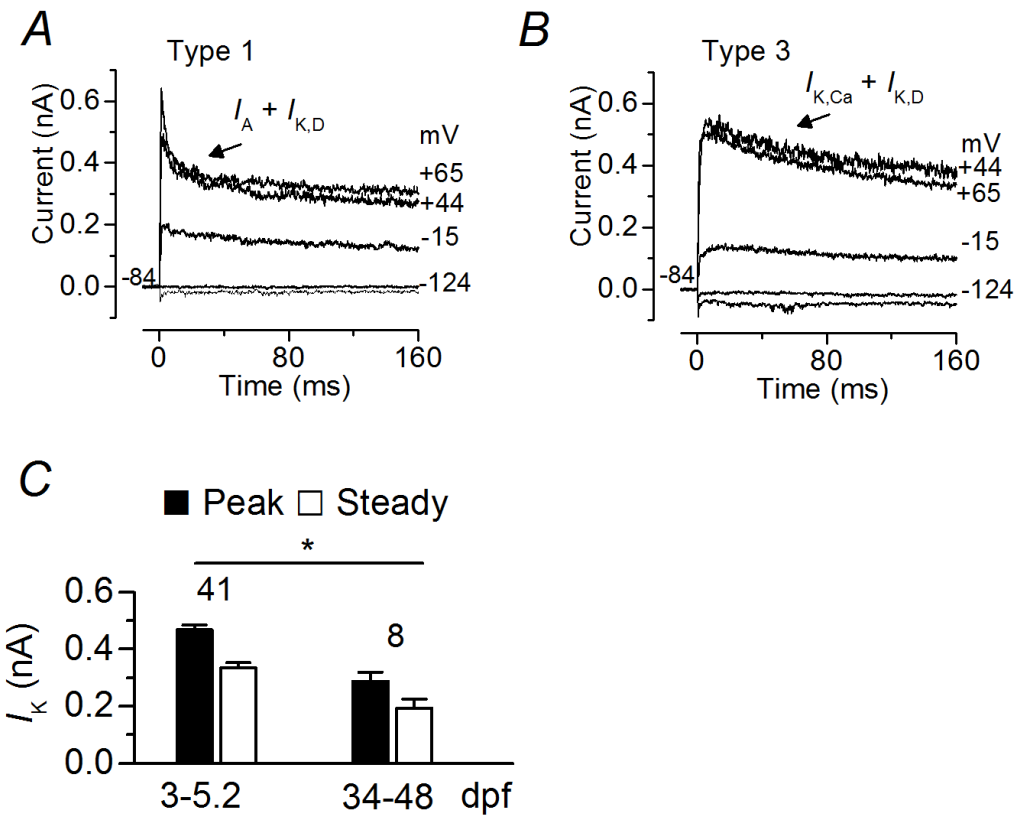

Figure 5.15 *In vivo* potassium currents in juvenile hair cells.

A, *B*, Examples of K^+ currents recorded from hair cells of 34 dpf (*A*) and 48 dpf (*B*) zebrafish. Currents were elicited by voltage steps as shown by the traces from the holding potential of – 84 mV. *C*, Comparison of the average size of the peak and steady state K^+ current values recorded *in vivo* from larval and juvenile zebrafish hair cells, asterisk indicates statistical significance at $P < 0.05$, two-tailed Student's *t* test. N-numbers are given above the data.

5.4 Summary

Zebrafish lateral line hair cells exhibit a variety of K^+ currents at larval stages with three different subtypes (Chapter 4). Investigating juvenile hair cells yielded the following results:

- Juvenile hair cells (> 20 dpf) exhibit all three K^+ current phenotypes as well.
- From larval to juvenile stages, the abundance of these types changes with the $I_{K,Ca}$ being dominant at larval stages and the I_A becoming the main type in juveniles.
- The synaptic machinery becomes more efficient at juvenile stages compared to larvae
- Juvenile hair cells become more sensitive to MS-222, a common anaesthetic for zebrafish

Furthermore, an approach to study older hair cells *in vivo* has been developed:

- The ideal anaesthetic for this is Benzocaine, which is nociceptive
- Benzocaine does not alter the basolateral membrane currents as well as the synaptic transmission

5.5 Discussion

Juvenile hair cell function

The most striking finding of this chapter is that the three types found in larval lateral line hair cells are also present in juvenile fish about 4 weeks later. Juvenile hair cells still express cells with either an A-type current (Type 1), a BK-current (Type 3) or delayed rectifier with small A-type (Type 2). The effect these current have on the voltage change appears to be also unaltered at later stages, with Type 3 cells mediating the fastest and smallest response, whereas Type 1 cells have slower and larger responses. This strengthens the notion, that these types are already functionally mature at larval stages.

Interestingly, the abundance of these types does change over time. There are several reason for this: Firstly, there could be a bias towards recording one type over the other, for reasons such as easier access or stability. Seeing that 146 cells were recorded in total in the juvenile and there was no great difficulty in obtaining recordings of any cell, this seems unlikely.

Secondly, the sensory environment of the fish changes in such a way, it would require more cells with a specific function over the other. Indeed, even though the fish is functional at 5 dpf, there are some crucial behavioural changes that occur in the next few weeks. For example, during larval stages fish exhibit burst like swimming and escapse responses (Buss and Drapeau, 2001) while later on, they are capable of undulating swimming at different velocities (Mueller and van Leeuwen, 2003). This is due to the increase in size of the fish and the acquirement of a more streamlined body shape (Mueller and van Leeuwen, 2003). Zebrafish sleep without moving, which creates a need for a fast escape response especially at later stages.

The fact that the types of currents do not change over time suggests that their function is still the same, but perhaps the requirement is altered. This is highly speculative, but if the Type 1 cells (A-type) are indeed required for continued transmission of stimulation, with a bigger gain and being involved in velocity sensing, this could become more important at later stages where the fish is able to swim faster and regulate it's swimming pattern more. This correlation might be reflected in the presence of more A-type expressing cells.

On the contrary, as for the Type 3 cells (BK-current) that allow fast transmission and almost on-off signalling, if these are still important for escape responses, it is not surprising that they are still present. It is unclear, why there are less of the Type 3 than Type 1, as certainly escape responses are more crucial for survival than velocity sensing. At the moment, details of the afferent innervation and escape circuitry at juvenile stages are unknown. But is has been shown that hair cell activity activates the Mauthner cell, which is directly involved in mediating the escape response (Lacoste et al., 2015). Perhaps, the number of Type 3 cells form stronger connections to the Mauthner cell over time, so there is no need for

a larger number of them. Equally, the Type 1 cells would be required in larger numbers. Since they seem to work in a more gradual fashion, more cells would be required to be recruited during stimulation, because the sensitivity of the individual cell is small. As for the Type 2 cells, it is intriguing whether they are similar to immature vestibular hair cells. Their expression of a delayed rectifier would make them functional in a basic way, but perhaps they acquire additional K^+ currents later on.

This hypothesis would need extensive further investigation, such as details on where the afferent neurons of each cell type go or whether there is any preference in innervation in the first place. It is very likely, that this is a complicated matter as has been shown in the vestibular system. Even though, it comprises two distinct cell types (Type I and II) and two distinct afferent neuron types (regular and irregular), the majority of synapses is mixed and there is no clear correlation between the types of hair cell and neuron but rather with position within the epithelium (Eatock and songer 2011). Equally the finding of different cell types in specific locations of the neuromast is puzzling and could be related to differentiation or regeneration in the periphery of the tissue. However, this does not rule out that most hair cells are functionally mature.

The finding that the synaptic machinery becomes more efficient is intriguing. Due to the nature of the experiment that involves blocking K^+ currents to isolate the I_{Ca}, it was not possible to determine which cell type was investigated. Despite the size of the calcium current staying small, the number of vesicles that fuse after a 1 second stimulation is increased by around threefold. The most straightforward explanation for this is a closer association of the calcium channel to the ribbon body. In mouse hair cells, it has been shown that the calcium channel is scattered around the basolateral membrane at pre-hearing stages. Later on, it then localises tightly to the ribbon bodies at the presynaptic zone. A similar scenario in fish could be the case. Also, in larval fish, it has been shown that the ribbon clusters calcium channels to the presynaptic zone and ribeye knockouts have scattered calcium channels (Sheets et al., 2012). Even though it is unknown whether the ribbon body changes after 5 dpf in fish, it has been shown in gerbils

that it develops from a round, ball like shape to a ovoid shape. If this is the case in the fish too, this could be responsible for the increase in efficiency.

Another possible explanation is an addition of more or different calcium sensors, that make the machinery more sensitive. Otoferlin or synaptotagmins would be candidates for this. Particularly synaptotagmin 4 has been shown to gain importance in adult IHC where it increases the sensitivity (Johnson et al., 2010). Finally, the increased vesicle release could be explained by alterations in intracellular calcium buffering at juvenile stages, where more calcium could be available to trigger release.

Understanding the underlying reasons for the change in efficiency could be extremely difficult, mainly because the signal is so small and the 1 second stimulation will recruit both the ready releasable and secondary pool. This makes investigating the role of different calcium sensors or buffers highly unfeasible using electrophysiological techniques.

On the other hand, TEM or immunostaining could give a very good idea as to whether the calcium channel cluster does indeed change and whether this is accompanied by a change in ribbon size or shape.

Using anaesthethics to study juvenile hair cells

The finding that the juvenile lateral line comprises a different number of hair cell types than the larvae and the fact that juvenile fish remains underexplored in general beyond 5 dpf has lead us to develop an approach to study juvenile fish *in vivo*. Benzocaine appears to be the ideal anaesthetic as it does not affect hair cell properties. However, as it works via blocking voltage gated sodium channels, it is expected to reduce neuronal firing. This poses a great obstacle for studies on afferent signalling from the hair cell and further investigations are required.

For other studies that do not involve primarily neurons, such as hair cell regeneration, infection and bone regeneration the use of benzocaine could be a useful approach to study the juvenile fish. But further investigations into its safety and effect on neurons are required.

Chapter 6 Biophysical Properties of Zebrafish Inner Ear Hair Cells

6.1 Introduction

The finding that the lateral line shows three different phenotypes for the basolateral membrane currents and the conclusion that these are likely to be linked to function consequently leads to the question of what the precise function is.

Answering this question is difficult and time consuming. However, a first and straightforward attempt would be to compare it to a known entity. How do the lateral line hair cells compare to the hair cells in the zebrafish inner ear? The inner ear consists of six sensory epithelia. The cristae at the end of the semicircular canals sense rotational acceleration, while the maculae sense linear acceleration. The utriclular macula senses balance, whereas the sacculus is responsible for audition and the lagena is presumably involved in both. Comparing the properties of their hair cells to the lateral line might provide an indication of their role. The development of the inner ear starts around the same time as the lateral line during the first day post fertilisation and by 2 dpf the first hair cells appear. By 3 dpf, electrical activity of hair cells can be measured, suggesting their functionality (Lu and DeSmidt, 2013).

In this chapter, the basolateral membrane properties, mainly the K^+ currents, of hair cells in the three maculae will be briefly described. Since all three tissues carry different functions, this is expected to be reflected in their K^+ profiles. Utricular hair cells might match vestibular hair cells in lower and higher vertrebrates with two distinct types. Saccular hair cells might exhibit electrical tuning, which is a common feature of lower vertebrate auditory hair cells. And finally lagenar hair cells potentially show a mixture of the two, reflecting their shared function.

6.2 Brief methods

For general methods about animal handling, electrophysiological recordings and statistical analysis see Chapter 2. Briefly, inner ear hair cells of all maculae of adult zebrafish (> 1 year) were investigated. For the lagena, hair cells of zebrafish

> 8 weeks could be dissected too. The dissection of the inner ear organs from the zebrafish are described in detail in Chapter 3.

Membrane potentials in voltage clamp were corrected for the voltage drop across the uncompensated residual series resistance (*R*s: 3.1 ± 0.2 MΩ, *n* = 54) and for a liquid junction potential (Chapter 2). Current responses are referred to a holding potential of −84 mV or −79 mV unless specified, and are set to 0-current for comparison between hair cells. All inner ear hair cells had a mean capacitance of 3.6 ± 0.1 pF (*n* = 54).

Calcium currents (I_{Ca}) were recorded in the presence of 2.8 mM extracellular calcium and at 28.5°C. The isolated I_{Ca} was obtained by blocking the known K^+ conductances with a cocktail of blockers contained in the intracellular solution (Chapter 2).

Phalloidin staining: Adult zebrafish were culled using 0.017 % MS-222 until cessation of blood circulation and then decapitated. Heads were placed in a fixative solution containing 4% formaldehyde in 0.1 M sodium phosphate for 2 hrs at room temperature. Whole otolithic organs were carefully dissected from the labyrinth and washed three times in PBS. The dissected organs were incubated for 2 hrs in a solution containing 10% heat-inactivated horse serum, 0.1% Triton X-100 (TX-100) and Texas Red-conjugated phalloidin to label F-actin (1:300; Molecular Probes, Inc., Eugene, Oregon, USA) in PBS. The tissue was then washed three times in PBS and mounted on glass coverslips using Vectashield mounting medium. Nail varnish was used to seal the coverslip onto the slide. Images were taken using an Olympus microscope equipped with a 20X objective and epifluorescence illumination.

6.3 Results

6.3.1 Electrical properties of saccular hair cells

The sacculus, which detects up to about 3000 Hz in the zebrafish, is supposed to be tonotopically organised along its anterior posterior axis (Smith et al., 2011), with the anterior part containing the highest and posterior part the lowest

frequencies (Smith et al., 2011). Recordings were performed in different locations (Figure 6.1) to assess whether the cell properties vary with frequency location. Phalloidin staining shows the two different regions within the sacculus used to record the electrophysiological properties of hair cells: edge (yellow cloud) and centre (red cloud) (Figure 6.1). Because of the difficulties associated with the dissecting procedure, only the posterior/caudal portion of the sacculus could be dissected, which contains hair cells responding to a frequency range between 100 Hz (most posterior) and 800 Hz (medial part) (Smith et al., 2011).

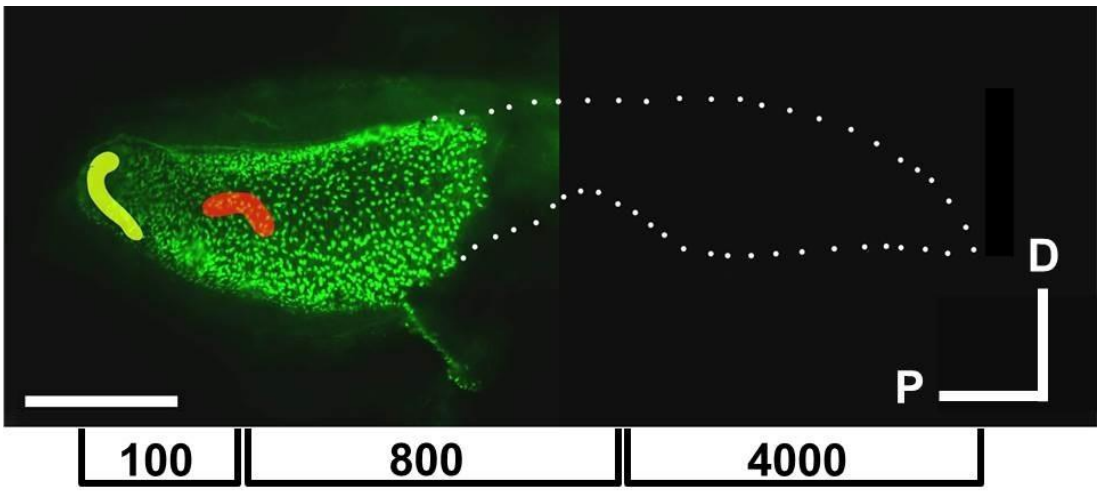

Figure 6.1 Recording sites in the adult sacculus.

Phalloidin-stained hair bundles of saccular hair cells from adult (>1 year) zebrafish showing the central region encoding medial frequencies (red) and the edge sensing a low frequency range (yellow). Both regions were sampled to obtain the electrophysiological recordings. 100, 800 and 4000 refers to the rough frequency range found in saccular hair cells (Smith et al., 2011). The dotted line delineates the entire sacculus, including the unlabelled portion that could not be successfully removed from the inner ear. P, posterior; D, dorsal. Scale bar: 120 μm.

6.2.1.1 Current responses of saccular hair cells

Voltage clamp experiments in saccular hair cells were used to record membrane ion currents elicited over a range of membrane potentials spanning from -140 mV to +40 mV. This voltage range was selected in order to determine the full composition of the different voltage-gated membrane currents expressed in hair cells. Saccular hair cells showed two main current profiles (Figure 6.2 *A, B*). Cells located in the central part of the tissue, where frequencies of 800 Hz are sensed, showed an inward rectifier K^+ current ($I_{K,1}$). $I_{K,1}$ is found in murine hair cells too and is characterised by its rapid activation, little inactivation and strong inward rectification negative to -80 mV (Marcotti et al., 1999). In zebrafish saccular hair cells, for the -140 mV step, the current showed time-dependent decay (Marcotti et al., 1999). These hair cells also have an outward delayed rectifier current termed $I_{K,D}$, which showed a much slower activation kinetics than $I_{K,1}$ (Figure 6.2 *B*). Hair cells from the edge, which encoded frequencies around 100 Hz of the tissue showed a different K^+ current profile with a slowly activating hyperpolarisation activated K^+-Na^+ current (I_h), and a rapidly activating and inactivating A-type outward current (I_A), which were combined with a delayed rectifier ($I_{K,D}$) (Figure 6.2 *C*). The current-voltage relation (*I-V* relation) for the two cell populations is shown in Figure 6.2 *D* and reveals no difference in the overall size of the peak outward currents. The presence of the different inward currents between hair cells of the edge and centre was also highlighted by the *I-V* relation (Figure 6.2 *C*). The above current types have been identified based on their characteristic kinetics and voltage-dependence (Figure 6.2 *C*) which match very closely those previously described in other systems (Sugihara and Furukawa, 1989, 1995; Eatock et al., 1998).

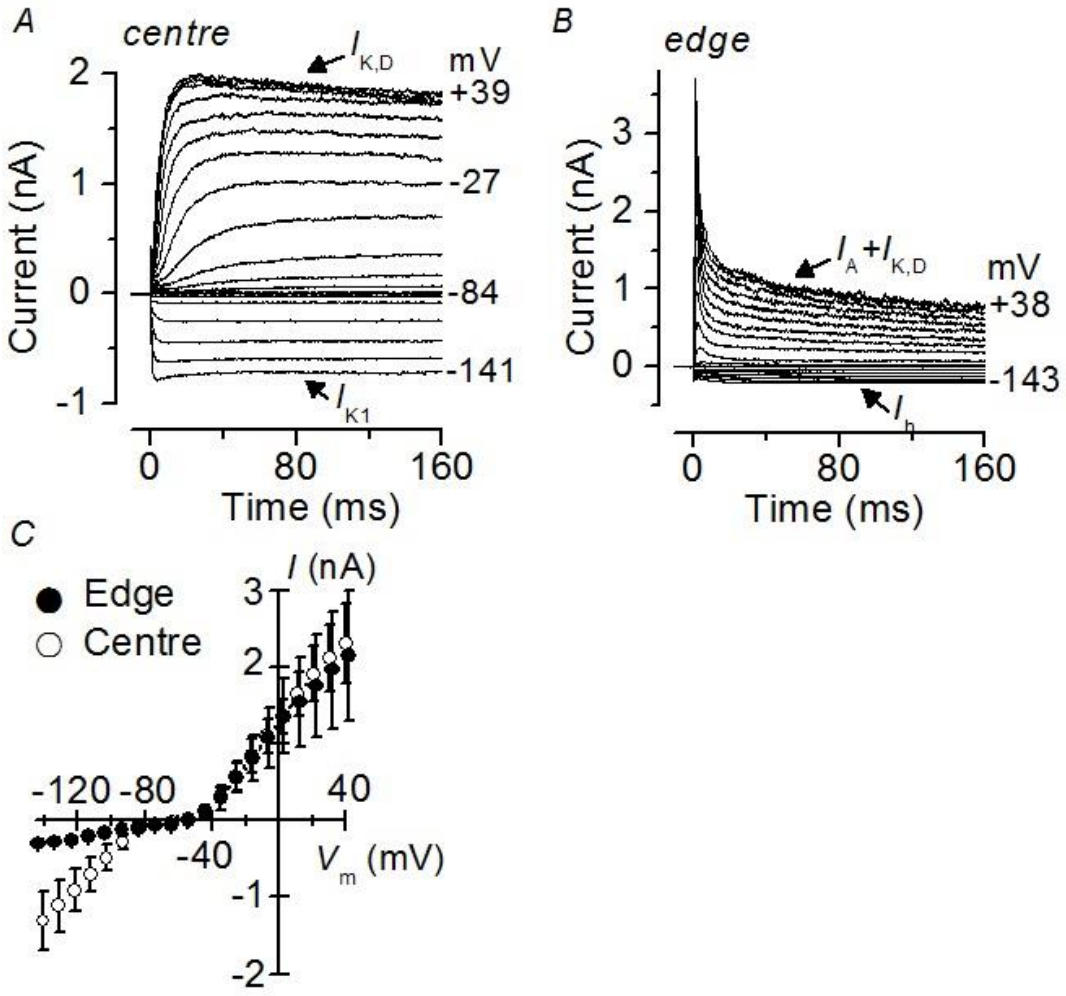

Figure 6.2 Membrane currents from hair cells in the sacculus of adult zebrafish.

A, B typical K^+ currents from hair cells positioned in the centre (*A*) and edge (*B*) of the sacculus in adult (> 1 year) zebrafish. Currents were elicited by depolarizing and hyperpolarizing voltage steps in 10 mV nominal increments from the holding potential of −84 mV to the various test potentials shown by some of the traces. Note that in the central region four hair cells showed the profile depicted in *A* and one showed that in *B*. In the edge, all three cells were as in *B. C*, average peak *I–V* curves from hair cells in the centre (n = 5) and edge (n = 3), including those in *A* and *B*.

6.2.1.2 Voltage responses of saccular hair cells

Next, I have investigated the functional role, in terms of size and speed of the voltage change, of these different K^+ current profiles on the membrane potential of saccular hair cells, which gives an indication of the speed and size of the response that the inner ear hair cells have in order to fulfil their task.

In current clamp experiments, single hair cells were injected with currents ranging from -30 pA to +70 pA in -10 pA nominal increments from the resting membrane potential of the individual cell. Saccular hair cells had an average V_m of −70.7 ± 3.5 mV (n = 7) and capacitance of 3.2 ± 0.4 pF (n = 8). The two cell types described above (Figure 6.3 *B, C*) showed distinct voltage responses. In the centre, hyperpolarising steps elicited small voltage changes in hair cells (Figure 6.3 *A*). This is due to the large, fast and sustained activation of I_{K1} which drives K^+ ions into the cell, thus preventing the membrane potential to hyperpolarise below about - 85 mV for a current injection of -30 pA. Depolarising steps elicited broad spikes or membrane oscillations lasting between 30 and 80 ms (Figure 6.3 *A*), which is due to the activation of the calcium current that initially depolarises the cell membrane. Hair cell repolarization is achieved by the slowly-activating $I_{K,D}$ (Figure 6.3 *A*). These spike-like changes in membrane potential resemble the electrical tuning found in many hair cells of lower vertebrate such as the frog and turtle (Fettiplace and Fuchs, 1999).

Hair cells from the edge showed a voltage sag upon hyperpolarising current injection, indicative of the h-current (Figure 6.3 *B*). Cells from the edge could hyperpolarise more compared to cells from the centre, which is due to the I_h being relatively small in these cells. Depolarising current steps did not lead to a big voltage change in the membrane potential, which was quickly clamped with no oscillations during the 240 ms tested, which was due to the fast activation of the outward I_A. The subsequent activation of the $I_{K,D}$ prevented further depolarisation.

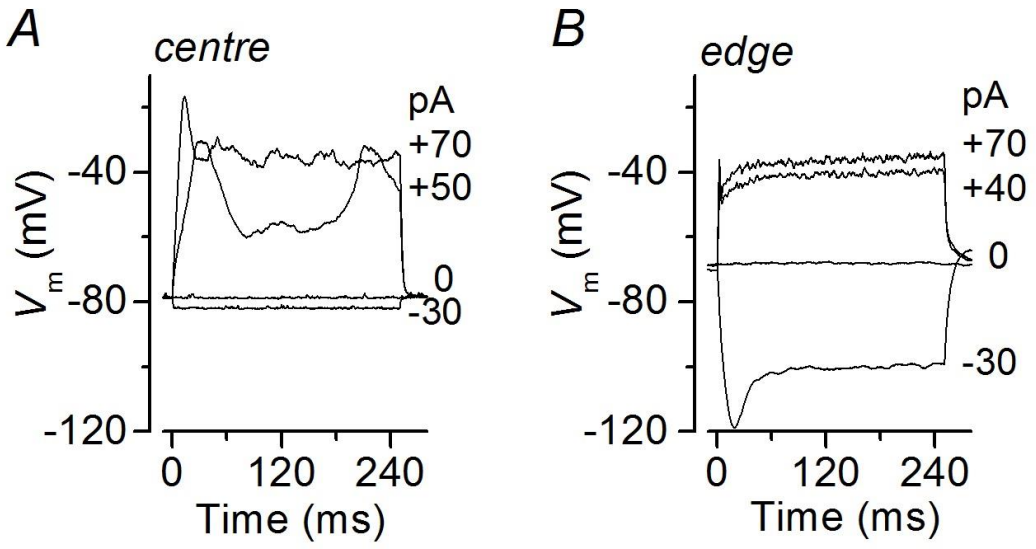

Figure 6.3 Membrane voltage responses from adult hair cells of the sacculus.

A, B, Voltage responses to the different current injections shown next to the traces in 10 pA nominal increments from the V_m of the individual cell. Voltage responses recorded from hair cells positioned in the centre (*A*) and edge (*B*) of the sacculus in the adult (> 1 year) zebrafish.

6.3.2 Electrical properties of utricular hair cells

Utricular hair cells are mainly associated with vestibular function and sense frequencies up to 10 Hz and their biophysical properties were investigated using the same protocols as described in Figure 6.2 and Figure 6.3. Similar to the sacculus, hair cells from the utricles were recorded from the centre and edge (Figure 6.4) in order to compare the current profile from the two different sensory organs. This was done to assess whether the two different functions carried by sacculus and utricle are reflected in their current profiles.

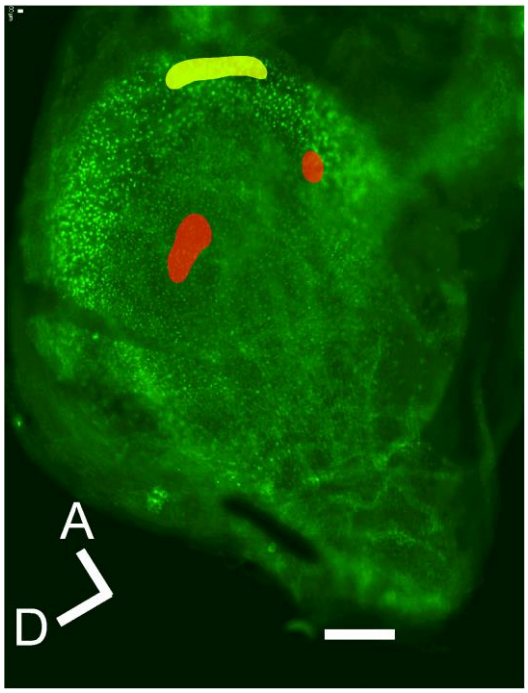

Figure 6.4 Recording sites in the adult utricle.

Phalloidin-stained hair bundles of utricular hair cells from adult (> 1 year) zebrafish showing the central (red) and edge (yellow) regions used for the recording. A, anterior; D, dorsal. Scale bar: 120 µm.

In voltage clamp experiments, the majority of utricular hair cells from both the centre and edge regions (nine out of 10 cells) expressed the fast outward I_A combined with outward $I_{K,D}$. The peak and steady-state overall size of the outward K^+ current at 0 mV was 1432 ± 197 pA and 397 ± 83 pA (n = 10), respectively. They also express a slowly activating inward I_h (Figure 6.5 *A*), which is also reflected in the *I-V* curve (Figure 6.5 *B*). These utricular hair cells show current profiles similar to those seen in the edge of the sacculus (Figure 6.2).

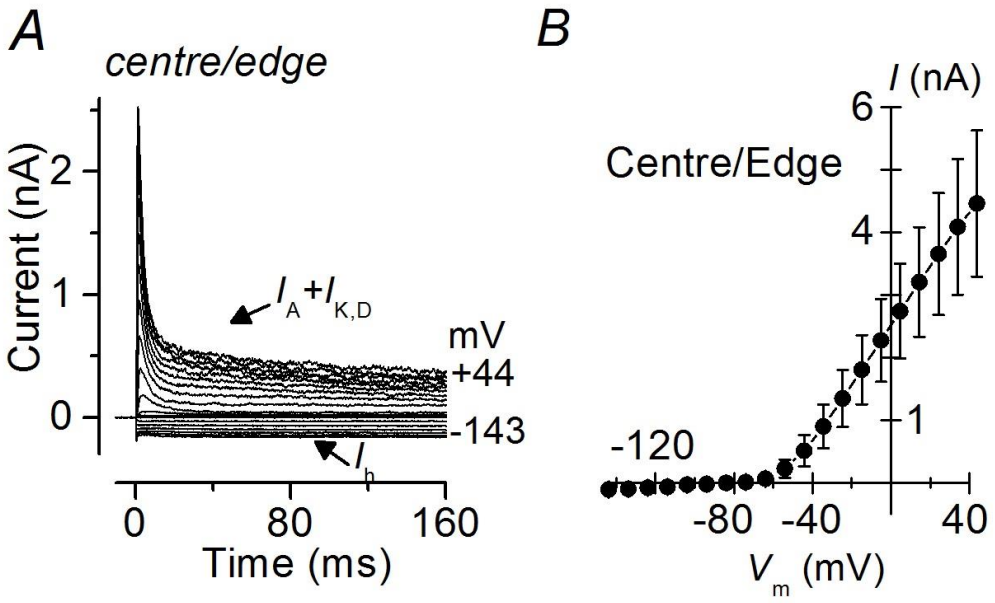

Figure 6.5 Currents responses from hair cells of the utricle in adult zebrafish.

A, Example of K^+ currents recorded from a utricular hair cell; Currents were elicited by depolarizing and hyperpolarizing voltage steps in 10 mV nominal increments from the holding potential of −84 mV to the various test potentials shown by some of the traces. *B,* Average peak *I*–*V* curves from all hair cells in the centre and edge, including that in *A*.

For the majority of the utricular hair cells, current clamp experiments revealed a similar behaviour of the membrane to current injection as seen in the sacculus (Figure 6.6). For negative current injections, utricular hair cells show a voltage sag that is due to the slowly activating I_h which prevents continued hyperpolarisation below 90 mV. To positive current injections, the cells respond with a small depolarisation that is quickly (~ 5 ms) clamped by I_A with no oscillations. However, I_A inactivates rapidly leading to a slow depolarisation, which is then maintained by the slow activating $I_{K,D}$ (Figure 6.6). Utricular hair cells had an average V_m of −71.2 ± 2.2 mV (n = 8) and capacitance of 3.2 ± 0.2 pF (n = 11).

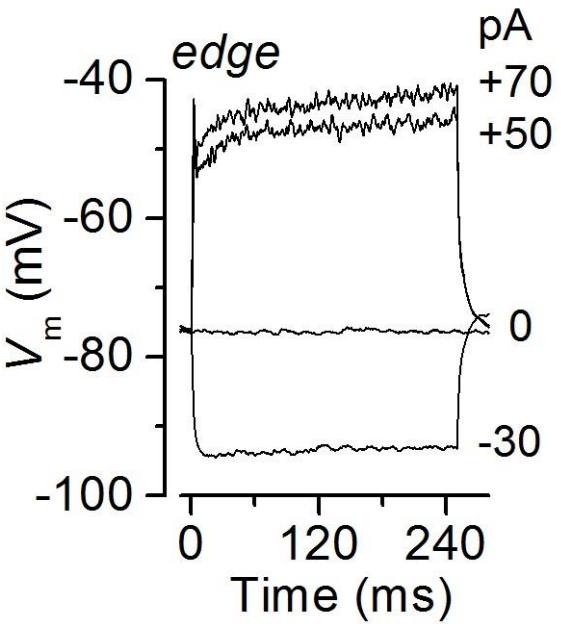

Figure 6.6 Voltage responses from a hair cell in the utricle in adult zebrafish.

Voltage responses to the different current injections shown next to the traces from the V_m. Voltage responses recorded from a hair cell positioned at the edge of the utricle.

Only one out of 10 cells investigated, which was positioned at the edge of the epithelium (Figure 6.7 *A, B*), showed an inward I_{K1} instead of I_h and a large $I_{K,D}$ with a smaller I_A This cell resembled that found in the centre of the sacculus but did not show any oscillations to positive current injections (Figure 6.7 *B*).

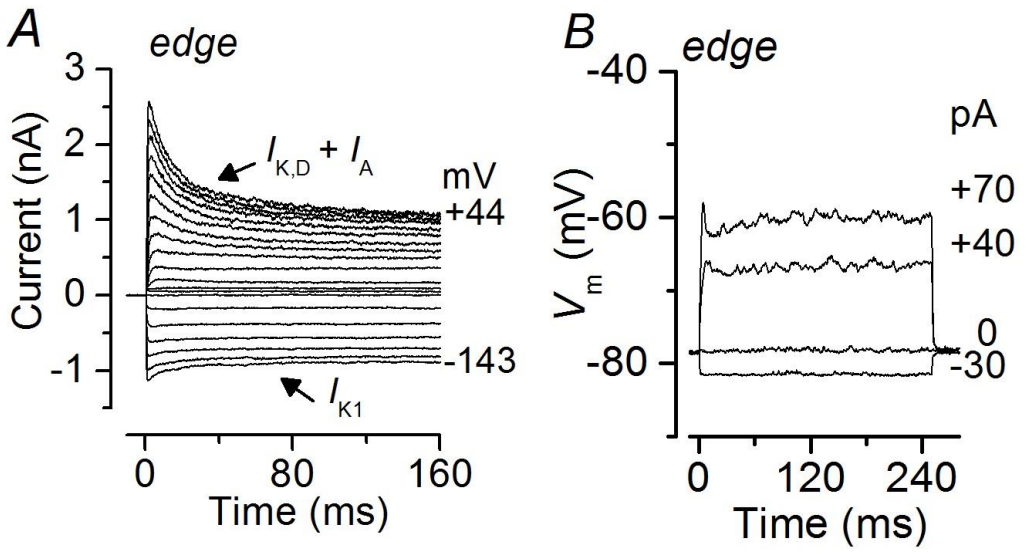

Figure 6.7 Membrane currents and voltage responses from a single hair cell in the edge of the utricle.

A, Currents were elicited by depolarizing and hyperpolarizing voltage steps in 10 mV nominal increments from the holding potential of −84 mV to the various test potentials shown by some of the traces. *B*, Voltage responses to the different current injections shown from the V_m. Voltage responses recorded from a hair cell positioned at the edge of the utricle of the adult (> 1 year) zebrafish.

6.3.3 Electrical properties of lagenar hair cells

6.3.3.1 Current and voltage responses from hair cells of the lagena

As for the sacculus and utricle, recordings were performed from hair cells located in the centre and edge of the lagena (Figure 6.8), the aim of which was to identify possible positional specialization in the biophysical properties of these cells.

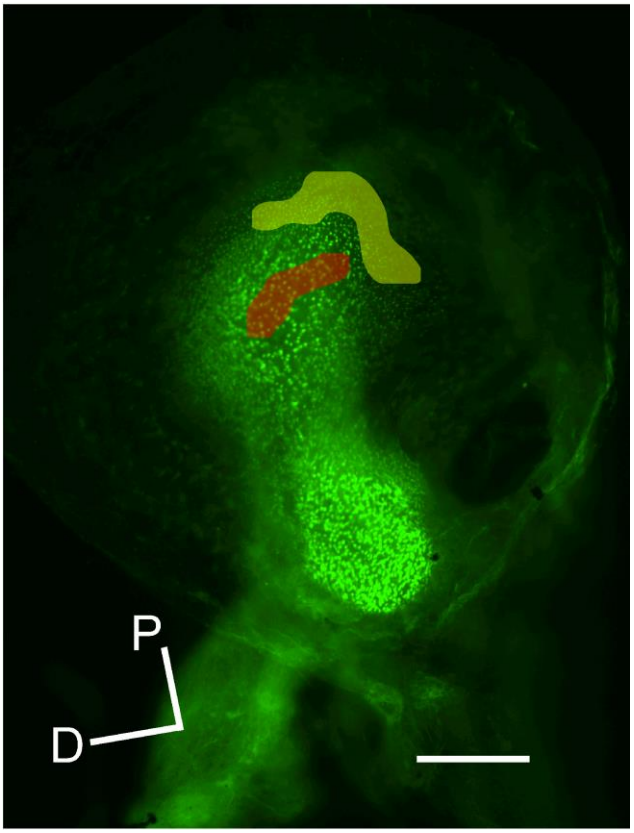

Figure 6.8 Recording sites in the adult lagena.

Phalloidin-stained hair bundles in an adult (> 1 year) zebrafish lagena showing the central (red) and edge (yellow) regions of the posterior sensory organ used for the recordings. P, posterior; D, dorsal. Scale bar: 120 μm.

In voltage clamp, hyper- and depolarising voltage steps caused hair cells to elicit two main current profiles (Figure 6.9 A and B). The current profile of hair cells located in the centre of the lagena is characterised by a slowly developing outward $I_{K,D}$ and an inward I_{K1} (Figure 6.9 *A*). The profile of cells positioned in the edge includes a rapid activating and inactivating I_A and delayed outward rectifier $I_{K,D}$ and slowly developing inward I_h (Figure 6.9 *B*).

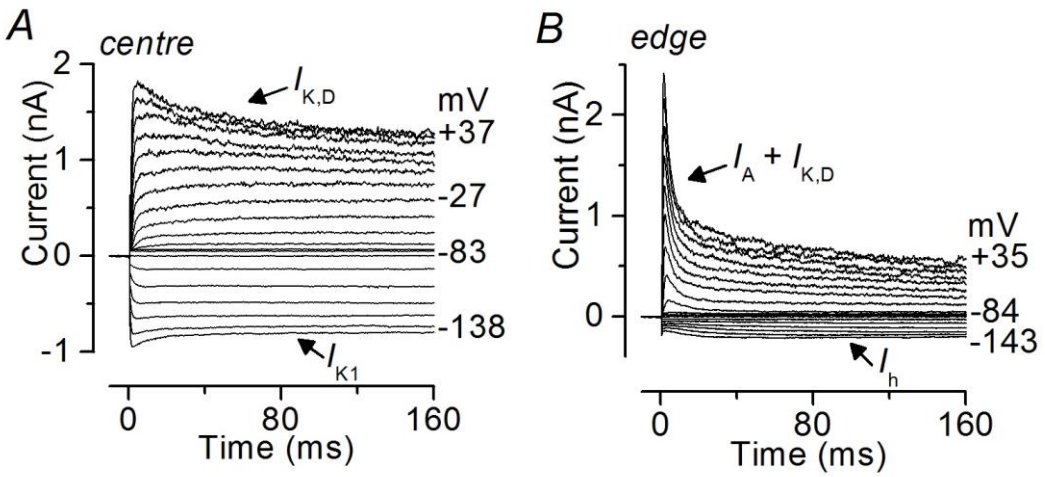

Figure 6.9 Membrane current responses from hair cells of the lagena in adult zebrafish.

A, B, typical K^+ currents from hair cells positioned in the centre (*A*) and edge (*B*) of the lagena. Note the different current profiles. Currents were elicited by depolarizing and hyperpolarizing voltage steps in 10 mV nominal increments from the holding potential of −84 mV to the various test potentials shown by some of the traces.

In Figure 6.10 *A,* the *I-V* relationship for the peak current for all cells recorded in the centre (n = 3) and edge (n = 4) is shown. Hair cell in the edge of the lagena have a larger peak current size at 0 mV than in the centre, while the steady-state current size is comparable (Figure 6.10 *B*).

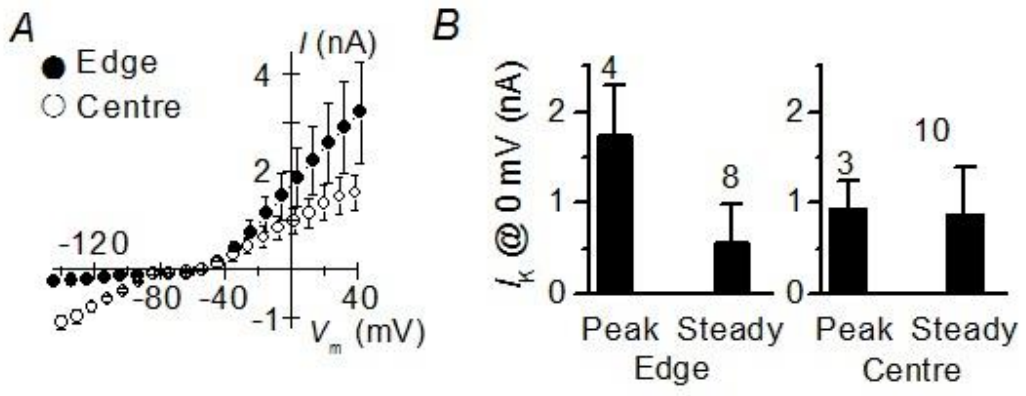

Figure 6.10 *I-V* curve and peak and steady current values from hair cells of the lagena.

A, Average peak *I–V* curves from hair cells in the centre (open circles) and edge (closed circles), including those in Figure 6.9 *A* and *B*. *B*, average peak and steady-state amplitudes of the total outward K^+ current in the two different regions from adult (> 1 year) zebrafish lagena.

Current clamp experiments from lagenar hair cells are shown in Figure 6.11. In the centre of the lagena, negative current injections caused small negative voltage changes in the order of ~ -85 mV, which was attributable to the large I_{K1} (Figure 6.11 *A*). Depolarizing current injections of +70 pA elicited broad spikes in the order of ~ 40 ms in hair cells from the centre, similar to the sacculus (Figure 6.3 *E*). In cells from the edge, hyperpolarising current injections of -30 pA elicited a larger change in V_m (~ -90 mV), including a small voltage sag that was due to the small I_h. Depolarising steps led to small voltage changes, that were clamped quickly (~ 5 ms) by I_A with no oscillations (Figure 6.11 *B*). Further depolarisation is prevented by $I_{K,D}$. Lagenar hair cells from the adult had a mean V_m of −74.4 ± 2.0mV, (n = 8) in the edge and −72.5 ± 3.4mV, (n=6) in the centre. The capacitance of lagena hair cells of both regions was 3.1 ± 0.1 pF (n = 36).

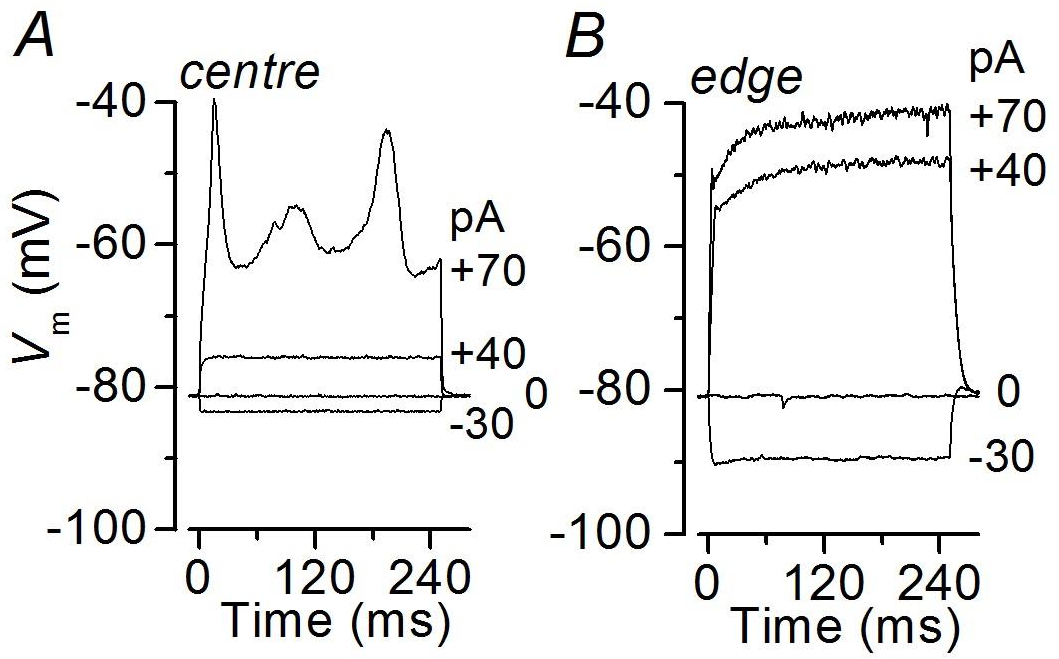

Figure 6.11 Membrane voltage responses from hair cells of the lagena in adult zebrafish.

A, B, Voltage responses from lagenar hair cells from the centre (*A*) and edge (*B*) of the adult (> 1 year) zebrafish. Note that only hair cells from the centre show membrane potential oscillations. Voltage responses to different current injections shown next to the traces from the V_m.

6.3.3.2 Electrical properties of juvenile lagenar hair cells

It has been shown that mouse cochlear hair cells undergo dramatic developmental changes in the basolateral membrane current profile up to around the onset of hearing (for review see Housley et al., 2006). Therefore, it was investigated whether lagenar hair cells undergo similar changes between young and adult stages. The lagena is the last macula to develop with hair cells appearing around three to four wpf (Bang et al., 2001). Recordings could first be performed at 7 wpf, because it was not until this stage that the tissue was big

enough to be dissected out from the inner ear. For zebrafish, 7 wpf is considered to be a juvenile stage.

Juvenile lagenar hair cells showed a larger set of of K^+ current profiles (Figure 6.12) compared to that recorded in adult cells (Figure 6.9). At least three different current profiles were found in hair cells from the centre (n = 10): 60 % of cells had a combination of $I_{K,D}$ with a Ca^{2+} activated K^+ current ($I_{K,Ca}$) and I_{K1} (Figure 6.12 *Ai*). Some cells showed $I_{K,D}$ with I_A and I_{K1} (20 %, Figure 6.12 *Aii*) and some showed I_A only (20%, Figure 6.12 *Aiii*). Cells in the edge had a more homogenous profile: the majority displays the I_A with I_h (75 %, Figure 6.12 *Bi*), which is already similar to the phenotype found in the adult. Only 25 % show an $I_{K,D}$ with $I_{K,Ca}$ and I_{K1} (Figure 6.12 *Bii*).

Despite the different current profile observed in hair cells from the centre of the larvae, the peak (1.7 ± 0.3 nA) and steady state (0.8 ± 0.1 nA, n = 9, measured at 0 mV) values of their overall outward K^+ current was similar to that of adult hair cells (Figure 6.12 C, black bar – adult, red bar - juvenile). The same was true for cells from the edge where the peak (2.1 ± 0.3 nA) and steady state values (0.5 ± 0.2 nA, n = 8) at 0 mV were not significantly different from those measured in hair cells from the same region of the adult lagena (Figure 6.12 *C*, black bar – adult, red bar - juvenile). However, even despite differences in the set of K^+ currents between 7wpf and 1 year old fish, it is unclear whether this reflects differences in function or maturity of the hair cells. Electrical activity in the inner ear can be measured as early as 3 dpf, therefore at least a subset of inner ear cells must be functional.

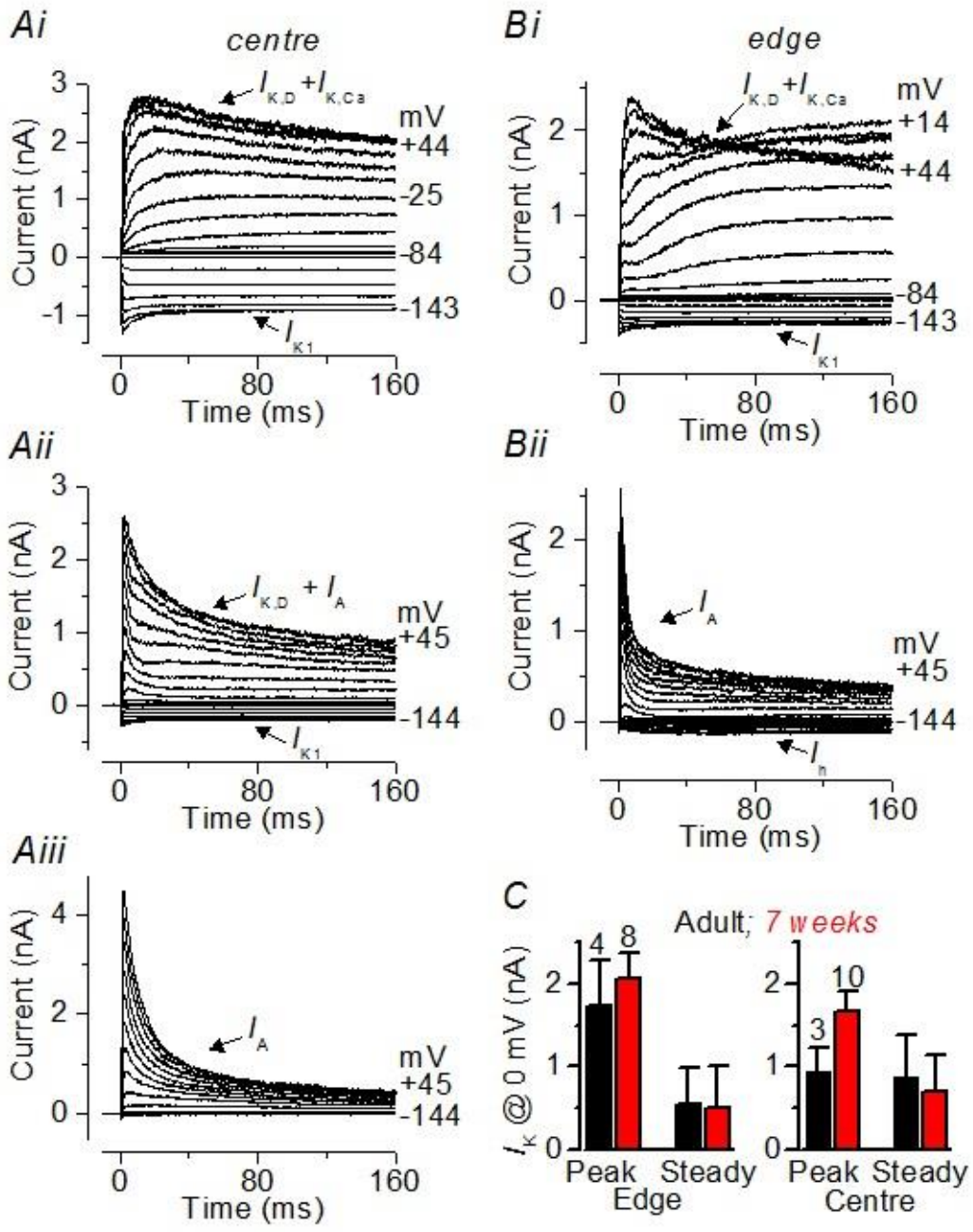

Figure 6.12 Membrane currents from hair cells of the juvenile lagena.

A, B, Typical K^+ currents from hair cells positioned in the centre (*Ai-Aiii*) and edge (*Bi-Biii*) of the lagena in a juvenile (7 wpf) zebrafish. Note that the current profile recorded within each region was variable. Currents were elicited by depolarizing and hyperpolarizing voltage steps in 10 mV nominal increments from the holding potential of −84 mV to the various test potentials shown by some of the traces. *C*, average peak and steady-state amplitudes of the total outward K+ current in the two different regions from adult (> 1 year) and juvenile (7 week) zebrafish.

6.3.3.3 Calcium currents in lagenar hair cells of the adult zebrafish

The receptor potential generated by the mechanoelectrical transducer current (I_{met}), and shaped by the basolateral membrane currents, leads to the opening of voltage gated calcium channels of the $Ca_v1.3$ subtype (Sidi et al., 2004). A typical example of the calcium current (I_{Ca}) recorded from lagenar hair cells at the edge is shown in Figure 6.13 *A*. I_{Ca} is a fast activating current that shows little inactivation (Moser and Beutner, 2000; Brandt et al., 2003). It activated at around −67 mV (5% of g_{max}) and reached its maximum size at −31 mV (−34 ± 6 pA, n = 6). It then reverses at around 46 mV (Figure 6.13 *B*). The average peak I_{Ca}-V curve (Figure 6.13 *B*) was fitted using Equation 2 (Chapter 4).

Measurements of vesicle release were not obtained, but they are likely to be small due to the small calcium current.

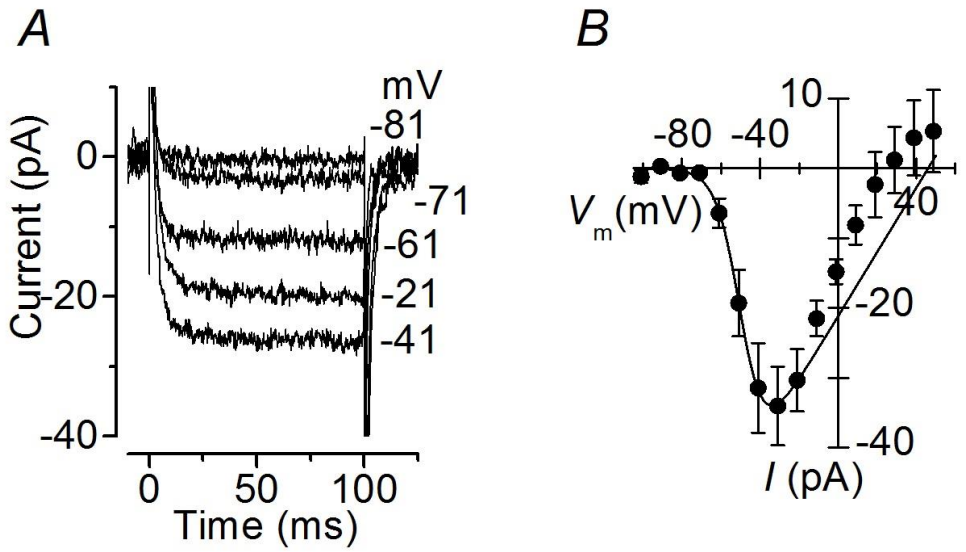

Figure 6.13 Calcium currents in lagenar hair cells of adult zebrafish.

A, Example of calcium currents (I_{Ca}) recorded from a lagenar hair cell at the edge of the adult (> 1 year) zebrafish. Currents were elicited by depolarizing and hyperpolarizing voltage steps in 10 mV nominal increments from the holding potential of −79 mV to the various test potentials shown by some of the traces. *B* Average peak *I*–*V* curve for the calcium currents (n = 6; from both regions), including that shown in *A*. The continuous line is a fit using Equation 2. Note that for values more depolarized than −20 mV, the fit was extrapolated. Recordings were obtained at 28 °C.

6.4 Summary and conclusion

In recent years the zebrafish inner ear has been an applicable model for studying the genetic basis of development. Yet, relatively little was known about the electrical properties of the sensory cells in the inner ear tissues.

This chapter has provided the first comprehensive description of the biophysical properties of the hair cells maintained in the sensory epithelium of the three maculae organs. I have identified two main current profiles:

–Hair cells expressing I_A + $I_{K,D}$ with I_h

- These cells are found in edge of all maculae
- Their membrane potential does not oscillate with depolarisation
- This profile is characteristic of vestibular organs in birds (Masetto and Correia, 1997; Masetto et al., 2000) and mice (Rüsch et al., 1998), but is different to that of mammalian cochlear hair cells (Marcotti et al., 1999; Marcotti et al., 2003a)

–Hair cells expressing $I_{K,D}$ with I_{K1}

- These cells are mainly found in the centre of the sacculus and lagena
- The membrane potential shows oscillations in response to depolarisation that resemble electrical tuning in other lower vertebrates (Fettiplace and Fuchs, 1999)
- The current profile is similar to auditory organs of other lower vertebrates: goldfish sacculus (Sugihara and Furukawa, 1989, 1995), and mammals, such as in immature mouse IHCs (Marcotti et al., 1999; Marcotti et al., 2003a)

6.5 Discussion

In the inner ear, I have investigated the biophysical properties of the basolateral membranes of hair cells positioned in different locations within each of three sensory epithelia, the maculae. I found two different current profiles in the sacculus and lagena, these maculae have a primary function in hearing (Abbas and Whitfield, 2010). One group of cells expressed a rapidly activating A-type current (I_A) together with an h-type K^+-Na^+ current (I_h), and the other expressed a delayed rectifier K^+ current ($I_{K,D}$) together with the inward rectifier K^+ current (I_{K1}). Hair cells with these different current profiles were spatially segregated within the macula, with those expressing I_A being present at the edge region of the sensory epithelium and those with $I_{K,D}$ been located in its centre. Different from the sacculus and the lagena, 90 % of utricular hair cells, which are only responsible for balance, showed one current profile (A-type and h-type currents).

The presence of two main current profiles in the sacculus and lagena agrees with that of an earlier preliminary study (Knirsch and Rüsch, 2003). However, a recent study reported a large variation in the current profile of enzymatically isolated hair cells from the zebrafish inner ear and up to six different combinations of K^+ currents (Haden et al., 2013). One possible explanation for this discrepancy may refer to alterations in channel properties when cells are treated with enzyme, which is also suggested by the fact that the A-type current was barely visible and the h-type current was absent in the earlier recordings (Haden et al., 2013).

Hair cells expressing the A-type, h-type and delayed rectifier currents have been shown to be characteristic of vestibular organs in bird (Masetto and Correia, 1997; Masetto et al., 2000) and mice (Holt and Eatock, 1995; Eatock et al., 1998; Rüsch et al., 1998). I_A and I_h are absent in hair cells of the mammalian cochlea (Marcotti and Kros, 1999; Marcotti et al., 2003a). Zebrafish hair cells expressing $I_{K,D}$ and I_{K1} resembled those present in early postnatal cochlear outer hair cells (OHCs) and IHCs (Marcotti et al., 1999; Marcotti and Kros, 1999; Marcotti et al., 2003a).

Similar current profiles to those recorded in the zebrafish inner ear have also been described in the goldfish sacculus. This macula senses sound up to 4000 Hz and is tonotopically organised, where cells at the edge or anterior region sense frequencies of around 100 Hz and cells more medial or central sense higher frequencies at around 800 Hz (Smith et al., 2011). The goldfish sacculus lacks micromechanical specialisations of the auditory organ, e.g. basilar membrane, such that frequency filtering has to be fulfilled by the hair cells. This is different to higher vertebrates and mammals, which have sophisticated mechanisms for extrinsic frequency filtering (Manley, 2000).

Adult goldfish saccular hair cells in the posterior region (sensing around 100 Hz) exhibit the A-type current, similar to my finding in the zebrafish inner ear. A crucial characteristic of the A-type current is that it activates very rapidly, and as such is able to repolarize the V_m very quickly. However, due to the inactivation kinetics of I_A it can only shape the V_m behaviour up to few hundred Hz. Its rapid effect on the V_m is particularly important for onset-encoding and phase-locking of the afferent fibre. Therefore, the presence of the A-type current in a low frequency region (up to 100 Hz) such as the anterior sacculus suggests that it could be involved in the precise transmission of stimulus timing at lower frequencies. This is in line with the properties of the afferent fibres in the rostral region of the sacculus that show vigorous phase-locking to sound (Sento and Furukawa, 1987).

Since the I_A cannot mediate stimulation above a few tens of Hz, due to its inactivation, a different current is required in the centre of the sacculus that senses around 800 Hz. This is a delayed rectifier K^+ current ($I_{K,D}$) (Sugihara and Furukawa, 1989) which is similar to my results in the zebrafish inner ear. In the zebrafish sacculus, cells in the centre showed membrane oscillations that resemble electrical tuning to higher frequencies (800 Hz) which is also found in other lower vertebrates (Fettiplace and Fuchs, 1999). Electrical tuning is a mechanism employed by lower vertebrates, including frogs and chicken, to precisely convey frequencies up to few hundred Hz where mechanical specialisation of the auditory organ is not well developed (Fettiplace and Fuchs,

1999; Manley, 2000). However, it needs to be noted, that the quality of electrical tuning is poorer in the zebrafish inner ear than in the turtle.

Currently, there is no information regarding the electrophysiological properties of the mechanoelectrical transducer current (I_{MET}) or the afferent fibres, which is crucial in order to understand the inner ear hair cell function. For example, the contribution of the I_{MET} to the resting V_m remains to be elucidated, as this has an impact on the electrical behaviour of the cell. Similarly, it is unknown whether the afferent fibres contacting different sensory organs have different properties, as described in the vestibular and auditory systems of mammals (Eatock and Songer, 2011). These omissions in our knowledge are currently preventing an in depth understanding of how sensory signals are processed by hair cells with such precision and the exact role that these membrane currents have on signal transduction.

Chapter 7 General Discussion

In this study I have provided the first detailed investigation of the basolateral membrane properties of zebrafish hair cells both in the inner ear and lateral line. Zebrafish hair cells show several different current profiles and the abundance of which changes over time from larval or juvenile to older stages (Chapter 5 and 6). I also described for the first time the properties of exocytosis at the ribbon synapses, allowing comparisons to be made with what we currently know in vertebrate hair cells and mammalian cochlear inner hair cells (IHCs).

7.1 Comparison of lateral line and inner ear hair cells.

The possible function of each of the individual hair cell types was discussed in detail in the respective chapter, but how do hair cells of the lateral line compare to the inner ear?

Both organs have common K^+ currents, such as the A-type current, but the roles seem to be very different. In the inner ear the A-type current mediates a faster voltage response, making it ideal to follow low frequencies. In the lateral line, it is much slower compared to the other Type 2 and 3 and making it likely to be involved in continued stimulation. How can the same current have two different functions? Firstly, the speed of the response has to be compared to the other cell types present and is unlikely to be different between inner ear and lateral line as can be estimated by the similar cell size (see Table 7.1). The inner ear I_A is faster than the $I_{K,D}$ expressing cells in the same tissue, but not necessarily faster than in the lateral line. Secondly, in the inner ear the I_A is much larger than in the lateral line, which will flatten the voltage response due to its inactivation. During fluid stimulation of the hair cell, when the transducer channel adapts and the I_{Met} becomes smaller, this can show in the I_A cells as a decrease in the voltage response, bringing the cell closer to a new activation of I_A. As for the other types that have been found, an $I_{K,D}$ involved in electrical tuning and an $I_{K,Ca}$ seem to have very distinct roles. While $I_{K,D}$ is involved in mediating higher frequency sounds, $I_{K,Ca}$ is important for fast onset encoding.

Apart from their K^+ current set, the cells in the lateral line and inner ear are remarkably similar in terms of their sizes (around 3-4 pF) and resting membrane potentials (around 70 mV) (Table 7.1). This is different to the vestibular system, where both types not only have different K+ currents but also different cell resistances. This could indicate that both the inner ear and lateral line are much less specialized than higher vertebrate sensory cells.

Table 7.1 Properties of lateral line and inner ear hair cells

Values given as mean ± S.E.M.

	All Hair cells (3- 36 dpf)	Larval Zebrafish (3-5.2 dpf) *In vivo*	Juvenile Zebrafish (> 20 dpf) *in vitro* – decapitated	
Capacitance (pF)	3.6 ± 0.1 (*n* = 208)	3.6 ± 0.1 (*n* = 62)	3.1 ± 0.1 (*n* = 146)	
Resistence (MΩ)	3.2 ± 0.1 (*n* = 208)	3.4 ± 0.1 (*n* = 62)	3.7 ± 0.1 (*n* = 146)	
V_m (mV)	-68.2 ± 1.5 (*n* = 50)	-70.7 ± 1.6 (*n* = 26)	centre: −69.9 ± 2.5 (*n* = 10)	edge: −68.3 ± 4.0 (*n* = 7)

	Lagena adult		Lagena juvenile		Sacculus adult	Utricle adult
	Centre	Edge	Centre	Edge		
Capacitance (pF)	3.1 ± 0.1 (*n* = 36)		4.8 ± 0.2 (*n* = 15)		3.2 ± 0.4 (*n* = 8)	3.2 ± 0.2 (*n* = 11)
Resistence (MΩ)	4.4 ± 0.3 (*n* = 16)		3.1 ± 0.2 (*n* = 15)		3.8 ± 0.3 (*n* = 8)	1.6 ± 0.3 (*n* = 11)
V_m (mV)	−74.4 ± 2.0 (*n* = 8)	−72.5 ± 3.4 (*n*=6)	-70.9 ± 3.7 (*n*= 5	-73.6 ± 2.1 (*n*= 7)	−70.7 ± 3.5 (*n* = 7)	−71.2 ± 2.2 (*n* = 8)

Another question remains as to why the inner ear and lateral line are still more similar to each other than the cochlea and the vestibular system in mammals. One possible explanation for this is a much lesser degree of specialization in the zebrafish. Firstly, neurons from both the inner ear and lateral line contact the Mauthner cells to mediate the escape response, meaning that any activity is enough to trigger a simple response. Secondly, both organs send axons into the same areas in the brain indicating that both inputs are needed to compute behaviour (Highstein et al., 1992). Even though this is also the case in the mammal, where several sensory inputs are combined at different levels of the CNS, each sensory system has a distinct area in the brain. Thirdly, several lateral line hair cells are innervated by the same neuron, indicating convergence at approximately 6:1. This means, that the individual hair cell is not characterized by great precision as is the mammalian IHC. Whether the inner ear neurons branch and innervate several hair cells is unknown, but it seems likely judging by their small calcium current.

Fourth, despite the properties of the afferent neurons in the lateral line not being fully explored, it seems certain that there are two populations (large and small diameter cell body) of neurons with spontaneous frequencies of 5-50 Hz (Haehnel et al., 2012). At the moment, it is not clear whether these neuron types preferentially innervate specific hair cells. What is clear is that they predominantly innervate neuromasts in certain position, e.g. in the tail or the dorsal lateral line. This could mean, that one single neuromast receives innervation by one type of fibre only.

The notion that the lateral line is less specialized than the vestibular system in the mammal or the bullfrog auditory hair cell is not surprising when looking at the role of this sensory system during behaviour. A number of studies have addressed the issue of rheotaxis, i.e. how fish align to stimulation. And it has been shown that the lateral line is crucial to mediate this response. However, if the lateral line is blocked, rheotaxis is still possible based on visual cues (REF Montgomery 1997). Finally, the sensitivity for the direction of the stimulus in the lateral line is achieved by turning the neuromast either in an anterior-posterior way or dorsal to ventral, rather than specializing the cell. All these features make

the lateral line a sensory system that functions reliably but with less precision and accuracy than found in hair cells of higher vertebrates.

7.2 Calcium current and exocytosis at hair cell ribbon synapses

The zebrafish lateral line, due to its optical transparency, has been particularly popular for studying synaptic transmission using imaging techniques. Using genetically encoded calcium indicators (Dreosti and Lagnado, 2011), calcium transients within cells and between cells can be measured as well as vesicle release. However, whole-cell patch clamp is a more accurate way to measure the absolute size of the calcium current and vesicles released.

In the zebrafish lateral line hair cells, I found a small but measurable calcium current (Chapter 4 and 5, Figure 4.12 and 5.7). This does not change between larval, early juvenile and later juvenile stages. The small I_{Ca} is consistent with what I found in the inner ear (Chapter 6, Figure 6.13) and that reported in frog, rat and goldfish vestibular hair cells (Sugihara and Furukawa, 1989; Prigioni et al., 1992; Bao et al., 2003) and with recent data from hair cells of the larval zebrafish lateral line (Ricci et al., 2013). The calcium current in the lateral line hair cells is carried by $Ca_v1.3$ calcium channels that are clustered to the presynaptic active zones (Sidi et al., 2004). This is similar to what has been shown for hair cells in the mammalian auditory and vestibular systems (Platzer et al., 2000; Bao et al., 2003; Brandt et al., 2003).

The elementary properties of $Ca_v1.3$ calcium channels are well known (Zampini et al., 2013; Zampini et al., 2014), and were used to estimate the number of channels present at the presynaptic zone (Chapter 3, Equation 1). Considering that the peak size of I_{Ca} is around -11 pA (juvenile hair cells), the total number of calcium channels is likely to be in the order of 150. Assuming that all 150 calcium channels are associated with ribbons (Sidi et al., 2004; Sheets et al., 2012), then each of the four ribbons that form active zones in zebrafish lateral line hair cells (Obholzer et al., 2008) is likely to contain about 38 calcium channels. This value is similar to what was previously estimated for the adult bullfrog ($\sim$ 36 channels

per ribbon, (Graydon et al., 2011) but is about five times smaller than that measured in cochlear hair cells (~180 calcium channels: Zampini et al., 2013; Zampini et al., 2014).

How does the number of channels relate to vesicle release? Even though, the size of I_{Ca} does not change during development, the efficacy of the neurotransmitter release does increase from larval (ΔCm 2.3 pF) to juvenile stages (ΔCm 7.7 pF) (Chapter 4 and 5, Figure 4.12 and 5.7). Assuming that each vesicle has a surface area of 37 aF (Lenzi et al., 1999), this means at larval stages on average 62 vesicles fuse to the hair cell membrane using a 1 s stimulus, whereas at juvenile stages the number increases to 178 vesicles (Olt et al., 2014).

Looking at the vesicle release per ribbon, these 178 vesicles in juvenile zebrafish equate to ~45 vesicles for each of the four active zones (Sidi et al., 2004; Obholzer et al., 2008). A similar depolarizing voltage step in mature mouse IHCs has been shown to recruit about 4000 vesicles which equals ~150 fF (Johnson et al., 2005) and ~270 vesicles per active zone. Even though, the values of vesicle release are different, the proportion of vesicles released per calcium channel in the fish is 1.2 (44 vesicles per 38 calcium channels) which is comparable to the mouse inner hair cell with a proportion of 1.5 (270 vesicles per 180 calcium channel), assuming a nanodomain control of exocytosis (Moser et al., 2006). This similarity in the proportions indicates that the efficiency of neurotransmitter release in hair cells is likely to be very similar between the mammalian cochlea and zebrafish lateral line. However, as mentioned above, the scale of the responses is very different making the lateral line hair cells less sensitive than their mammalian counterparts.

At the moment, it is unclear how the different basolateral membrane properties of developing hair cells affect synaptic signal encoding at the afferent fibre, mainly because we still know little about lateral line function and organization in the adult zebrafish. However, we do know that the neuromasts and afferent fibres of the zebrafish lateral line undergo extensive growth and reorganization during larval stages that result in a more complex organization in the adult, which is

likely to be essential to the fine-tuning of sensitivity to movement direction (Haehnel et al., 2012; Liao and Haehnel, 2012).

7.3 Benzocaine as an anaesthetic to study the lateral line after 5.2 dpf

Since I am mostly interested in studying the role of hair cells in their adult configuration, which appears to happen from juvenile stages onwards where there are more Type 1 hair cells, I had to develop an *in vivo* approach (Chapter 5, Section 5.3.2). I found that MS-222 blocks part of the hair cell potassium current and as such alters their physiology. Therefore, there was the need to using a new anaesthetic and Benzocaine was selected based on its analgesic properties and the fact that it did not alter the basolateral membrane currents nor synaptic transmission (Chapter 5, Figure 5.11 – 5.14).

The use of adult zebrafish has wider implications outside of zebrafish hair cell research. At the moment, the full potential of the zebrafish for functional *in vivo* studies is limited by the fact that most of the work is carried out at larval stages (Ampatzis et al., 2013; Stil and Drapeau, 2015). Currently, electrophysiological studies of neuronal activity from functionally mature systems such as in the olfactory system, motoneurons and specific brain areas are performed from *in vitro* dissected preparations (Sato et al., 2007; Gabriel et al., 2011; Vargas et al., 2011; Vargas et al., 2012). Using Benzocaine and the intubation of the zebrafish to maintain oxygenation could be a useful approach for *in vivo* studies of older fish involving behaviour (Kalueff et al., 2014; Stewart et al., 2014; Tabor et al., 2014), optical imaging and electrophysiology (e.g. *motoneurons*: Ampatzis et al., 2013; Fidelin and Wyart, 2014; *Purkinje cells*: Hsieh et al., 2014; *retina horizontal and ganglion cells*: Sun et al., 2012; Johnston et al., 2014; *hair cells*: Olt et al., 2014).

7.4 Future and ongoing experiments

7.4.1 Role of different hair cells types on afferent fibre activity in the lateral line

The present study has provided a better understanding into the properties of lateral line hair cells. However, it is still unclear how the afferent neurons that contact the hair cells behave in terms of biophysical properties during development. We know that the migrating primordium drags fibres with it as it provides the first innervation of the hair cells (Metcalfe, 1985; Gilmour et al., 2004). Afferent fibres also branch and innervate at least two neuromasts and only contact hair cells from the same polarity (Nagiel et al., 2008; Liao, 2010).

Not only are the properties of the lateral line afferent fibres unclear, but it is also unknown how the different hair cell types are able to influence neurotransmitter release to those fibres. It would also be interesting to know whether the newly formed hair cells that express BK- channels receive innervation or if it is only the A-type current expressing cells, that are innervated. This is crucial for understanding the potential regeneration of the system. Performing a combination of dual patch between hair cells, single neuron recordings and morphological studies should address at least some of these unknown aspects of sensory development and function in the lateral line.

7.4.2 Patch-clamp electrophysiology as a tool to study transgenic zebrafish lines

The ability to perform electrophysiological recordings from single zebrafish hair cells can also be used to screen transgenic lines with genetic modifications. In particular, zebrafish have been used to study the function of ribbon synapses in the hair cells *in vivo* and it was found that the removal of ribbons, leads to the presynaptic calcium channel being scarcely clustered (Sheets et al., 2011; Sheets et al., 2012; Nicolson, 2015).

Very recently, I have received a transgenic line from T. Nicolson and K. Kindt, that has a ribeye-b overexpression (myo6-ribB-GFP) leading to very large ribbons

and supernumerary tethered vesicles. Performing patch-clamp electrophysiology, I found that the size of the calcium current is significantly increased in myo6-ribB-GFP (−13.2 ± 1.8 pA, n = 10) compared to that measured in wild-type hair cells (−7.0 ± 1.4 pA, n = 13, $P < 0.05$, two-tailed Student's t test) (Figure 7.1 *A* and *B*). This is in line with previous studies, showing that the ribbon is important to cluster $Ca_v1.3$ to the presynaptic membrane and these results could indicate that this happens in a fashion that is dependent on the amount of ribeye protein present (Sheets et al., 2011).

However, the increase in I_{Ca} was not accompanied by an increase in transmitter release ΔC_m, which is similar between wild-type (9.0 ± 3.0 fF, n = 6) and myo6-ribB-GFP (6.8 ± 1.0 fF, n = 7) (Figure 7.1 *C* and *D*). This indicates that despite the larger ribbon, the overall number of releasable vesicles is not increased in myo6-ribB-GFP cells. The finding that I_{Ca} is increased is intriguing as it has been shown using TEM that myo6-ribB-GFP hair cells have significantly more vesicles tethered to the ribbon. This means that ribeye is important for clustering the channel and the vesicles, but parts of the machinery that are important for vesicle recruitment are missing. These could be the calcium sensor, buffer or proteins involved in vesicle priming. Alternatively, a larger ribbon might pose a physical obstacle for the calcium entry and might prevent it from reaching the higher up rows in the transgenic. This questions might be very difficult to answer experimentally in the fish, as the cells are small and manipulation of calcium signalling difficult. One way to find out, might be applying computational modelling to assess whether the size of the ribbon impacts on the diffusion distance of calcium.

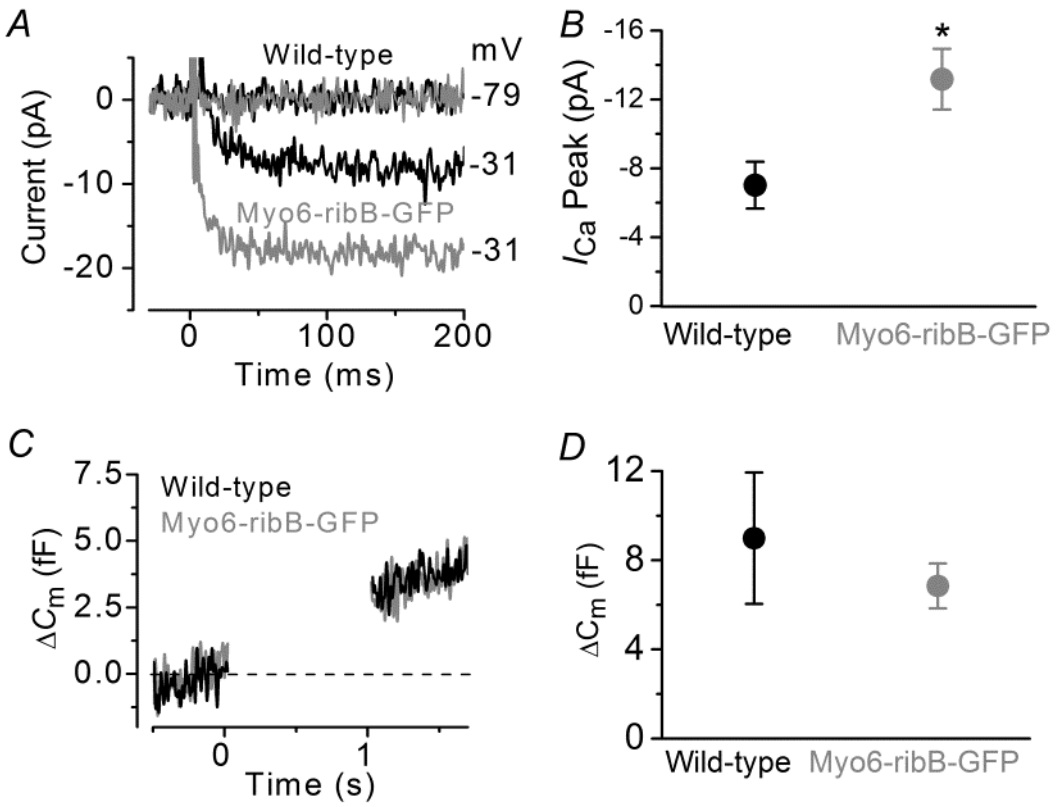

Figure 7.1 Calcium currents and neurotransmitter release in wild-type and myo6-ribB-GFP lateral line hair cells.

A, Calcium currents (I_{Ca}) recorded from wild-type (7 dpf, black) and myo6-ribB-GFP (5 dpf, grey) zebrafish lateral line hair cells. Currents were elicited by a series of depolarizing voltage steps in 10 mV increments (200 ms in duration) from the holding potential of −79 mV. For clarity, only the trace at the holding potential and at the peak of I_{Ca} are shown. *B*, Average I_{Ca} peak size at −31 mV from wild-type (black) and transgenic (grey) including cells in *A. C*, Changes in membrane capacitance (ΔCm) recorded from hair cells of larval wild-type (5 dpf, black) and myo6-ribB-GFP (6 dpf, grey) zebrafish. Recordings were obtained in response to 1 s voltage steps from the holding potential of −79 mV to near the peak of I_{Ca} (−31 mV). *D*, Average ΔCm elicited following 1s depolarization step to −31 mV from hair cells of both wild-type (6 – 8 dpf, black) and myo6-ribB-GFP (5 – 8 dpf, grey). Recordings were performed at 28 °C.

7.5 Conclusion

In this study I have established a near physiological method to record electrical activity from hair cells of both the inner ear as well as the lateral line. I have shown that hair cells express several different current profiles both in the lateral line and inner ear. The newly developed *in vivo* approach to study juvenile hair cells using benzocaine and intubation of the fish, will help future studies utilise the full potential of the adult zebrafish lateral line for investigations into the function of hair cells *in vivo*.

References

Abbas L, Whitfield TT (2010) The zebrafish inner ear. Zebrafish 29:123-171.

Alexandre D, Ghysen A (1999) Somatotopy of the lateral line projection in larval zebrafish. Proceedings of the National Academy of Sciences of the United States of America 96:7558-7562.

Almanza A, Vega R, Soto E (2003) Calcium current in type I hair cells isolated from the semicircular canal crista ampullaris of the rat. Brain Research 994:175-180.

Ampatzis K, Song J, Ausborn J, El Manira A (2013) Pattern of innervation and recruitment of different classes of motoneurons in adult zebrafish. Journal of Neuroscience 33:10875-10886.

Art JJ, Fettiplace R (1987) Variation of membrane properties in hair cells isolated from the turtle cochlea. Journal of Physiology 385:207-242.

Art JJ, Wu YC, Fettiplace R (1995) The calcium activated potassium channels of turtle hair cells. Journal of General Physiology 105:49-72.

Bang PI, Sewell WF, Malicki JJ (2001) Morphology and cell type heterogeneities of the inner ear epithelia in adult and juvenile zebrafish (Danio rerio). Journal of Comparative Neurology 438:173-190.

Bao H, Wong WH, Goldberg JM, Eatock RA (2003) Voltage-gated calcium channel currents in type I and type II hair cells isolated from the rat crista. Journal of Neurophysiology 91:589-589.

Beurg M, Fettiplace R, Nam J-H, Ricci AJ (2009) Localization of inner hair cell mechanotransducer channels using high-speed calcium imaging. Nature Neuroscience 12:553-558.

Beutner D, Voets T, Neher E, Moser T (2001) Calcium Dependence of Exocytosis and Endocytosis at the Cochlear Inner Hair Cell Afferent Synapse. Neuron 29:681-690.

Brandt A, Striessnig J, Moser T (2003) Ca(V)1.3 channels are essential for development and presynaptic activity of cochlear inner hair cells. Journal of Neuroscience 23:10832-10840.

Buss RR, Drapeau P (2001) Synaptic drive to motoneurons during fictive swimming in the developing zebrafish. Journal of Neurophysiology 86:197-210.

Carter KM, Woodley CM, Brown RS (2011) A review of tricaine methanesulfonate for anesthesia of fish. Reviews in Fish Biology and Fisheries 21:51-59.

Corns L, Bardhan T, Houston O, Olt J, Holley M, Masetto S, Johnson S, Marcotti W (2014) Functional development of hair cells in the mammalian inner ear. In: Development of Auditory and Vestibular Systems, 4 Edition (Romand R, Varela-Nieto I, eds), pp 155-188: Elsevier.

Corwin JT, Oberholtzer JC (1997) Fish n' chicks: Model recipes for hair-cell regeneration? Neuron 19:951-954.

Dick O, Dieck ST, Altrock WD, Ammermuller J, Weiler R, Garner CC, Gundelfinger ED, Brandstatter JH (2003) The presynaptic active zone protein bassoon is essential for photoreceptor ribbon synapse formation in the retina. Neuron 37:775-786.

Dou HV, Vazquez AE, Namkung Y, Chu H, Cardell EL, Nie LP, Parson S, Shin H, Yamoah EN (2004) Null mutation of alpha(1D) Ca2+ channel gene results in deafness but no vestibular defect in mice. Jaro-Journal of the Association for Research in Otolaryngology 5:215-226.

Dreosti E, Lagnado L (2011) Optical reporters of synaptic activity in neural circuits. Experimental Physiology 96:4-12.

Eatock R, Hutzler M (1992) Ionic currents of mammalian vestibular hair cells. Annals of the New York Academy of Science 656:58-74.

Eatock RA, Songer JE (2011) Vestibular hair cells and afferents: two channels for head motion signals. Annual Review of Neuroscience 34:501-534.

Eatock RA, Rusch A, Lysakowski A, Saeki M (1998) Hair cells in mammalian utricles. Otolaryngology-Head and Neck Surgery 119:172-181.

Faucherre A, Pujol-Marti J, Kawakami K, Lopez-Schier H (2009) Afferent neurons of the zebrafish lateral line are strict selectors of hair cell orientation. Plos One 4:doi:10.1371/journal.pone.0004477.

Fettiplace R, Fuchs PA (1999) Mechanisms of hair cell tuning. Annual Review of Physiology 61:809-834.

Fettiplace R, Kim K (2014) The physiology of mechanoelectrical transduction in hearing. Physiological Reviews 94:951-986.

Fidelin K, Wyart C (2014) Inhibition and motor control in the developing zebrafish spinal cord. Current Opinion in Neurobiology 26:103-109.

Flock A, Wersall J (1962) A study of orientation of sensory hairs of receptor cells in lateral line organ of fish, with special reference to function of receptors. Journal of Cell Biology 15:19-17.

Flock A, Bretscher A, Weber K (1982) Immunohistochemical localisation of several cytoskeleton proteins in inner ear sensory and supporting cells. Hearing Research 7:75-89.

Furness DN, Hackney CM (1985) Cross-links between stereocilia in the guinea pig cochlea. Hearing Research 18:177-188.

Gabriel JP, Ausborn J, Ampatzis K, Mahmood R, Eklof-Ljunggren E, El Manira A (2011) Principles governing recruitment of motoneurons during swimming in zebrafish. Nature Neuroscience 14:93-U125.

Gale JE, Marcotti W, Kennedy HJ, Kros CJ, Richardson GP (2001) FM1-43 dye behaves as a permeant blocker of the hair-cell mechanotransducer channel. Journal of Neuroscience 21:7013-7025.

Ghysen A, Dambly-Chaudiere C (2004) Development of the zebrafish lateral line. Current Opinion in Neurobiology 14:67-73.

Ghysen A, Dambly-Chaudiere C (2007) The lateral line microcosmos. Genes & Development 21:2118-2130.

Gilmour D, Knaut H, Maischein HM, Nusslein-Volhard C (2004) Towing of sensory axons by their migrating target cells in vivo. Nature Neuroscience 7:491-492.

Glowatzki E, Fuchs PA (2000) Cholinergic synaptic inhibition of inner hair cells in the neonatal mammalian cochlea. Science 288:2366-2368.

Graydon CW, Cho S, Li G-L, Kachar B, von Gersdorff H (2011) Sharp Ca2+ Nanodomains beneath the Ribbon Promote Highly Synchronous Multivesicular Release at Hair Cell Synapses. Journal of Neuroscience 31:16637-16650.

Hackney C, Furness D (2013) The composition and role of cross links in mechanoelectrical transduction in vertebrate sensory hair cells. Journal of Cell Science 126:1721-1731.

Hackney CM, Fettiplace R, Furness DN (1993) The functional morphology of stereociliary bundles on turtle cochlear hair cells. Hearing Research 69:163-175.

Haddon C, Lewis J (1996) Early ear development in the embryo of the zebrafish, Danio rerio. Journal of Comparative Neurology 365:113-128.

Haden M, Einarsson R, Yazejian B (2013) Patch clamp recordings of hair cells isolated from zebrafish auditory and vestibular organs. Neuroscience 248:79-87.

Haehnel M, Taguchi M, Liao JC (2012) Heterogeneity and dynamics of lateral line afferent innervation during development in zebrafish (Danio rerio). Journal of Comparative Neurology 520:1376-1386.

Hamill OP, Marty A, Neher E, Sakmann B, Sigworth FJ (1981) Improved Patch-Clamp Techniques for High-Resolution Current Recording from Cells and Cell-Free Membrane Patches. Pflugers Archiv-European Journal of Physiology 391:85-100.

Heidelberger R, Thoreson WB, Witkovsky P (2005) Synaptic transmission at retinal ribbon synapses. Progress in Retinal and Eye Research 24:682-720.

Higgs DM, Souza MJ, Wilkins HR, Presson JC, Popper AN (2002) Age- and size-related changes in the inner ear and hearing ability of the adult zebrafish (Danio rerio). Jaro 3:174-184.

Highstein S, Kitch R, Carey J, Baker R (1992) Anatomical organization of the brainstem octavolateralis area of the oyster toadfish, Opsanus tau. Journal of Comparative Neurology 319(4):501-518.

Holmberg K (1971) Hagfish retina - electron microscopic study comparing receptor and epithelial cells in pacific and hagfish, polistotrema-stouti, with those in atlantic hagfish, myxine-glutinosa. Zeitschrift Fur Zellforschung Und Mikroskopische Anatomie 121:249-269.

Holt JR, Eatock RA (1995) Inwardly rectifying currents from the saccular hair cells from the leopard frog. Journal of Neurophysiology 73:1484-1502.

Housley GD, Marcotti W, Navaratnam D, Yamoah EN (2006) Hair cells - beyond the transducer. Journal of Membrane Biology 209:89-118.

Hsieh J-Y, Ulrich B, Issa FA, Wan J, Papazian DM (2014) Rapid development of Purkinje cell excitability, functional cerebellar circuit, and afferent sensory input to cerebellum in zebrafish. Frontiers in neural circuits 8:147-147.

Johnson SL, Thomas MV, Kros CJ (2002) Membrane capacitance measurement using patch clamp with integrated self-balancing lock-in amplifier. Pflugers Archiv-European Journal of Physiology 443:653-663.

Johnson SL, Marcotti W, Kros CJ (2005) Increase in efficiency and reduction in Ca2+ dependence of exocytosis during development of mouse inner hair cells. Journal of Physiology 563:177-191.

Johnson SL, Beurg M, Marcotti W, Fettiplace R (2011) Prestin-Driven Cochlear Amplification Is Not Limited by the Outer Hair Cell Membrane Time Constant. Neuron 70:1143-1154.

Johnson SL, Forge A, Knipper M, Muenker S, Marcotti W (2008) Tonotopic variation in the calcium dependence of neurotransmitter release and vesicle pool replenishment at mammalian auditory ribbon synapses. Journal of Neuroscience 28:7670-7678.

Johnson SL, Kennedy HJ, Holley MC, Fettiplace R, Marcotti W (2012) The resting transducer current drives spontaneous activity in prehearing mammalian cochlear inner hair cells. Journal of Neuroscience 32:10479-10483.

Johnson SL, Kuhn S, Franz C, Ingham N, Furness DN, Knipper M, Steel KP, Adelman JP, Holley MC, Marcotti W (2013) Presynaptic maturation in auditory hair cells requires a critical period of sensory-independent spiking activity. Proceedings of the National Academy of Sciences of the United States of America 110:8720-8725.

Johnson SL, Franz C, Kuhn S, Furness DN, Ruettiger L, Muenkner S, Rivolta MN, Seward EP, Herschman HR, Engel J, Knipper M, Marcotti W (2010) Synaptotagmin IV determines the linear Ca2+ dependence of vesicle fusion at auditory ribbon synapses. Nature Neuroscience 13:45-U201.

Johnston J, Ding H, Seibel SH, Esposti F, Lagnado L (2014) Rapid mapping of visual receptive fields by filtered back projection: application to multi-neuronal electrophysiology and imaging. Journal of Physiology 592:4839-4854.

Kachar B, Parakkal M, Kurc M, Zhao Y, Gillespie PG (2000) High-resolution structure of hair-cell tip links. Proceedings of the National Academy of Sciences of the United States of America 97:13336-13341.

Kalueff AV, Stewart AM, Gerlai R (2014) Zebrafish as an emerging model for studying complex brain disorders. Trends in Pharmacological Sciences 35:63-75.

Kharkovets T, Hardelin JP, Safieddine S, Schweizer M, El-Amraoui A, Petit C, Jentsch TJ (2000) KCNQ4, a K+ channel mutated in a form of dominant deafness, is expressed in the inner ear and the central auditory pathway. Proceedings of the National Academy of Sciences of the United States of America 97:4333-4338.

Khonsari RH, Li B, Vernier P, Northcutt RG, Janvier P (2009) Agnathan brain anatomy and craniate phylogeny. Acta Zoologica 90:52-68.

Kimmel CB, Ballard WW, Kimmel SR, Ullmann B, Schilling TF (1995) Stages of embryonic development of the zebrafish. Developmental Dynamics 203:253-310.

Kindt KS, Finch G, Nicolson T (2012) Kinocilia mediate mechanosensitivity in developing zebrafish hair cells. Developmental Cell 23:329-341.

Knirsch M, Rüsch A (2003) Two Classes of Hair Cells with different Potassium Currents in the Hearing Organ of the Zebrafish (Danio rerio). In: Association for Research in Otolaryngology, Midwinter meeting.

Lacoste AMB, Schoppik D, Robson DN, Haesemeyer M, Portugues R, Li JM, Randlett O, Wee CL, Engert F, Schier AF (2015) A convergent and essential interneuron pathway for mauthner-cell-mediated escapes. Current Biology 25:1526-1534.

Ledent V (2002) Postembryonic development of the posterior lateral line in zebrafish. Development 129:597-604.

Lenzi D, Runyeon JW, Crum J, Ellisman MH, Roberts WM (1999) Synaptic vesicle populations in saccular hair cells reconstructed by electron tomography. Journal of Neuroscience 19:119-132.

Lewis RS, Hudspeth AJ (1983) Voltage depdendent and ion dependent conductances in solitary vertebrate hair cells. Nature 304:538-541.

Li G-L, Cho S, von Gersdorff H (2014) Phase-locking precision is enhanced by multiquantal release at an auditory hair cell ribbon synapse. Neuron 83:1404-1417.

Liao JC (2010) Organization and physiology of posterior lateral line afferent neurons in larval zebrafish. Biology Letters 6:402-405.

Liao JC, Haehnel M (2012) Physiology of afferent neurons in larval zebrafish provides a functional framework for lateral line somatotopy. Journal of Neurophysiology 107:2615-2623.

Lindau M, Neher E (1988) Patch-clamp techniques for time-resolved capacitance measurements in single cells. Pflügers Archiv - European Journal of Physiology 411:137-146.

Lopez-Schier H, Hudspeth AJ (2007) A two-step mechanism underlies the planar polarization of regenerating sensory hair cells. Proceedings of the National Academy of Sciences of the United States of America 103:18615-18620.

Lopez-Schier H, Starr CJ, Kappler JA, Kollmar R, Hudspeth AJ (2004) Directional cell migration establishes the axes of planar polarity in the posterior lateral-line organ of the zebrafish. Developmental Cell 7:401-412.

Lu Z, DeSmidt AA (2013) Early Development of Hearing in Zebrafish. Jaro-Journal of the Association for Research in Otolaryngology 14:509-521.

Ma EY, Raible DW (2009) Signaling pathways regulating zebrafish lateral line development. Current Biology 19:R381-R386.

Manley G (2000) Cochlear mechanisms from a phylogenetic viewpoint. Proceedings of the National Academy of Sciences 97:11736–11743.

Marcotti W, Kros CJ (1999) Developmental expression of the potassium current I-K,I-n contributes to maturation of mouse outer hair cells. Journal of Physiology 520:653-660.

Marcotti W, van Netten SM, Kros CJ (2005) The aminoglycoside antibiotic dihydrostreptomycin rapidly enters mouse outer hair cells through the mechano-electrical transducer channels. Journal of Physiology 567:505-521.

Marcotti W, Geleoc GSG, Lennan GWT, Kros CJ (1999) Transient expression of an inwardly rectifying potassium conductance in developing inner and outer hair cells along the mouse cochlea. Pflugers Archiv-European Journal of Physiology 439:113-122.

Marcotti W, Johnson SL, Holley MC, Kros CJ (2003a) Developmental changes in the expression of potassium currents of embryonic, neonatal and mature mouse inner hair cells. Journal of Physiology 548:383-400.

Marcotti W, Johnson SL, Rusch A, Kros CJ (2003b) Sodium and calcium currents shape action potentials in immature mouse inner hair cells. Journal of Physiology 552:743-761.

Martini M, Rossi ML, Rubbini G, Rispoli G (2000) Calcium currents in hair cells isolated from semicircular canals of the frog. Biophysical Journal 78:1240-1254.

Masetto S, Correia MJ (1997) Electrophysiological properties of vestibular sensory and supporting cells in the labyrinth slice before and during regeneration. Journal of Neurophysiology 78:1913-1927.

Masetto S, Russo G, Prigioni I (1994) Differential expression of potassium currents by hair cells in thin slices of frog crista ampullaris. Journal of Neurophysiology 72:443-455.

Masetto S, Perin P, Malusa A, Zucca G, Valli P (2000) Membrane properties of chick semicircular canal hair cells in situ during embryonic development. Journal of Neurophysiology 83:2740-2756.

Matthews G, Fuchs P (2010) The diverse roles of ribbon synapses in sensory neurotransmission. Nature Reviews Neuroscience 11:812-822.

Metcalfe WK (1985) Sensory neuron growth cones comigrate with posterior lateral line primordial cells in zebrafish. Journal of Comparative Neurology 238:218-224.

Mo W, Chen F, Nechiporuk A, Nicolson T (2010) Quantification of vestibular-induced eye movements in zebrafish larvae. Bmc Neuroscience 11:doi:10.1186/1471-2202-1111-1110.

Moser T, Beutner D (2000) Kinetics of exocytosis and endocytosis at the cochlear inner hair cell afferent synapse of the mouse. Proceedings of the National Academy of Sciences of the United States of America 97:883-888.

Moser T, Brandt A, Lysakowski A (2006) Hair cell ribbon synapses. Cell and Tissue Research 326:347-359.

Mueller K, van Leeuwen J (2003) Swimming of larval zebrafish: ontogeny of body waves and implications for

locomotory development. The Journal of Experimental Biology 207:853-868.

Mulroy MJ, Williams RS (1987) Auditory stereocilia in the alligator lizard. Hearing Research 25:11-21.

Nagiel A, Andor-Ardo D, Hudspeth AJ (2008) Specificity of afferent synapses onto plane-polarized hair cells in the posterior lateral line of the zebrafish. Journal of Neuroscience 28:8442-8453.

Nicolson T (2005) The genetics of hearing and balance in zebrafish. Annual Review of Genetics 39:9-22.

Nicolson T (2015) Ribbon synapses in zebrafish hair cells. Hearing Research:doi: 10.1016/j.heares.2015.1004.1003.

Nicolson T, Rusch A, Friedrich RW, Granato M, Ruppersberg JP, Nusslein-Volhard C (1998) Genetic analysis of vertebrate sensory hair cell mechanosensation: the zebrafish circler mutants. Neuron 20:271-283.

Norris CH, Ricci AJ, Housley GD, Guth PS (1992) The inactivating potassium currents of hair cells isolated from the crista ampullaris of the frog. Journal of Neurophysiology 68:1642-1653.

Obholzer N, Wolfson S, Trapani JG, Mo W, Nechiporuk A, Busch-Nentwich E, Seiler C, Sidi S, Soellner C, Duncan RN, Boehland A, Nicolson T (2008) Vesicular glutamate transporter 3 is required for synaptic transmission in zebrafish hair cells. Journal of Neuroscience 28:2110-2118.

Olt J, Johnson SL, Marcotti W (2014) In vivo and in vitro biophysical properties of hair cells from the lateral line and inner ear of developing and adult zebrafish. Journal of Physiology 592:2041-2058.

Olt J, Ordoobadi AJ, Marcotti W, Trapani jG (2016) Physiological recordings from the zebrafish lateral line. In: Methods in Cell Biology, Volume 135: The Zebrafish: Genetics, Genomics, and Transcriptomics, 4 Edition (Detrich HW, Zon L, Westerfield M, eds), Elsevier. In Press

Parichy DM, Elizondo MR, Mills MG, Gordon TN, Engeszer RE (2009) Normal table of postembryonic zebrafish development: staging by externally visible anatomy of the living fish. Developmental Dynamics 238:2975-3015.

Pelkowski SD, Kapoor M, Richendrfer HA, Wang X, Colwill RM, Creton R (2011) A novel high-throughput imaging system for automated analyses of avoidance behavior in zebrafish larvae. Behavioural Brain Research 223:135-144.

Perin P, Soto E, Vega R, Botta L, Masetto S, Zucca G, Valli P (2000) Calcium channels functional roles in the frog semicircular canal. Neuroreport 11:417-420.

Pickles JO, Comis SD, Osborne MP (1984) Cross links between stereocilia in the guinea pig organ of corti and their possible relation to sensory transduction. Hearing Research 15:103-112.

Platt C (1993) Zebrafish inner ear sensory surfaces are similar to those in goldfish. Hearing Research 65:133-140.

Platzer J, Engel J, Schrott-Fischer A, Stephan K, Bova S, Chen H, Zheng H, Striessnig J (2000) Congenital deafness and sinoatrial node dysfunction in mice lacking class D L-type Ca2+ channels. Cell 102:89-97.

Popper AN, Fay RR (1997) Evolution of the ear and hearing: issues and questions. Brain Behavior and Evolution 50:213-221.

Posner L, Burns P (2009) Injectable anesthetic agents. In: Veterinary Pharmacology and Therapeutics, 9 Edition, pp 265-301.

Prigioni I, Masetto S, Russo G, Taglietti V (1992) Calcium currents in solitary hair cells isolated from frog crista ampullaris. Journal of vestibular research : equilibrium & orientation 2:31-39.

Pujol-Marti J, Lopez-Schier H (2013) Developmental and architectural principles of the lateral-line neural map. Frontiers in Neural Circuits:doi: 10.3389/fncir.2013.00047.

Readman GD, Owen SF, Murrell JC, Knowles TG (2013) Do Fish Perceive Anaesthetics as Aversive? Plos One 8.

Ricci AJ, Bai J-P, Song L, Lv C, Zenisek D, Santos-Sacchi J (2013) Patch-Clamp Recordings from Lateral Line Neuromast Hair Cells of the Living Zebrafish. Journal of Neuroscience 33:3131-3134.

Roberts WM, Jacobs RA, Hudspeth AJ (1990) Colocalization of ion channels involved in frequency-selectivity and synaptic transmission at presynaptic active zones of hair cells. Journal of Neuroscience 10:3664-3684.

Rodriguez-Contreras A, Yamoah EN (2001) Direct measurement of single-channel Ca2+ currents in bullfrog hair cells reveals two distinct channel subtypes. Journal of Physiology 534:669-689.

Rombough PJ (2007) Ontogenetic changes in the toxicity and efficacy of the anaesthetic MS222 (tricaine methanesulfonate) in zebrafish (Danio rerio) larvae. Comparative Biochemistry and Physiology a-Molecular & Integrative Physiology 148:463-469.

Russell IJ, Sellick PM (1976) Measurement of potassium and chloride ion concentrations in cupulae of lateral lines of xenopus laevis. Journal of Physiology-London 257:245-255.

Rüsch A, Eatock RA (1996) A delayed rectifier conductance in type I hair cells of the mouse utricle. Journal of Neurophysiology 76:995-1004.

Rüsch A, Lysakowski A, Eatock RA (1998) Postnatal development of type I and type II hair cells in the mouse utricle: Acquisition of voltage-gated conductances and differentiated morphology. Journal of Neuroscience 18:7487-7501.

Sakaguchi H, Tokita J, Müller U, Kachar B (2009) Tip links in hair cells: molecular composition and role in hearing loss. Current Opinion in Otolaryngology and Head and Neck Surgery 17:388-393.

Sapede D, Dyballa S, Pujades C (2012) Cell lineage analysis reveals three different progenitor pools for neurosensory elements in the otic vesicle. Journal of Neuroscience 32:16424-16434.

Sapede D, Gompel N, Dambly-Chaudiere C, Ghysen A (2002) Cell migration in the postembryonic development of the fish lateral line. Development 129:605-615.

Sato Y, Miyasaka N, Yoshihara Y (2007) Hierarchical regulation of odorant receptor gene choice and subsequent axonal projection of olfactory sensory neurons in zebrafish. Journal of Neuroscience 27:1606-1615.

Schofield BR (2011) Central Descending Auditory Pathways. In: Auditory and Vestibular Efferents, pp 261-290.

Scholz A (2002) Mechanisms of (local) anaesthetics on voltage-gated sodium and other ion channels. British Journal of Anaesthesia 89:52-61.

Schwander M, Kachar B, Mueller U (2010) The cell biology of hearing. Journal of Cell Biology 190:9-20.

Sento S, Furukawa T (1987) Intraaxonal labeling of saccular afferents in the goldfish, carassius-auratus - correlations between morphological and physiological characteristics. Journal of Comparative Neurology 258:352-367.

Sheets L, Kindt KS, Nicolson T (2012) Presynaptic Ca(V)1.3 channels regulate synaptic ribbon size and are required for synaptic maintenance in sensory Hair Cells. Journal of Neuroscience 32:17273-17286.

Sheets L, Trapani JG, Mo W, Obholzer N, Nicolson T (2011) Ribeye is required for presynaptic Ca(V)1.3a channel localization and afferent innervation of sensory hair cells. Development 138:1309-1319.

Sidi S, Busch-Nentwich E, Friedrich R, Schoenberger U, Nicolson T (2004) gemini encodes a zebrafish L-type calcium channel that localizes at sensory hair cell ribbon synapses. Journal of Neuroscience 24:4213-4223.

Sjostrand FS (1953) The ultrastructure of the retinal rod synapses of the guinea pig eye. Journal of Applied Physics 24:1422-1422.

Sjostrand FS (1958) Ultrastructure of retinal rod synapses of the guinea pig eye as revealed by 3-dimensional reconstructions from serial sections. Journal of Ultrastructure Research 2:122-170.

Smith ME, Schuck JB, Gilley RR, Rogers BD (2011) Structural and functional effects of acoustic exposure in goldfish: evidence for tonotopy in the teleost saccule. Bmc Neuroscience 12:doi:10.1186/1471-2202-1112-1119.

Smith SC, Lannoo MJ, Armstrong JB (1990) Development of the mechanoreceptive lateral line system in the axolotl - placode specification, guidance of migration and the origin of neuromast polarity. Anatomy and Embryology 182:171-180.

Sneary MG (1988) Auditory receptor of the red-eared turtle. 1. General ultrastructure. Journal of Comparative Neurology 276:573-587.

Sneddon LU (2012) Clinical anesthesia and analgesia in fish. Journal of Exotic Pet Medicine 21:32-43.

Stewart AM, Braubach O, Spitsbergen J, Gerlai R, Kalueffl AV (2014) Zebrafish models for translational neuroscience research: from tank to bedside. Trends in Neurosciences 37:264-278.

Stil A, Drapeau P (2015) Neuronal labeling patterns in the spinal cord of adult transgenic Zebrafish. Developmental neurobiology:doi: 10.1002/dneu.22350.

Stone LS (1922) Experiments on the development of the cranial ganglia and the lateral line sense organs in amblystoma punctatum. Journal of Experimental Zoology 35:420-496.

Stone LS (1937) Further experimental studies of the development of lateral-line sense organs in amphibians observed in living preparations. Journal of Comparative Neurology 68:83-115.

Straehle U, Scholz S, Geisler R, Greiner P, Hollert H, Rastegar S, Schumacher A, Selderslaghs I, Weiss C, Witters H, Braunbeck T (2012) Zebrafish embryos as an alternative to animal experiments-A commentary on the definition of the onset of protected life stages in animal welfare regulations. Reproductive Toxicology 33:128-132.

Sugihara I, Furukawa T (1989) Morphological and functional aspects of two different types of hair cells in the goldfish sacculus. Journal of Neurophysiology 62:1330-1343.

Sugihara I, Furukawa T (1995) Potassium currents underlying the oscillatory response in hair cells of the goldfish sacculus. Journal of Physiology 489:443-453.

Sugihara I, Furukawa T (1996) Inwardly rectifying currents in hair cells and supporting cells in the goldfish sacculus. Journal of Physiology 495:665-679.

Sun Z, Risner ML, van Asselt JB, Zhang D-Q, Kamermans M, McMahon DG (2012) Physiological and molecular characterization of connexin hemichannels in zebrafish retinal horizontal cells. Journal of Neurophysiology 107:2624-2632.

Tabor KM, Bergeron SA, Horstick EJ, Jordan DC, Aho V, Porkka-Heiskanen T, Haspel G, Burgess HA (2014) Direct activation of the Mauthner cell by electric field pulses drives ultrarapid escape responses. Journal of Neurophysiology 112:834-844.

Tilney LG, Saunders JC (1983) Actin-filaments, stereocilia, and hair cells of the bird cochlea. 1. Length, number, width, and distribution of stereocilia of each hair cell are related to the position of the hair cell on the cochlea. Journal of Cell Biology 96:807-821.

Toro C, Trapani JG, Pacentine I, Maeda R, Sheets L, Mo W, Nicolson T (2015) Dopamine Modulates the Activity of Sensory Hair Cells. Journal of Neuroscience 35:16494-16503.

Trapani J, Nicolson T (2010) Physiological recordings from zebrafish lateral-line hair cells and afferent neurons. In: Methods in cell biology, 3 Edition (Detrich H, Westerfield M, Zon L, eds), pp 219-231.

Trapani JG, Nicolson T (2011) Mechanism of spontaneous activity in afferent neurons of the zebrafish lateral-line organ. Journal of Neuroscience 31:1614-1623.

Trapani JG, Obholzer N, Mo W, Brockerhoff SE, Nicolson T (2009) synaptojanin1 Is Required for Temporal Fidelity of Synaptic Transmission in Hair Cells. Plos Genetics 5.

Vargas R, Porsteinsson H, Karlsson KAE (2012) Spontaneous neural activity of the anterodorsal lobe and entopeduncular nucleus in adult zebrafish: A putative homologue of hippocampal sharp waves. Behavioural Brain Research 229:10-20.

Vargas R, Johannesdottir IP, Sigurgeirsson B, Porsteinsson H, Karlsson KAE (2011) The zebrafish brain in research and teaching: a simple in vivo and in vitro model for the study of spontaneous neural activity. Advances in Physiology Education 35:188-196.

Vemaraju S, Kantarci H, Padanad M, Riley B (2012) A spatial and temporal gradient of Fgf differentially regulates distinct stages of neural development in the zebrafish inner ear. PLoS Genetics:e1003068.

Wan L, Almers W, Chen WB (2005) Two ribeye genes in teleosts: the role of ribeye in ribbon formation and bipolar cell development. Journal of Neuroscience 25:941-949.

Wangemann P, Schacht J (1996) Homeostatic mechanisms in the cochlea. In: The cochlea (Dallos P, Popper A, Fay R, eds), pp 130-185. New York: Springer.

Weber ES, III (2011) Fish Analgesia: Pain, Stress, Fear Aversion, or Nociception? Veterinary Clinics of North America Exotic Animal Practice 14:21-32.

Whitfield TT, Riley BB, Chiang MY, Phillips B (2002) Development of the zebrafish inner ear. Developmental Dynamics 223:427-458.

Williams JA, Holder N (2000) Cell turnover in neuromasts of zebrafish larvae. Hearing Research 143:171-181.

Wu YC, Art JJ, Goodman MB, Fettiplace R (1995) A kinetic description of the calcium-activated potassium channel and its application to electrical tuning of hair cells. Progress in Biophysics and Molecular Biology 63:131-158.

Young HS, Herbette LG, Skita V (2003) alpha-bungarotoxin binding to acetylcholine receptor membranes studied by low angle X-ray diffraction. Biophysical Journal 85:943-953.

Zahl IH, Samuelsen O, Kiessling A (2012) Anaesthesia of farmed fish: implications for welfare. Fish Physiology and Biochemistry 38:201-218.

Zampini V, Johnson SL, Franz C, Knipper M, Holley MC, Magistretti J, Masetto S, Marcotti W (2013) Burst activity and ultrafast activation kinetics of Ca(V)1.3 Ca2+ channels support presynaptic activity in adult gerbil hair cell ribbon synapses. Journal of Physiology 591:3811-3820.

Zampini V, Johnson SL, Franz C, Knipper M, Holley MC, Magistretti J, Russo G, Marcotti W, Masetto S (2014) Fine Tuning of Ca(V)1.3 Ca2+ Channel Properties in Adult Inner Hair Cells Positioned in the Most Sensitive Region of the Gerbil Cochlea. Plos One 9.